IEEE Access
Multidisciplinary ⋮ Rapid Review ⋮ Open Access Journal

Received 17 April 2024, accepted 6 May 2024, date of publication 8 May 2024, date of current version 15 May 2024.

Digital Object Identifier 10.1109/ACCESS.2024.3398351

SURVEY

A Comprehensive Review of Direction-of-Arrival Estimation and Localization Approaches in Mixed-Field Sources Scenario

AMIR MASOUD MOLAEI[1], (Senior Member, IEEE), BIJAN ZAKERI[2], (Member, IEEE), SEYED MEHDI HOSSEINI ANDARGOLI[2], MUHAMMAD ALI BABAR ABBASI[1], (Member, IEEE), VINCENT FUSCO[1], (Fellow, IEEE), AND OKAN YURDUSEVEN[1], (Senior Member, IEEE)

[1]Institute of Electronics, Communications and Information Technology (ECIT), Queen's University Belfast, BT3 9DT Belfast, U.K.
[2]Electrical and Computer Engineering Faculty, Babol Noshirvani University of Technology, Babol 47148-71167, Iran

Corresponding author: Amir Masoud Molaei (a.molaei@qub.ac.uk)

This work was supported by the Leverhulme Trust under the Research Leadership Award under Grant RL-2019-019.

ABSTRACT Direction-of-arrival (DOA) estimation plays a crucial role in array signal processing across various domains, including radar, sonar, wireless communications, and seismic exploration. However, traditional DOA techniques often assume either far-field (FF) or near-field (NF) propagation, limiting their applicability in scenarios involving mixed-field sources. DOA estimation and localization in scenarios involving mixed NF and FF sources is a complex and dynamic field that has garnered significant research attention in recent years. This multifaceted and evolving area holds promise for addressing challenges in radar, wireless communications, and acoustic sensing applications. This review paper provides a comprehensive overview of the methodologies, techniques, and advancements in this domain. We categorize existing methodologies, discussing their advantages and limitations. Furthermore, we delve into the mathematical modeling of mixed-field sources and essential signal processing techniques for parameter estimation. Special attention is given to technical issues such as aperture loss, computational complexity, and hardware considerations. The paper discusses the various sources of noise in the mentioned scenario and highlights the importance of modeling noise accurately for effective estimation. It also explores different scenarios and assumptions considered in the literature, ranging from non-Gaussian and non-stationary noise environments to scenarios involving multipath propagation and unknown mutual coupling effects. A detailed examination of the statistical approaches used in DOA estimation and localization reveals a diverse range of methods, including higher-order statistics and second-order statistics, each with its own advantages and applications. A comparative evaluation of various approaches highlights their performance in terms of estimation accuracy, resolution, aperture loss and computational efficiency. This provides insights into the trade-offs involved in choosing between different approaches. The review also identifies promising future research directions, such as the exploration of advanced signal processing techniques like compressive sensing and deep learning, exact NF modeling, estimation based on one-bit measurements, the integration of polarization diversity, employing metasurface antennas, tracking parameters, and the utilization of full-wave or experimental data for a more realistic representation of the challenges. By reviewing advances in methodologies and techniques, as well as outlining future research directions aimed at addressing the complexities of mixed-field scenarios, this paper paves the way for the development of more robust and reliable localization systems capable of handling real-world complexities.

The associate editor coordinating the review of this manuscript and approving it for publication was Chen Chen.

INDEX TERMS Antenna array, array signal processing, azimuth/elevation angle and range estimations, DOA estimation, Fresnel region, mixed-field sources, NF and FF sources, passive localization, wireless communication.

I. INTRODUCTION

Array signal processing (ASP) is one of the most important branches of signal processing, which is widely used in various fields of science and engineering, such as radar, sonar, seismic event prediction, microphone sensors, navigation, air traffic control and wireless communication systems [1], [2], [3]. The structure of the array can be defined as a set of sensors/antennas that are placed next to each other in a special arrangement. In radar and sonar systems, sensor arrays are often used to determine the number of sources and estimate their position, or estimate the speed of targets such as airplanes, missiles, and submarines [4], [5]. Seismic arrays are used for oil exploration and detection of underground nuclear tests [6], [7]. For example, the Norwegian Seismic Array (NORSAR), an internationally recognized independent research foundation, now with 50 primary and 120 auxiliary seismic stations around the world, is working on improving array processing to improve an international monitoring system for seismic activity. Since the strength of the desired signals is reduced to some extent due to the distance between the source and the microphones, in speech and audio signal processing, microphone arrays are often used to extract the desired signals by improving reception in one or more specific directions [8], [9]. The array antenna method [10], [11] is known as one of the key features of the third generation and beyond wireless communication systems, which can dramatically improve the operational parameters of the system such as capacity, quality and coverage.

Estimating the direction-of-arrival (DOA) [12] of one or more plane waves impinging on an array of sensors from noisy data is one of the most important aspects of ASP, which has been the focus of many researchers in the past decades. The signals to be processed can be in the form of electromagnetic (EM)/radio or sound waves. The necessity of DOA estimation arises from the necessity of locating and tracking signal sources in military applications as well as civilian applications (such as search and rescue, sonar, seismology, and locating wireless emergency calls). An antenna array can be designed to detect incoming signals so that it only accepts signals from certain directions and filters out unintended signals that are known as interference [13]. The estimation accuracy, resolution, applicability for real environments, computational complexity and hardware implementation cost have always been discussed in different DOA estimation techniques [14], [15], [16], [17].

DOA estimation techniques can be divided into three general categories, including classical methods, subspace-based methods, and maximum likelihood (ML) methods [18], [19]. Classical methods such as the delay-and-sum method, and minimum variance distortionless response (MVDR) method, are conceptually simple but have relatively poor performance, and are not computationally efficient [19]. In comparison, the ML technique performs well, especially when the signal-to-noise ratio (SNR) is low or the number of snapshots is small, but it is computationally very complex [20]. Subspace-based methods also perform well and are known as high-resolution methods; besides, they are also more efficient in terms of computation [21]. By taking advantage of the orthogonality of subspaces, two common techniques including multiple signal classification (MUSIC) [22] and estimation of signal parameters through rotational invariance techniques (ESPRIT) [23] and their different versions are widely used. The above DOA estimators can be designed and implemented based on spatial, frequency and time filtering or their combination. In the case of wideband signals (i.e. signals that occupy a relatively large portion of the frequency spectrum and have a bandwidth that is significant compared to the carrier frequency), using spatial filtering to separate the signals is not cost-effective. This is because it requires the calculation of the spatial statistics matrix for each frequency bin and the use of a separate estimator for each signal, which greatly increases the computational complexity and makes its practical applications difficult. However, frequency filtering is widely used in broadband DOA estimation methods [24], [25]. In this way, wideband signals are decomposed into several narrowband signals (which means that the time delays are small compared to the inverse of the signal bandwidth) by a filter bank or discrete Fourier transform.

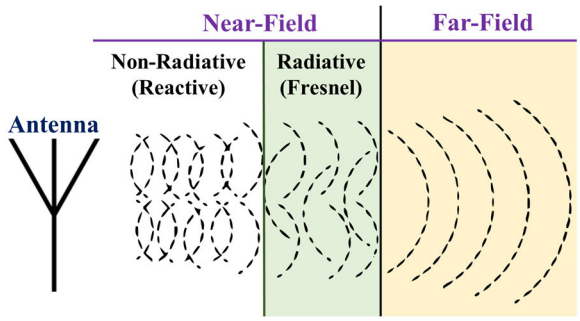

FIGURE 1. A schematic of the regions of Fraunhofer (reactive NF), Fresnel (radiative NF), and far-field (FF) [38]. In the reactive NF zone, energy decays very rapidly with distance. In the radiative NF region, the average energy density remains fairly constant at different distances from the antenna, although there are localized energy fluctuations [39], [40]. Note that in the mixed-field sources scenario, in the literature and throughout this paper, the NF region always refers to the Fresnel region (green region in the figure).

Although the plane wave assumption can simplify the modeling and processing, in practical applications of the near-field (NF), such an assumption is not valid and will lead to errors in the analysis [26]. When the radiation source is in the NF (Fresnel region of the array aperture) [27], the shape of the spherical wavefront changes nonlinearly with the position of the array and is determined by both angle (DOA) and range parameters (see Fig. 1) [28], [29]. As a result, conventional

DOA estimation algorithms of far-field sources (FFSs) are not directly applicable to NF sources (NFSs).

On the other hand, in various practical applications such as wireless communication, radar systems, medical imaging, acoustic sensing, seismic exploration, electronic supervision and guidance systems, the coexistence of NF and FF sources (relative to the sensing position) may occur [30], [31], [32]. For example, in wireless communication systems, base stations and mobile devices can be located in such a way that some signals are received in the NF, especially when devices are close to each other, while others may be in the FF when the distance between transmitter (TX) and receiver (RX) is significant [33]. Similarly, in radar systems, targets at varying distances from the radar antenna may fall into either the NF or FF region, depending on their proximity [34]. Medical imaging techniques like magnetic resonance imaging (MRI) and ultrasound imaging also encounter scenarios where sources exhibit both NF and FF characteristics. For instance, in MRI, the interaction between the radiofrequency coil and the body tissues may lead to a combination of NF and FF signals [35]. Similarly, in ultrasound imaging, reflections from structures close to the transducer can generate NF signals (NSs), while those from deeper tissues may produce FF signals (FSs) [36]. Acoustic sensing applications, such as microphone arrays used for speaker localization or environmental monitoring, encounter similar situations. Sources emitting sounds at varying distances from the microphone array may generate both NF and FF signals, depending on their proximity [37]. In all these scenarios, conventional techniques face problems; because these techniques are inherently limited to resolving only pure FSs or pure NSs, rather than dealing with scenarios where they co-exist. This has motivated the increasing attention to the issue of parameter estimation of mixed-field source signals in recent years.

Each of the approaches presented in the literature for the problem of mixed FFSs and NFSs has advantages and disadvantages. Among the disadvantages and limitations that can be found in some of them are severe loss of aperture (degree of freedom), creation of spurious peaks in the spatial spectrum, low estimation accuracy, high computational complexity, low resolution, inability to estimate the parameters of sources with the same angle, the failure in complex propagation environments, the limited dimensions of estimation, etc. In this review paper, in addition to introducing the problem, and stating the technical limitations, existing/possible strategies to deal with some special problems/challenges will be presented and discussed. In addition, suggestions for future work in this area are provided.

The rest of this paper is organized as follows. In Section II, the essentials of the problem of estimating the parameters of mixed-field sources, including mathematical modeling of the data are presented. In Section III, basic approaches for solving the mixed-field sources problem are described. In Section VI, the special technical issues and challenges, both in the processing layer and in the hardware part, are described for the mentioned problem. In Section V, a summarized general comparison of various aspects of the approaches available in the literature is provided. Finally, concluding remarks are drawn in Section VI.

Notation: Throughout the paper, superscripts $(\cdot)^T$, $(\cdot)^*$, $(\cdot)^H$ and $(\cdot)^\dagger$ represent the transpose, complex conjugate, conjugate transpose, and pseudoinverse, respectively. The symbols $\mathbb{E}\{\cdot\}$, j, $\ln(\cdot)$, $\log_2(\cdot)$, $\text{cum}\{\cdot\}$, $\hat{x}$, $\text{eig}(\cdot)$, $|\cdot|$, $\text{rem}(a,\ b)$, $\text{LCM}(\cdot)$, $\text{diag}[\cdot]$, $\text{blkdiag}[.]$, $\angle$, $\lceil\cdot\rceil$, $\lfloor\cdot\rfloor$, $\delta[\cdot]$, $\min\{\cdot\}$ and $\max\{\cdot\}$ denote the expected value operator, imaginary unit, natural logarithm, binary logarithm, cumulant function, estimation of x, eigenvalue, absolute value, remainder after the division of a by b, lowest common multiple, diagonal matrix, block diagonal matrix, angle, integer ceiling and floor functions, Dirac delta function, and the minimum and maximum values in the set, respectively. $\mathbf{I}_m$ and $\mathbf{J}_m$, respectively, stand for the $m \times m$ identity matrix and $m \times m$ exchange matrix.

Acronym: In Table 1, all acronyms used throughout the paper are presented.

II. THE PROBLEM OF MIXED FF AND NF SOURCES

A. BASIC CONCEPTS AND PREREQUISITES

In many applications of passive array processing, the wavefront is assumed to be planar; this means that the radiating sources are located in the FF (Fraunhofer region) relative to the position of the array, and their range is considered infinite. In this case, the task of locating the source is limited only to the estimation of DOAs. As mentioned in the previous section, although the plane wave assumption can simplify the modeling and processing, in practical applications of the NF, such an assumption is not correct and will lead to errors in the analysis. In fact, when the radiation source is in the NF (the Fresnel area of the array aperture), that is [28]

$$0.62\sqrt{\frac{D^3}{\lambda}} < R_{\text{D}} < 2\frac{D^2}{\lambda}, \tag{1}$$

the shape of the spherical wavefront has a phase difference that changes nonlinearly with the position of the array and is determined by both angle and range parameters. In (1), R_{D}, λ and D represent the distance from the source to the reference element in the array, the wavelength of the emitter and the array aperture size, respectively. As a result, conventional DOA estimation algorithms for FFSs are not applicable to estimate the location of NFSs. On the other hand, in some practical applications, FFSs and NFSs can coexist. Algorithms presented to deal with pure FFSs or pure NFSs fail in mixed sources scenario.

Considering that many solutions related to the mixed-field sources problem, which will be reviewed in the next sections, use fourth-order statistics (FOS), here is a short introduction to the concepts of cumulant [29]. The moment generating function (MGF) is a widely used function in mathematics and is defined as follows for a random variable X [41]:

$$M_X(t) = \mathbb{E}\left\{e^{tX}\right\}, \quad t \in \mathbb{R}. \tag{2}$$

TABLE 1. List of acronyms.

Acronym	Description
ADC	Analog-to-Digital Converter
ASP	Array Signal Processing
CDF	Cumulative Distribution Function
CF	Characteristic Function
CFN	Calibration for mixed Far-field and Near-field signals
CNN	Convolutional Neural Network
CRB	Cramér–Rao Bound
CS	Compressive Sensing
CSA	Components Separation Algorithm
CVMD	Complex Variational Mode Decomposition
DL	Deep Learning
DOA	Direction-of-Arrival
EVD	Eigenvalue Decomposition
EM	Electromagnetic
ESNA	Extended Symmetric Nested Array
ESPRIT	Estimation of Signal Parameters through Rotational Invariance Techniques
FC	Fading Coefficient
FF	Far-Field
FFS	Far-Field Source
FM	Far-field sources in Mixed signals
FMW	Far-field sources in Mixed Wideband signals
FOC	Fourth-Order Cumulant
FOS	Fourth-Order Statistics
FOSA	Fourth-Order Spatio-temporal Algorithm
FS	Far-Field Signal
GESPRIT	Generalized Estimation of Signal Parameters through Rotational Invariance Techniques
HODA	High-Order Differencing Algorithm
HOC	High-Order Cumulant
HOS	High-Order Statistics
HOSTA	High-Order Spatial-Temporal Algorithm
LS	Least-Squares
MC	Mutual Coupling
MCC	Mutual Coupling Coefficient
MCM	Mutual Coupling Matrix
MGF	Moment Generating Function
ML	Maximum Likelihood
MOS	Mixed-Order Statistics
MPR	Modified Polar Representation
MRI	Magnetic Resonance Imaging
MUSIC	Multiple Signal Classification
MVDR	Minimum Variance Distortionless Response
NC	Non-Circular
NF	Near-Field
NFIM	Near-Field Interference Mitigation
NFS	Near-Field Source
NORSAR	Norwegian Seismic Array
NS	Near-Field Signal
OPMUSIC	Oblique Projection Multiple Signal Classification
PDF	Probability Density Function
RARE	Rank Reduction
RMSE	Root Mean Square Error
RX	Receiver
SBL	Sparse Bayesian Learning
SDNA	Symmetric Double-Nested Array
SFNA	Symmetric Flipped Nested Array
SLA	Sparse Linear Array
SNR	Signal-to-Noise Ratio
SOS	Second-Order Statistics
SS	Spatial Smoothing
SSLA	Sparse Symmetric Linear Array
STCA	Symmetric Thinned Coprime Array
SULA	Symmetric Uniform Linear Array
SVD	Singular Value Decomposition
TDOA	Time Difference of Arrival
TSMDA	Two-Stage Matrix Differencing Algorithm
TSMUSIC	Two-Stage Multiple Signal Classification Algorithm
TSRARE	Two-Stage Rank Reduction
TTSNA	Translation and Transformation Symmetric Nested Array
2-D	Two-Dimensional
TX	Transmitter
UCA	Uniform Circular Array
ULA	Uniform Linear Array

By having the MGF of a random variable, its probability distribution can be fully defined. In addition to univariate distributions, the MGF can also be defined for vector- or matrix-valued random variables. In general, if $\mathbf{X}$ is a multivariate random variable, then [42]

$$M_{\mathbf{X}}(\mathbf{t}) = \mathbb{E}\left\{e^{\mathbf{t}^T\mathbf{X}}\right\}. \tag{3}$$

The MGF, unlike the characteristic function (CF) [43], cannot always be defined; because the implicit integral $\mathbb{E}\left\{e^{tX}\right\}$ need not converge, in general [44]. According to the definition, the CF of X is [45]

$$\Phi_X(j\omega) = \mathbb{E}\left\{e^{j\omega X}\right\}. \tag{4}$$

The CF is actually the Fourier transform of the probability density function (PDF), by converting $\omega \in [0, \infty)$ to $-\omega$. MGF and CF both have the same information. The n-th moment of a random variable can be obtained simply by the MGF and without the need to take the integral as follows [46]:

$$\mathbb{E}\left\{X^n\right\} = M_X^{(n)}(0), \tag{5}$$

where n a nonnegative integer.

In probability theory and statistics, the cumulants of a probability distribution are sets of values that provide an alternative for the moments of the distribution [47]. Any two probability distributions that have the same moments have the same cumulants and vice versa. The first cumulant is the mean, the second the variance and the third cumulant is the third central moment. But fourth and higher cumulants are not equal to central moments. Note that the 0-th moment for a random variable is equal to the total probability or the value 1. In some cases, the use of cumulants is preferred over moments. In particular, when two or more random variables are statistically independent, the n-th order cumulant of their sum is equal to the sum of their n-th order cumulants. Also, the third and higher cumulants of the normal distribution are zero. The cumulants of X are defined using the cumulant generating function $K_X(t)$, which is the natural logarithm of the MGF [48]

$$K_X(t) = \ln\left(M_X(t)\right). \tag{6}$$

Cumulants are obtained from the expansion of the power series (Maclaurin series) [49].

B. GENERAL DATA MODEL

In this section, the general mathematical model that is mainly considered the base problem in the scenario of mixed-field sources in the literature is presented. In the next section, more specific models are also reviewed.

Consider K uncorrelated narrowband sources, consisting of K_{N} NFSs and K_{F} FFS, where $K_{\mathrm{F}} = K - K_{\mathrm{N}}$. The signals transmitted by these sources from the azimuth directions $\theta_1, \theta_2, \ldots, \theta_K$ impinge on a symmetric uniform linear array (SULA) of $N = 2M + 1$ isotropic sensors with inter-spacing d (Fig. 2). Each antenna element is denoted by the index m, where $m = -M, -M+1, \ldots, 0, \ldots, M-1, M$. The spatial phase-shift factor between the reference element and m-th one for the k-th impinging signal is defined as [50] and [51]:

$$a_{m,k} = e^{j\tau_{m,k}}, \tag{7}$$

where $\tau_{m,k}$ represents the phase shift associated with the propagation time delay of the k-th signal between the reference sensor (array physical center in Fig. 2) and the m-th sensor, and $k = 1, 2, \ldots, K$. By considering the array center as the phase reference, the exact value of $\tau_{m,k}$ is obtained from the following equation [50], [52]:

$$\tau_{m,k} = \frac{2\pi}{\lambda} r_k \left(\sqrt{1 - \frac{2}{r_k} md \sin\theta_k + \left(\frac{md}{r_k}\right)^2} - 1 \right), \tag{8}$$

where r_k is the range of k-th source. If the k-th source is located in the NF, $\tau_{m,k}$ can be approximated as follows [53], [54]:

$$\tau_{m,k} \simeq \gamma_k m + \chi_k m^2, \tag{9}$$

where the electric angles γ_k and χ_k are obtained from the following equations [50], [55]:

$$\gamma_k = -2\pi \frac{d}{\lambda} \sin\theta_k, \tag{10}$$

$$\chi_k = \pi \frac{d^2}{\lambda r_k} \cos^2\theta_k. \tag{11}$$

On the other hand, if the signal source is located in the FF ($r_k \to \infty$), $\tau_{m,k}$ can be considered in the following form [50], [56]:

$$\tau_{m,k} \simeq \gamma_k m. \tag{12}$$

With a proper sampling rate that satisfies the Nyquist rate [57], the l-th signal sample observed by the m-th sensor can be expressed as follows [58], [59]:

$$x_m(l) = \sum_{k=1}^{K} s_k(l)\, e^{j\tau_{m,k}} + n_m(l), \quad l = 1, 2, \ldots, L, \tag{13}$$

where L is the number of snapshots, $s_k(l)$ is the baseband signal of the k-th source, and $n_m(l)$ is the noise corresponding to the m-th sensor. Without the loss of generality, it can be assumed that the first K_N signals are received from the NF and the remaining K_{F} signals are received from the FF. Therefore, according to (9)-(12), (13) can be rewritten in the following form:

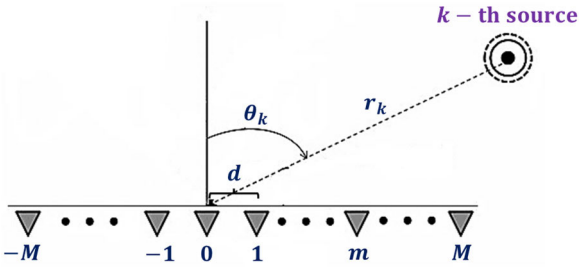

FIGURE 2. A SULA consisting of $N = 2M + 1$ sensors.

$$x_m(l) = \sum_{k=1}^{K_{\mathrm{N}}} s_k(l)\, e^{j(\gamma_k m + \chi_l m^2)} + \sum_{k=K_{\mathrm{N}}+1}^{K} s_k(l)\, e^{j\gamma_k m} + n_m(l). \tag{14}$$

In the matrix form, the output vector of the array, $\mathbf{x}(l) = \sum_{k=1}^{K} \mathbf{a}(\theta_k, r_k)\, s_k(l) + \mathbf{n}(l)$, can be expressed as follows:

$$\mathbf{x}(l) = \mathbf{A}\,\mathbf{s}(l) + \mathbf{n}(l) = \mathbf{A}_{\mathrm{N}}\mathbf{s}_{\mathrm{N}}(l) + \mathbf{A}_{\mathrm{F}}\mathbf{s}_{\mathrm{F}}(l) + \mathbf{n}(l), \tag{15}$$

where

$$\mathbf{x}(l) = \left[x_{-M}(l) \ldots x_0(l) \ldots x_M(l) \right]^T \in \mathbb{C}^{N\times 1}, \tag{16}$$

$$\mathbf{s}(l) = \left[\mathbf{s}_{\mathrm{N}}^T(l)\ \mathbf{s}_{\mathrm{F}}^T(l) \right]^T \in \mathbb{C}^{K\times 1}, \tag{17}$$

$$\mathbf{s}_{\mathrm{N}}(l) = \left[s_1(l)\ s_2(l) \ldots s_{K_{\mathrm{N}}}(l) \right]^T \in \mathbb{C}^{K_{\mathrm{N}}\times 1}, \tag{18}$$

$$\mathbf{s}_{\mathrm{F}}(l) = \left[s_{K_{\mathrm{N}}+1}(l)\ s_{K_{\mathrm{N}}+2}(l) \ldots s_K(l) \right]^T \in \mathbb{C}^{K_{\mathrm{F}}\times 1}, \tag{19}$$

$$\mathbf{n}(l) = \left[n_{-M}(l) \ldots n_0(l) \ldots n_M(l) \right]^T \in \mathbb{C}^{N\times 1}, \tag{20}$$

where $\mathbf{s}_{\mathrm{N}}(t)$, $\mathbf{s}_{\mathrm{F}}(t)$, and $\mathbf{n}(t)$ are the source vector of NSs, the source vector of FSs and the additive Gaussian noise vector with zero mean and variance σ^2, respectively. In (15), $\mathbf{A}$ is a steering matrix whose columns are the steering vectors corresponding to K signals and can be written as follows:

$$\mathbf{A} = \left[\mathbf{A}_{\mathrm{N}}\ \mathbf{A}_{\mathrm{F}} \right] \in \mathbb{C}^{N\times K}, \tag{21}$$

$$\mathbf{A}_{\mathrm{N}} = \left[\mathbf{a}_1\ \mathbf{a}_2 \ldots \mathbf{a}_{K_{\mathrm{N}}} \right] \in \mathbb{C}^{N\times K_{\mathrm{N}}}, \tag{22}$$

$$\mathbf{A}_{\mathrm{F}} = \left[\mathbf{a}_{K_{\mathrm{N}}+1}\ \mathbf{a}_{K_{\mathrm{N}}+2} \ldots \mathbf{a}_K \right] \in \mathbb{C}^{N\times K_{\mathrm{F}}}, \tag{23}$$

$$\mathbf{a}_k = \left[a_{-M,k}\ a_{-M+1,k} \ldots a_{M,k} \right]^T \in \mathbb{C}^{N\times 1}, \tag{24}$$

where $\mathbf{a}(\theta_k, r_k) = \mathbf{a}_k$, and $a_{m,k}$ is obtained from (7).

Two-dimensional (2)-D DOA estimation (estimation of both azimuth and elevation angles) [60] is an important issue in some applications, especially radar, mobile communication, sonar, seismology and industrial measurements [61], [62], [63]. Due to the increase in dimension, and as a result of the increase in the complexity of the problem, 2-D DOA

estimation in the scenario of mixed sources, despite its great importance, has been studied less. It should be noted that since the 1-D DOA estimation algorithms for the mixed sources scenario are completely dependent on the array geometry, they cannot be directly generalized for the 2-D problem. Among the 2-D arrays, uniform circular array (UCA) is usually preferred due to its 360° azimuthal coverage and almost unchanged directional pattern [54], [64]. Moreover, the resolution of UCA is relatively uniform around the azimuth angle [65], [66]. In addition, UCAs are capable of forming beam patterns that are relatively invariant with frequency [66], [67]. In the following, the general mathematical data model for the problem of mixed-field sources using UCA is expressed.

Suppose K signals transmitted by K_{N} NFSs and K_{F} FFSs impinge on a UCA with radius R consisting M sensors, plus a center sensor at the phase reference point (see Fig. 3). The center sensor is used to normalize the data [68], [69]. Each antenna element is denoted by the index m, where $m' = 0, 1, \ldots, M$. NFSs and FFSs are located at (θ_k, ϕ_k, r_k) and (θ_k, ϕ_k), where $\theta_k \in [0, 2\pi)$, $\phi_k \in \left[0, \pi/2\right)$ and r_k represent the azimuth angle, elevation angle, and range measured by the array set, respectively. With a proper sampling rate, the l-th sample of the signal observed by the m'-th sensor is expressed as [54] and [70]

$$x_{m'}(l) = \sum_{k=1}^{K} s_k(l)\, e^{j\frac{2\pi}{\lambda}\left(r_k - r_{m'}(\theta_k, \phi_k, r_k)\right)} + n_{m'}(l), \quad (25)$$

where $r_{m'}(\theta_k, \phi_k, r_k)$ is the distance between the k-th source and the m'-th sensor, which can be calculated by the following equation [54]:

$$r_{m'}(\theta_k, \phi_k, r_k) = \sqrt{r_k^2 - R^2 - 2r_k R\eta_{m'}(\theta_k, \phi_k)}, \quad m' = 1, 2, \ldots, M, \quad (26)$$

where $\eta_{m'}(\theta_k, \phi_k) = \cos\left(2\pi m'/M - \theta_k\right)\sin\phi_k$. Assuming $R \ll r_k$ and according to the second-order Taylor series expansion [71], (26) can be approximated as

$$r_k - R\eta_{m'}(\theta_k, \phi_k) + \frac{R^2}{2r_k}\left(1 - \eta_{m'}^2(\theta_k, \phi_k)\right). \quad (27)$$

Note that for $m' = 0$, $r_{m'}(\theta_k, \phi_k, r_k) = r_k$. Since if the source is located in the FF, it is assumed that $r_k \to \infty$, so substituting the above expression into (25) yields

$$x_{m'}(l) = \begin{cases} \sum_{k=1}^{K} s_k(l) + n_{m'}(l), & m' = 0, \\ \sum_{k=1}^{K_{\mathrm{N}}} s_k(l)\, e^{j\frac{2\pi R}{\lambda}\left(\eta_{m'}(\theta_k, \phi_k) - \frac{R}{2r_k}\left(1 - \eta_{m'}^2(\theta_k, \phi_k)\right)\right)} \\ \quad + \sum_{k=K_{\mathrm{N}}+1}^{K} s_k(l)\, e^{j\frac{2\pi R}{\lambda}\eta_{m'}(\theta_k, \phi_k)} + n_{m'}(l), \\ \quad m' = 1, 2, \ldots, M. \end{cases} \quad (28)$$

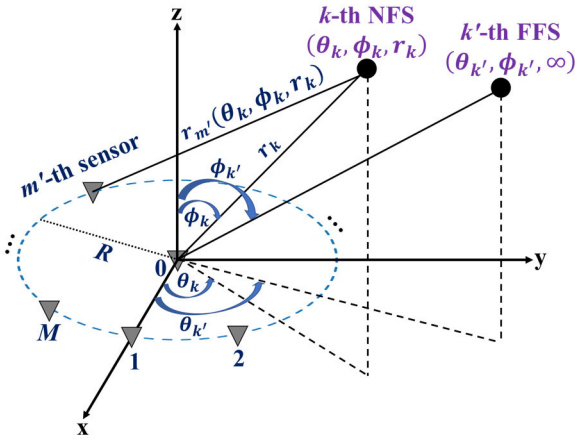

FIGURE 3. The geometry of a UCA with a center sensor in the mixed-field sources scenario.

The general matrix form of the output vector of the array (i.e. $\mathbf{x}(l) \in \mathbb{C}^{(M+1)\times 1}$) is similar to (15), with the difference that in the case of the array in Fig. 3, its components are defined as follows:

$$\mathbf{n}(l) = \left[n_0(l)\ n_1(l)\ \ldots\ n_M(l)\right]^T \in \mathbb{C}^{(M+1)\times 1}, \quad (29)$$

$$\mathbf{A}_{\mathrm{N}} = \left[\mathbf{a}_{\mathrm{N}}(\theta_1, \phi_1, r_1)\ \mathbf{a}_{\mathrm{N}}(\theta_2, \phi_2, r_2) \ldots \mathbf{a}_{\mathrm{N}}\left(\theta_{K_N}, \phi_{K_N}, r_{K_N}\right)\right] \in \mathbb{C}^{(M+1)\times K_N}, \quad (30)$$

$$\mathbf{A}_{\mathrm{F}} = \left[\mathbf{a}_{\mathrm{F}}\left(\theta_{K_N+1}, \phi_{K_N+1}\right)\ \mathbf{a}_{\mathrm{F}}\left(\theta_{K_N+2}, \phi_{K_N+2}\right) \ldots \mathbf{a}_{\mathrm{F}}(\theta_K, \phi_K)\right] \in \mathbb{C}^{(M+1)\times K_F}, \quad (31)$$

$$\mathbf{a}_{\mathrm{N}}(\theta_k, \phi_k, r_k) = \left[1\ e^{j\frac{2\pi R}{\lambda}\left(\eta_{1,k}(\theta_k, \phi_k) - \frac{R}{2r_k}\left(1 - \eta_{1,k}^2(\theta_k, \phi_k)\right)\right)} \ldots e^{j\frac{2\pi R}{\lambda}\left(\eta_{M,k}(\theta_k, \phi_k) - \frac{R}{2r_k}\left(1 - \eta_{M,k}^2(\theta_k, \phi_k)\right)\right)}\right] \in \mathbb{C}^{(M+1)\times 1}, \quad (32)$$

$$\mathbf{a}_{\mathrm{F}}(\theta_k, \phi_k) = \left[1\ e^{j\frac{2\pi R}{\lambda}\eta_{1,k}(\theta_k, \phi_k)}\ e^{j\frac{2\pi R}{\lambda}\eta_{2,k}(\theta_k, \phi_k)} \ldots e^{j\frac{2\pi R}{\lambda}\eta_{M,k}(\theta_k, \phi_k)}\right] \in \mathbb{C}^{(M+1)\times 1}. \quad (33)$$

The basic assumptions that are usually considered in modeling are:

[A1] The array is calibrated.

[A2] Signals $\{s_k(l)\}_{k=1}^{K}$ are statistically independent, narrowband stationary processes.

[A3] The sensor noise is additive Gaussian and is statistically independent of the sources' signals.

[A4] The total number of sources (i.e. K) is known or properly estimated by conventional methods [72], [73], [74].

Remark 1: All the methods that will be reviewed in the following sections estimate both the DOA and the range r of the source in locating NFSs. By having these two parameters and using the conversion of polar coordinates to Cartesian coordinates, it is easy to calculate the position of NFSs in

Cartesian coordinates. For more details and access to the relevant equations, refer to [75] and [76]. Note that logically, the 3-D position of the source in Cartesian coordinates (i.e. (x, y, z)) is only achievable for approaches that use 2-D arrays to estimate both the azimuth angle θ and the elevation angle ϕ. In the case of linear arrays, it is usually assumed that the antennas and sources are located in the horizontal plane, i.e. $\phi = 0$, and the elevation angle is ignored. In this case, the corresponding array manifold is only a function of the signal azimuth angle and range. As a result, in the latter case, it is possible to calculate the position of the source in Cartesian coordinates in the plane $\phi = 0$.

III. BASIC APPROACHES

In this section, some basic approaches to estimating spatial parameters when NFSs and FFSs coexist are briefly reviewed. In the next section, the challenges and limitations of the basic approaches in more practical and complex scenarios are described along with solutions.

The two-stage MUSIC algorithm (TSMUSIC) [77], as the first research in the area of mixed-sources passive estimation, uses two fourth-order cumulant (FOC) matrices $\mathbf{C}_1$ and $\mathbf{C}_2$ to localization of combining FFSs and NFSs. The first matrix (i.e. $\mathbf{C}_1$) is obtained from the cumulant $\text{cum}\left\{x_m(l), x_{-m}^*(l), x_p^*(l), x_{-p}(l)\right\}$, where x represents the received signal, and $p = -M, -M+1, \ldots, M$ [77], [78]. The second matrix (i.e. $\mathbf{C}_2$) is obtained by combining the information of the following four cumulants [77]:

$$\text{cum}\left\{x_m(l), x_M^*(l), x_p^*(l), x_M(l)\right\}, \tag{34}$$

$$\text{cum}\left\{x_m(l), x_M^*(l), x_M^*(l), x_q(l)\right\}, \tag{35}$$

$$\text{cum}\left\{x_M(l), x_n^*(l), x_p^*(l), x_M(l)\right\}, \tag{36}$$

$$\text{cum}\left\{x_M(l), x_n^*(l), x_M^*(l), x_q(l)\right\}, \tag{37}$$

where $q = M-1, M-2, \ldots, -M$ and $n = M-1, M-2, \ldots, -M$. In this way, the virtual steering vector $\mathbf{d}(\gamma_k, \chi_k)$ is separated into two parts $\mathbf{d}_1(\gamma_k)$ and $\mathbf{d}_2(\chi_k)$. The first part is a function of the electric angle common in both the FF and NF signal models, and the second part is a function of the electric angle that exists only in the NS model. The DOA of all sources is obtained using the MUSIC algorithm, in which the search interval of the azimuth angle parameter is divided into uniform steps of size Δ_θ in degrees. Then, by substituting the estimated common electric angle $\hat{\gamma}_k$ into a specific Hermitian matrix [77] formed from another MUSIC spectrum function, the range of NFSs is obtained from the eigenvector of the Hermitian matrix as follows [77]:

$$\hat{\chi}_k = \min_{\chi} \mathbf{d}_2^H(\chi)\, \mathbf{d}_1^H\left(\hat{\gamma}_k\right) \bar{\mathbf{U}}_\text{n} \bar{\mathbf{U}}_\text{n}^H \mathbf{d}_1\left(\hat{\gamma}_k\right) \mathbf{d}_2(\chi), \tag{38}$$

where $\bar{\mathbf{U}}_\text{n}$ contains the eigenvectors of the noise subspace of the cumulant matrix $\mathbf{C}_2$. Although the parameters of the mixed sources are successfully estimated by the TSMUSIC algorithm, due to the construction of high-order cumulant (HOC) matrices along with the spectral search operation and the application of several eigendecomposition operations, its computational complexity is very high [79], [80].

To reduce the computational burden, an algorithm called oblique projection MUSIC (OPMUSIC) was presented in [81] for the localization and classification of narrowband mixed FFSs and NFSs. The FF MUSIC estimator $F(\theta)$ and the NF MUSIC estimator $F(\varpi)$ are constructed to separately extract FF and NF angles, where $\varpi \triangleq 2\gamma$ [81]. The FF estimator is calculated from the following equation [81]:

$$F(\theta) = \left[\mathbf{a}_\text{N}^H(\theta, \infty)\, \mathbf{E}_\text{n} \mathbf{E}_\text{n}^H \mathbf{a}_\text{N}(\theta, \infty)\right]^{-1}, \tag{39}$$

where $\mathbf{a}_\text{N}$ represents the NF steering vector and $\mathbf{E}_\text{n}$ is the noise subspace matrix resulting from the eigendecomposition of the covariance matrix of the array ($\mathbf{R} = \mathbb{E}\left\{\mathbf{x}(l)\, \mathbf{x}^H(l)\right\}$) [29], [81]. The NF MUSIC estimator $F(\varpi)$ is built based on the symmetry property of the array geometry (as shown in Fig. 2) and the extraction of the spectral signature of the signal, which is only dependent on the DOA of the sources. The oblique projection technique is used to separate NFSs from FFSs [81]. The range NFSs are obtained by performing K_N 1-D searches, in which the range parameter search interval in the NF region is divided into uniform steps of size Δ_r in wavelength. The OPMUSIC method uses only second-order statistics (SOS) and does not need a multidimensional search. However, this algorithm suffers from a severe loss of array aperture [50], [82]. In fact, due to the creation of overlapping subvectors, it faces a fifty percent array aperture loss, and the maximum number of resolvable sources is equal to $(N-1)/2$.

In [83], an ESPRIT-like algorithm was developed for the problem of localization of mixed cyclostationary sources [84] using a SULA. This algorithm is based on the third-order cyclic moment [85]. By it, the NF direction and range parameters are automatically paired. The algorithm first constructs two special third-order cyclic moment matrices, where the rotational factor is a function of DOA and range of sources. The DOAs of the sources are estimated by performing singular value decomposition (SVD) [86] to a matrix merged from these matrices and MUSIC spectral search. Despite the relatively low computational complexity of this method, the array aperture loss and low range estimation accuracy are two limitations of this method.

The authors of the study [87], by using a symmetric sparse linear array (SLA), extended the array aperture. By exploiting the special geometry of the array and the construction of a cumulant matrix, the DOAs of the FFSs and NFSs are estimated using the MUSIC technique. With the estimated DOAs and covariance matrix of the sparse array, FF and NF sources are identified, and the range parameter of NFSs is obtained by defining the range spectrum. Compared to the previous algorithms, research [87] has moderate computational complexity and better resolution and has improved the accuracy of parameter estimation, but its range estimation suffers from the problem of spurious peaks [29], [88].

Based on the generalized ESPRIT (GESPRIT) algorithm [89], [90], several methods for the localization of mixed sources have been proposed [91], [92], [93], [94], which are reviewed below.

In the study [91], first, the steering vectors of two subarrays are combined to eliminate the range parameter to create a new steering vector. This steering vector only contains DOA information. Then, based on the polynomial rooting and ESPRIT-like methods [95], [96], the DOAs of all sources are obtained. Then, with the estimated DOAs and using MUSIC, the range parameter is estimated. According to the number of roots close to the unit circle, the number of sources in the same direction can be determined. Finally, based on the size of the range parameters, the source type (NFS or FFS) can be determined. The algorithm [91] does not need high-order statistics (HOS) and spectral search, and as a result, it has a low computational cost. It is also able to determine the number of FFSs that have the same angle as the NFSs (denoted by K', where $0 \leq K' \leq K_{\mathrm{F}}$ and $0 \leq K' \leq K_{\mathrm{N}}$). However, this method uses a series of additional assumptions about the signal type, which limits the practical application of this method.

A method based on the SOS is given in [92]. To improve the estimation accuracy, after estimating the DOAs and power of the FSs, the components related to the FF are eliminated from the signal subspace. Then, based on the symmetry in the SULA geometry, an NF estimator is used without the need for 2-D search and parameter pairing. Compared to other methods based on SOS, the algorithm [92] has achieved a more logical classification of the types of signals. However, the technique of eliminating FF components in it leads to additional estimation errors.

The two-stage matrix differencing algorithm (TSMDA) [93], [94], facing the problem of localization of mixed sources, provides a reasonable classification of the source type. By exploiting the structural differences between the FF covariance matrix $\mathbf{R}_{\mathrm{F}}$ (Toeplitz structure) and the NF covariance matrix $\mathbf{R}_{\mathrm{N}}$ (non-Toeplitz structure), the spatial differencing method is used to classify the type of signals and eliminate the FF components. As a result, the pure components of the NF can be found in the covariance difference matrix $\mathbf{R}_{\mathrm{D}}$ in the following form [93], [94]:

$$\mathbf{R}_{\mathrm{D}} = \mathbf{J}_N \Delta_{\mathbf{R}} \mathbf{J}_N = \mathbf{R}_{\mathrm{N}} - \mathbf{J}_N \mathbf{R}_{\mathrm{N}}^{*} \mathbf{J}_N, \tag{40}$$

where $\Delta_{\mathbf{R}} \triangleq \mathbf{J}_N \mathbf{R} \mathbf{J}_N - \mathbf{R}^T$, and according to the properties of the Toeplitz structure [97], it can be written $\mathbf{R}_{\mathrm{F}}^T = \mathbf{J}_N \mathbf{R}_{\mathrm{F}} \mathbf{J}_N$, and as a result, $\Delta_{\mathbf{R}} = \mathbf{J}_N \mathbf{R}_{\mathrm{N}} \mathbf{J}_N - \mathbf{R}_{\mathrm{N}}^T$. NF DOA and range estimators based on a hybrid ESPRIT-like and MUSIC-like method are implemented by taking advantage of the symmetry feature in the SULA geometry, without the need for parameter pairing. After the localization of NFSs, the covariance matrix of the FF information is reconstructed as follows [93], [94]:

$$\hat{\mathbf{R}}_{\mathrm{F}} = \mathbf{U}_{\mathrm{s}} \left(\Delta_{\mathrm{s}} - \hat{\sigma}^2 \mathbf{I}_N \right) \mathbf{U}_{\mathrm{s}}^H - \hat{\mathbf{R}}_{\mathrm{N}}, \tag{41}$$

where Δ_{s} and $\mathbf{U}_{\mathrm{s}}$ include the eigenvalues and eigenvectors of the signal subspace of $\mathbf{R}$, respectively. In fact, after estimating the power of the NSs, the NF components can be eliminated from the signal subspace, and the DOAs of the FFSs can be estimated by finding the peaks of the following spectral function [93], [94]:

$$f\left(\bar{\gamma}\right) = \left[\mathbf{a}_{\mathrm{F}}^H\left(\gamma\right) \tilde{\mathbf{U}}_{\mathrm{n}} \tilde{\mathbf{U}}_{\mathrm{n}}^H \mathbf{a}_{\mathrm{F}}\left(\gamma\right) \right]^{-1}, \tag{42}$$

where $\mathbf{a}_{\mathrm{F}}$ and $\tilde{\mathbf{U}}_{\mathrm{n}}$ represent the steering vector and noise subspace of $\hat{\mathbf{R}}_{\mathrm{F}}$, respectively, and $\bar{\gamma}$ denotes the electric angle of the FFSs. TSMDA has better resolution than the method [81]. However, the low accuracy of estimation due to the remaining effects of other components in the differencing operation and the need to know the number of NFSs are the most important drawbacks of TSMDA [56], [98].

It is worth mentioning that for GESPRIT-based algorithms [91], [92], [93], [94], the number of NFSs they can resolve is less than half of the number of array sensors [98], [99].

In [100], [101], and [102], the authors use the sparse signal reconstruction method for the passive localization of mixed sources. Algorithms [100] and [101] are based on the construction of FOC matrices and vectors, while in [102], the anti-diagonal elements of the second-order covariance matrix of the array are employed.

In the work [100], the DOAs of all sources are estimated by constructing an array cumulant domain data that is only related to the DOA parameter of the mixed sources. Then the range parameter is estimated and the FFSs are separated from the mixed sources. Unlike many algorithms that consider only the NF region for range estimation or source classification, in the approach [100], a range grids set with the number of N_{r} elements is also defined for FFSs. Compared to the TSMUSIC algorithm, the method [100] provides better estimation accuracy.

In the study [101], two special cumulant vectors are constructed sequentially, the first to obtain the direction of all signals and the second to distinguish mixed sources as well as estimate the range of NFSs.

In the study [102], by constructing the data from the SOS domain of the array, which is only related to the DOA parameter of the mixed sources, the DOA estimation of all sources is obtained by using weighted norm minimization concerning an overcomplete basis matrix with $\bar{K}$ columns, where in general $\bar{K} \gg K$ [103]. The weighted norm minimization problem is defined based on the division of the sparse signal representation framework into N_{L} overlapping subvectors, where $N_{\mathrm{L}} > K$. After that, the MUSIC spectral function is used to distinguish the mixed sources as well as find the more accurate DOA of the FFSs. Finally, based on the DOA estimation, the range parameter is estimated.

In general, algorithms based on sparse reconstruction [100], [101], [102] contain a huge amount of calculations. Moreover, it is difficult to determine the regulatory parameter that makes the trade-off between norms [50].

A method based on the construction of FOCs is presented in [104], which does not need to know the number of sources. In the first step, this method separates the DOA estimation from the range estimation by using the following cumulant with time lag ι [104]:

$$\text{cum}\left\{x_m\left(l-\iota\right),\, x_{-m}^{*}\left(l\right),\, x_p^{*}\left(l\right),\, x_{-p}\left(l\right)\right\}, \tag{43}$$

where $\iota = 1, 2, \ldots, \rho$ and ρ is the number of time lags. To obtain DOAs estimate of FFSs and NFSs, based on the structure of cumulant matrix $\mathbf{C}$ composed of spatial-temporal cumulant of (43), the 1-D spectral function $P\left(\theta\right)$ is extracted in the following form [104]:

$$P\left(\theta\right) = \left[N - \max\ \text{eig}\left(\mathbf{Q}^{H}\left(\theta\right)\mathbf{C}^{\dagger}\mathbf{Q}\left(\theta\right)\right)\right]^{-1}, \tag{44}$$

where $\mathbf{Q}$ is also made from spatial-temporal cumulant of (43) [104]. Then, the range parameter of NFSs is estimated based on the following MVDR beamformer [104]:

$$P_{\text{MVDR}}\left(\theta,\, r\right) = \left[\mathbf{a}^{H}\left(\theta,\, r\right)\mathbf{R}^{-1}\mathbf{a}\left(\theta,\, r\right)\right]^{-1}. \tag{45}$$

The method [104] requires the construction of many spatial-temporal cumulant matrices to improve the estimation accuracy. Along with that, the application of angle and range spectral search operations (based on MUSIC and MVDR techniques) greatly increases its computational complexity.

An algorithm based on polynomial decomposing and using FOC is presented in [51]. First, the SULA is divided into two subarrays with different phase reference points. Three FOC matrices $\bar{\mathbf{C}}_1$, $\bar{\mathbf{C}}_2$ and $\bar{\mathbf{C}}_3$ are formed by the following cumulants [51]:

$$\text{cum}\left\{x_{m'}\left(l\right),\, x_{-1-n'}\left(l\right),\, x_{-1-m'}^{*}\left(l\right),\, x_{n'}^{*}\left(l\right)\right\}, \tag{46}$$
$$\text{cum}\left\{x_{m''}\left(l\right),\, x_{1-n''}\left(l\right),\, x_{1-m''}^{*}\left(l\right),\, x_{n''}^{*}\left(l\right)\right\}, \tag{47}$$
$$\text{cum}\left\{x_{m'}\left(l\right),\, x_{1-n''}\left(l\right),\, x_{-1-m'}^{*}\left(l\right),\, x_{n''}^{*}\left(l\right)\right\}, \tag{48}$$

where $m' = -M, -M+1, \ldots, M-1, n' = -M, -M+1, \ldots, M-1, m'' = -M+1, -M+2, \ldots, M, n'' = -M+1, -M+2, \ldots, M$. Cumulant matrices are designed so that the range parameter of NFSs in steering vectors is omitted and only contain DOA information. By collecting the above three cumulant matrices in the form of a Hermite matrix $\begin{bmatrix}\mathbf{C}_1 & \mathbf{C}_3^{H}\\ \mathbf{C}_3 & \mathbf{C}_2\end{bmatrix}$ and based on an ESPRIT technique, the DOA of each source is estimated at the phase reference point. By having the DOA estimate, the coefficient matrix of the k-th source is formed in the following form [51]:

$$T_k = \begin{bmatrix}\sin\theta_{k,\,-d/2} & -\sin\theta_{k,\,d/2}\\ \cos\theta_{k,\,-d/2} & -\cos\theta_{k,\,d/2}\end{bmatrix}, \tag{49}$$

where $\theta_{k,\,-d/2}$ and $\theta_{k,\,d/2}$ are defined as the DOAs of the k-th source at two different center points. Sources are classified according to determinant of T_k. Finally, the range of NFSs is obtained. Despite the low computational complexity and preventing aperture loss, the classification mechanism in this method requires setting a threshold that may change in each experiment [56]. This makes the practical application of the algorithm difficult. In addition, this method suffers from low accuracy in DOA estimation [56].

A method based on SOS is presented in [105] to estimate the parameters of DOA, range and frequency of sources, which avoids multi-dimensional spectral search.

An algorithm named mixed-order statistics (MOS) has been developed using the combination of SOS and FOS [106], which provides a reasonable classification of signals. However, it imposes strict limits on the DOA intervals of incoming signals [56].

In the study [107], a method of mixed-order statistics [108] based on the reconstruction of the cumulant matrix and the use of the MUSIC spectrum is presented, which provides good estimation accuracy.

Most of the methods reviewed above require heavy computations related to spectral search. In addition, some of them, due to the combined use of spectral search and FOS, have an extra processing volume. On the other hand, the relatively severe loss of aperture, which can be seen in some of them, is another issue that should be considered in employing a sufficient number of sensors. Since in the case of NFSs, in addition to estimating the angle and range parameters, pairing between these two parameters should also be done, even in some ESPRIT-based methods such as [109] and [110], an additional process is required to pair these two parameters. The differencing operations presented in [93] and [94] are only valid for SOS, and as shown in [111], for methods based on FOS, the Toeplitz property used in them to separate the FF and NF components will no longer be effective.

In [111], a method called high-order differencing algorithm (HODA) is presented, which in addition to the effective separation of FF and NF components in the field of HOS, estimates the location of NFSs and FFSs without the need for complex spectral searches, the pairing process and the sharp aperture loss. The use of HOS, in addition to increasing the accuracy of estimation, also enables saving the number of sensors [112]. In addition, the FOC is not sensitive to Gaussian noise types [113]. Some advantages of HODA are:

- It does not require heavy searches.
- The parameter pairing operation is performed automatically and does not require an additional process.
- It has low aperture loss compared to similar works.
- It is the first research that provides a technique for performing spatial differencing operations in the field of HOS.
- In addition to the main parameters, it also provides an estimate of the frequencies and kurtosis [114] of the sources.

The block diagram of HODA is given in Fig. 4. The matrices $\mathbf{C}_1$, $\mathbf{C}_2$, $\mathbf{C}_3$, $\mathbf{C}_4$ and $\mathbf{C}_5$ are respectively constructed from the following five cross-cumulant functions from the array output stationary signals with different sensor lags [111]:

$$\text{cum}\left\{x_{u+1}^{*}\left(l\right), x_{u+2}\left(l\right), x_{v+2}^{*}\left(l\right), x_{v+1}\left(l\right)\right\}, \tag{50}$$
$$\text{cum}\left\{x_{u+1}^{*}\left(l\right), x_{u+2}\left(l\right), x_{v+1}^{*}\left(l\right), x_{v}\left(l\right)\right\}, \tag{51}$$

$$\text{cum}\left\{x_u^*(l), x_{u+1}(l), x_{M-v}^*(l), x_{M+1-v}(l)\right\}, \quad (52)$$

$$\text{cum}\left\{x_{u+1}^*(l), x_{u+2}(l), x_{M-v}^*(l), x_{M+1-v}(l)\right\}, \quad (53)$$

$$\text{cum}\left\{x_{-p}^*(l), x_{-m}(l), x_m^*(l), x_p(l)\right\}, \quad (54)$$

where $u = -M, -M+1, \ldots, M-2$ and $v = -M, -M+1, \ldots, M-2$. The *angle estimation matrix* $\mathbf{C}_\text{A}$ is formed as follows [111]:

$$\mathbf{C}_\text{A} \triangleq \mathbf{C}_{51}^\dagger \mathbf{C}_{52}, \quad (55)$$

where $\mathbf{C}_{51}$ and $\mathbf{C}_{52}$ consist of $2M$ first row and $2M$ last row of $\mathbf{C}_5$, respectively. By applying the eigenvalue decomposition (EVD) to $\mathbf{C}_\text{A}$, one can write [111]

$$\mathbf{C}_\text{A} = \tilde{\mathbf{U}}\Sigma\tilde{\mathbf{U}}^{-1}, \quad (56)$$

where $\Sigma = \text{diag}\left[\sigma_1\ \sigma_2\ \ldots\ \sigma_N\right]$ is a diagonal matrix with ordered eigenvalues $|\sigma_1| \geq |\sigma_2| \geq \ldots \geq |\sigma_K| > |\sigma_{K+1}| > \ldots > |\sigma_N|$ and part of $\mathbf{U} \in \mathbb{C}^{N\times N}$ contains K eigenvectors corresponding to eigenvalues $\sigma_1, \sigma_2, \ldots, \sigma_K$, spanning the signal subspace of the matrix $\mathbf{C}_\text{A}$. The DOA of k-the signal can be extracted from the following equation [111]:

$$\hat{\theta}_k = \arcsin\left(\frac{\lambda \angle\sigma_k}{4\pi d}\right), \quad (57)$$

where $\sigma_k = e^{-j2\hat{\gamma}_k}$. Also, the appropriate number of snapshots (L_P) to use in HODA is obtained from the following formula [111]:

$$L_\text{P} = L - \text{rem}\left(L, f_\text{s} \times \text{LCM}\left(\left[\frac{1}{\hat{f}_1}\right], \left[\frac{1}{\hat{f}_2}\right], \ldots, \left[\frac{1}{\hat{f}_K}\right]\right)\right), \quad (58)$$

where f_s is the sampling frequency, and f_k represents the linear frequency of the k-th signal. The frequencies of the signals are estimated by extracting the pseudospectrum using the MUSIC approach with frequency search step Δ_f in Hz [115], [116].

The vast majority of methods for the problem of parameters estimation in mixed scenarios use MUSIC-like approaches completely or in stages. Although MUSIC-based approaches have been studied more and have advantages (including in hardware implementation) [117], [118], in ESPRIT-based approaches, the search step on the parameter space, which is inherent in all MUSIC, ML, and maximum entropy techniques, is omitted. In addition to the lower computational load, the storage cost is also lower in them and they are more robust against calibration errors [98], [112], [119]. In ASP, it has been more common to use only spatial information [120], [121]. However, when the DOAs of the signals are close to each other, the sources cannot be satisfactorily resolved by spatial information alone. By exploiting spatial and temporal features, the resolution and accuracy of estimation can be improved [122], [123]. Presented in [98] is an all-ESPRIT method called the high-order spatial-temporal algorithm (HOSTA). In this algorithm, by constructing special spatio-temporal cumulant matrices, it is possible to localize NFSs and FFSs with good accuracy, high resolution, relatively small computational volume and without the need for any spectral search and pairing process. In addition, it is able to perform the estimation of NFS and FFS parameters with the same angle well. In summary, some of the key features of HOSTA are:

- It is all-ESPRIT and does not require any spectrum search.
- The parameter pairing operation is performed automatically and does not require an additional process.
- It has a low aperture loss compared to similar works.
- It is possible to estimate NFS and FFS parameters that are at the same angle with good accuracy.
- Unlike some methods, it does not suffer from errors caused by statistical differencing.

The block diagram of HOSTA is given in Fig. 5. The sensor complex cross-cumulant matrices $\mathbf{C}_1^\iota$ and $\mathbf{C}_2$ are constructed from two cumulants obtained from the array output stationary signals with a time lag ι and different sensor lags in the following form [98]:

$$\text{cum}\left\{x_0^*(l), x_0(l), x_p^*(l), x_m(l+\iota)\right\}, \quad (59)$$

$$\text{cum}\left\{x_{-p}^*(l), x_{-m}(l), x_m^*(l), x_p(l)\right\}, \quad (60)$$

where $\iota = il_\text{s}$, l_s is the sampling interval from signal $x_m(l)$, $i = 0, 1, \ldots, \rho$. $\tilde{\mathbf{C}}_2$ is reconstructed from $\mathbf{C}_2$ so that its rank is equal to the known value of K. This is called the rank-matching operation [50], [98]. Assuming that $\mathbf{U} = \left[\mathbf{u}_1\ \mathbf{u}_2\ \ldots\ \mathbf{u}_N\right] \in \mathbb{C}^{N\times N}$ is the left singular vector of $\mathbf{C}_2$, $\mathbf{V} = \left[\mathbf{v}_1\ \mathbf{v}_2\ \ldots\ \mathbf{v}_N\right] \in \mathbb{C}^{N\times N}$ is its right singular vector, and $\Sigma = \text{diag}\left[\sigma_1\ \sigma_2\ \ldots\ \sigma_N\right] \in \mathbb{R}^{N\times N}$ is its singular values (where $\sigma_1 \geq \sigma_2 \geq \ldots \geq \sigma_N$), the reconstructed matrix $\tilde{\mathbf{C}}_2$ can be formed in the following form [98]:

$$\tilde{\mathbf{C}}_2 = \mathbf{U}'\Sigma'\mathbf{V}'^H, \quad (61)$$

where $\mathbf{U}' = \left[\mathbf{u}_1\ \mathbf{u}_2\ \ldots\ \mathbf{u}_K\right] \in \mathbb{C}^{N\times K}$, $\mathbf{V}' = \left[\mathbf{v}_1\ \mathbf{v}_2\ \ldots\ \mathbf{v}_K\right] \in \mathbb{C}^{N\times K}$ and $\Sigma' = \text{diag}\left[\sigma_1\ \sigma_2\ \ldots\ \sigma_K\right] \in \mathbb{R}^{K\times K}$. The *angle estimation matrix* $\mathbf{C}_\text{A}$ is formed as follows [98]:

$$\mathbf{C}_\text{A} \triangleq \mathbf{C}_{21}^\dagger \mathbf{C}_{22}, \quad (62)$$

where $\mathbf{C}_{21}$ and $\mathbf{C}_{22}$ are created from $2M$ first row and $2M$ last row of Hermitian matrix $\tilde{\mathbf{C}}_2$, respectively. The matrix $\mathbf{C}_1^{\iota,\iota'} \in \mathbb{C}^{N\times N}$ C is defined as follows [98]:

$$\mathbf{C}_1^{\iota,\iota'} \triangleq \mathbf{C}_1^\iota \mathbf{C}_1^{\iota'\dagger}, \quad (63)$$

where $\iota \in \{l_\text{s}, 2l_\text{s}, \ldots, \rho l_\text{s}\}$, $\iota' \in \{\iota - l_\text{s}, \iota - 2l_\text{s}, \ldots, \iota - \rho l_\text{s}\}$ and $\rho \geq 1$. The rank-matching operation [50], [98] is also applied to $\mathbf{C}_1^\iota$ and $\mathbf{C}_1^{\iota'}$ so that the rank of the corresponding reconstructed matrices $\mathbf{D}_1^\iota$ and $\mathbf{D}_1^{\iota'\dagger}$ is equal to K. The *parameter estimation matrix* $\mathbf{D}_1^{\iota,\iota'} \in \mathbb{C}^{N\times N}$ is obtained in the following form [98]:

$$\mathbf{D}_1^{\iota,\iota'} \triangleq \mathbf{D}_1^\iota \mathbf{D}_1^{\iota'\dagger}. \quad (64)$$

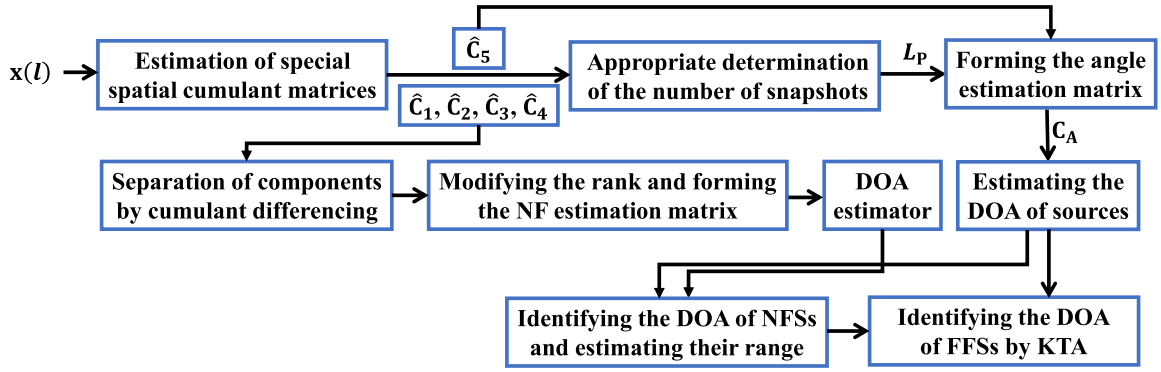

FIGURE 4. HODA block diagram.

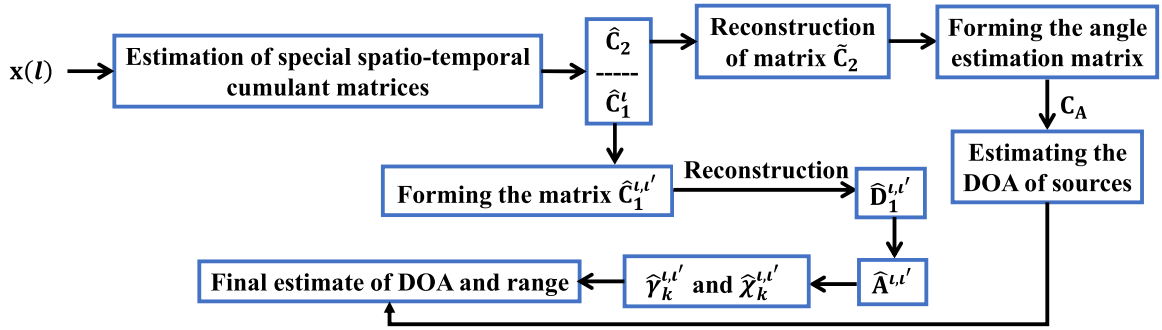

FIGURE 5. HOSTA block diagram.

$\hat{\mathbf{A}}^{\iota,\iota'}$ is an estimate of $\mathbf{A}$ that is obtained by exploiting the cumulant matrices $\mathbf{C}_1^{\iota}$ and $\mathbf{C}_1^{\iota'}$ [98].

HOSTA does not have any restrictions on the type of signal field; in other words, even all sources can be pure NF or pure FF. Whereas in HODA, the maximum number of NFSs that can be estimated is less than half the number of array elements.

The paper [124] introduces an NF interference mitigation (NFIM) beamformer to address challenges in passive sonar arrays caused by NF interferences masking FFSs. The proposed beamformer utilizes N_v configurable subarrays and an azimuth-domain filter to separate FFS beams from NF interferences without source constraints. Computer simulations demonstrate that the NFIM beamformer improves DOA estimation performance compared to conventional methods by effectively mitigating interferences.

In studies [125], [126], techniques based on orthogonal projection have been presented to deal with 2-D DOA estimation of mixed sources using UCA. In [125], the differencing matrix and the orthogonal projection matrix of the signal subspace are constructed to classify signals and estimate 2-D DOAs. Then, the covariance matrix of the signals is decomposed to obtain the noise subspace. In [126], cumulant matrices are employed to estimate 2-D DOAs using the orthogonal projection matrix of the signal subspace and obtain the noise subspace using eigendecomposition. In these studies, spatial SOS and FOS are used, respectively. Both methods, like those of [127] and [128], require very complex multidimensional searches, which can seriously hamper their performance in real-time applications. In addition, the methods [125], [126] suffer from estimation error due to spatial differencing.

In the approach [54] called the fourth-order spatio-temporal algorithm (FOSA), by constructing two spatial-temporal cumulant matrices, without range information, and considering the fourth-order stationarity property, the 2-D DOA estimation matrix is extracted. By using EVD, a virtual steering matrix is estimated. During the implementation process, a rank-matching mechanism is used to improve accuracy. Then, the 2-D DOAs are estimated by the least-squares (LS) technique [129], [130]. The ranges of NFSs are estimated by constructing a spatial cumulant matrix and using the 1-D MUSIC technique. Spectral search is implemented in an interval beyond the Fresnel region, so that the positive factors $\zeta < 1$ and $\beta > 1$ are multiplied by the beginning and the end of the Fresnel zone as interval expansion coefficients, respectively [54]. This approach provides a reasonable classification of the type of signals.

IV. SPECIAL TECHNICAL ISSUES AND CHALLENGES

In the previous section, the basic approaches to resolving the mixed-field sources problem were reviewed. However, they and similar approaches may face challenges in practice, including more complex assumptions/scenarios, or implementation limitations. In this section, special technical issues

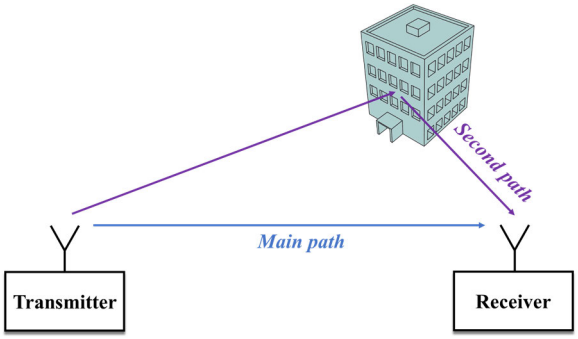

FIGURE 6. Interference due to multipath.

and challenges are discussed, and solutions/suggestions for future research are provided.

A. MULTIPATH ENVIRONMENT

In practical multi-path environments and some applications such as wireless communications and smart jammers, the received signals may be uncorrelated (independent), partially correlated, or coherent [60], [131], [132]. In the illustration in Fig. 6, an object (building) affects the received signal by adding a second path. The signal reaches the RX through two different paths that have different lengths. The main path is the direct path, while the second is caused by reflections from the building.

The problem of DOA estimation for all incoming signals to sensors (including uncorrelated, partially correlated and coherent signals [133], [134], [135]), in some practical scenarios of array processing where multipath propagation usually causes various returns (for example, multipath fading channel estimation [136], [137], processing of back-scattered acoustic signal [138], [139], spatially distributed signal [140], [141], etc.), is of great importance. Although error sources such as gain/phase mismatch and mutual coupling (MC) between antennas also affect the angle estimation accuracy, multipath distortion is the main source of gross errors in the results [142], [143], [144]. For more details about the effects of gain/phase mismatch and MC, refer to Section IV-E and [145], [146].

Conventional DOA estimation algorithms were initially developed with the assumption that the received signals are uncorrelated; that is, there is no signal due to multipath propagation [147]. But in real environments, signals received from a target/source/user may experience reflection, resulting in multiple return signals, which are actually phase-delayed along with amplitude-weighted replicas of the direct signal [148], [149]. Consequently, these signals are coherent [149], [150]. Coherent signals decrease the rank of spatial statistics matrices, and as a result, conventional algorithms do not perform well in the presence of multipath propagation [56], [151]. Also, the inability to distinguish uncorrelated signals from coherent signals leads to the waste of a significant number of sensors [60], [152].

Now let us describe the data model for a mixed-field sources scenario in multipath environments [153]. Consider

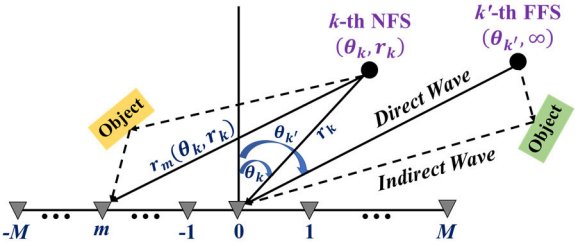

FIGURE 7. A SULA consisting of $N = 2M + 1$ sensors in a mixed sources scenario in a multipath environment.

a SULA consisting of $N = 2M + 1$ isotropic sensors (Fig. 7), which receives K narrowband signals, consisting of a mixture of K_{n} noncoherent signals (including K_{nN} uncorrelated or partially correlated NSs, and K_{nF} uncorrelated or partially correlated FSs), and K_{c} coherent signals (including K_{cN} NSs in G_{N} groups and K_{cF} FSs in G_{F} groups). With a proper sampling rate, the l-th sample of the signal observed by the m-th sensor can be written in the following form [54], [56]:

$$\begin{aligned} x_m(l) = &\sum_{k=1}^{K_{nN}} s_k(l)\, a_m(\theta_k, r_k) + \sum_{k=K_{nN}+1}^{K_n} s_k(l)\, a_m(\theta_k) \\ &+ \sum_{g=1}^{G_N}\sum_{\mu=1}^{P_g} \alpha_{g,\mu} s_{K_n+g}(l)\, a_m\left(\theta_{K_n+g,\mu}, r_{K_n+g,\mu}\right) \\ &+ \sum_{g=G_N+1}^{G}\sum_{\mu=1}^{P_g} \alpha_{g,\mu} s_{K_n+g}(l)\, a_m\left(\theta_{K_n+g,\mu}\right) + n_m(l). \end{aligned} \tag{65}$$

$a_m(\theta, r)$ and $a_m(\theta)$ are the m-th element of the steering vector of NFSs ($\mathbf{a}(\theta, r) \in \mathbb{C}^{N\times 1}$) and steering vector of FFSs ($\mathbf{a}(\theta) \in \mathbb{C}^{N\times 1}$), respectively. $\alpha_{g,\mu}$ and P_g respectively represent the complex fading coefficient (FC) corresponding to the μ-th signal from the g-th coherent group, and the number of coherent signals in the g-th group, such that $P_1 + P_1 + \ldots + P_{G_{\mathrm{N}}} = K_{\mathrm{cN}}$ and $P_{G_{\mathrm{N}}+1} + P_{G_{\mathrm{N}}+2} + \ldots + P_G = K_{\mathrm{cF}}$.

In matrix form, the array output can be expressed as follows [56], [154]:

$$\begin{aligned} \mathbf{x}(l) = &\mathbf{A}_{\mathrm{nN}}\mathbf{s}_{\mathrm{nN}}(l) + \mathbf{A}_{\mathrm{nF}}\mathbf{s}_{\mathrm{nF}}(l) + \mathbf{A}_{\mathrm{cN}}\boldsymbol{\Gamma}_{\mathrm{N}}\mathbf{s}_{\mathrm{cN}}(l) \\ &+ \mathbf{A}_{\mathrm{cF}}\boldsymbol{\Gamma}_{\mathrm{F}}\mathbf{s}_{\mathrm{cF}}(l) + \mathbf{n}(l) = \mathbf{A}\boldsymbol{\Gamma}\mathbf{s}(l) + \mathbf{n}(l), \end{aligned} \tag{66}$$

where $\mathbf{x}(l) \in \mathbb{C}^{N\times 1}$ and [56], [154]

$$\begin{aligned} \mathbf{A} = &\left[\mathbf{A}_{\mathrm{nN}}\ \mathbf{A}_{\mathrm{nF}}\ \mathbf{A}_{K_{\mathrm{n}}+1}\ \mathbf{A}_{K_{\mathrm{n}}+2}\ \ldots\ \mathbf{A}_{K_{\mathrm{n}}+G_{\mathrm{N}}}\right. \\ &\left.\mathbf{A}_{K_{\mathrm{n}}+G_{\mathrm{N}}+1}\ \mathbf{A}_{K_{\mathrm{n}}+G_{\mathrm{N}}+2}\ \ldots\ \mathbf{A}_{K_{\mathrm{n}}+G_{\mathrm{N}}}\right] \in \mathbb{C}^{N\times K}, \end{aligned} \tag{67}$$

$$\mathbf{A}_{\mathrm{nN}} = \left[\mathbf{a}(\theta_1, r_1)\ \mathbf{a}(\theta_2, r_2)\ \ldots\ \mathbf{a}\left(\theta_{K_{\mathrm{nN}}}, r_{K_{\mathrm{nN}}}\right)\right] \in \mathbb{C}^{N\times K_{\mathrm{nN}}}, \tag{68}$$

$$\mathbf{A}_{\mathrm{nF}} = \left[\mathbf{a}\left(\theta_{K_{\mathrm{nN}}+1}\right)\ \mathbf{a}\left(\theta_{K_{\mathrm{nN}}+2}\right)\ \ldots\ \mathbf{a}\left(\theta_{K_{\mathrm{n}}}\right)\right] \in \mathbb{C}^{N\times K_{\mathrm{nF}}}, \tag{69}$$

$$\begin{aligned} \mathbf{A}_{K_{\mathrm{n}}+g} = &\left[\mathbf{a}\left(\theta_{K_{\mathrm{n}}+g,1}, r_{K_{\mathrm{n}}+g,1}\right)\ \mathbf{a}\left(\theta_{K_{\mathrm{n}}+g,2}, r_{K_{\mathrm{n}}+g,2}\right)\right. \\ &\left.\ldots\ \mathbf{a}\left(\theta_{K_{\mathrm{n}}+g,P_g}, r_{K_{\mathrm{n}}+g,P_g}\right)\right] \in \mathbb{C}^{N\times P_g}, \end{aligned} \tag{70}$$

$$\mathbf{A}_{K_{\mathrm{n}}+g'} = \left[\mathbf{a}\left(\theta_{K_{\mathrm{n}}+g',1}\right)\ \mathbf{a}\left(\theta_{K_{\mathrm{n}}+g',2}\right)\ \ldots\ \mathbf{a}\left(\theta_{K_{\mathrm{n}}+g',P_{g'}}\right)\right] \in \mathbb{C}^{N\times P_{g'}}, \tag{71}$$

$$\mathbf{s}(l) = \left[\mathbf{s}_{\mathrm{nN}}^T(l)\ \mathbf{s}_{\mathrm{nF}}^T(l)\ \mathbf{s}_{\mathrm{cN}}^T(l)\ \mathbf{s}_{\mathrm{cF}}^T(l)\right]^T \in \mathbb{C}^{(K_{\mathrm{n}}+G)\times 1}, \tag{72}$$

$$\mathbf{s}_{\mathrm{nN}}(l) = \left[s_1(l)\ s_2(l)\ \ldots\ s_{K_{\mathrm{nN}}}(l)\right]^T \in \mathbb{C}^{K_{\mathrm{nN}}\times 1}, \tag{73}$$

$$\mathbf{s}_{\mathrm{nF}}(l) = \left[s_{K_{\mathrm{nN}}+1}(l)\ s_{K_{\mathrm{nN}}+2}(l)\ \ldots\ s_{K_{\mathrm{n}}}(l)\right]^T \in \mathbb{C}^{K_{\mathrm{nF}}\times 1}, \tag{74}$$

$$\mathbf{s}_{\mathrm{cN}}(l) = \left[s_{K_{\mathrm{n}}+1}(l)\ s_{K_{\mathrm{n}}+2}(l)\ \ldots\ s_{K_{\mathrm{n}}+G_{\mathrm{N}}}(l)\right]^T \in \mathbb{C}^{G_{\mathrm{N}}\times 1}, \tag{75}$$

$$\mathbf{s}_{\mathrm{cF}}(l) = \left[s_{K_{\mathrm{n}}+G_{\mathrm{N}}+1}(l)\ s_{K_{\mathrm{n}}+G_{\mathrm{N}}+2}(l)\ \ldots\ s_{K_{\mathrm{n}}+G}(l)\right]^T \in \mathbb{C}^{G_{\mathrm{F}}\times 1}, \tag{76}$$

$$\mathbf{\Gamma} = \mathrm{blkdiag}\left[\mathbf{I}_{K_{\mathrm{n}}}\ \mathbf{\Gamma}_{\mathrm{c}}\right] \in \mathbb{C}^{K\times(K_{\mathrm{n}}+G)}, \tag{77}$$

$$\mathbf{\Gamma}_{\mathrm{c}} = \mathrm{blkdiag}\left[\boldsymbol{\alpha}_1\ \boldsymbol{\alpha}_2\ \ldots\ \boldsymbol{\alpha}_G\right] \in \mathbb{C}^{K_{\mathrm{c}}\times G}, \tag{78}$$

$$\mathbf{n}(l) = \left[n_{-M}(l)\ n_{-M+1}(l)\ \ldots\ n_M(l)\right]^T \in \mathbb{C}^{N\times 1}, \tag{79}$$

where $g = 1, 2, \ldots, G_{\mathrm{N}}$ and $g' = G_{\mathrm{N}}+1, G_{\mathrm{N}}+2, \ldots, G$. In the above equations, $\mathbf{s}_{\mathrm{nN}}(l)$, $\mathbf{s}_{\mathrm{nN}}(l)$, $\mathbf{s}_{\mathrm{nN}}(l)$, and $\mathbf{s}_{\mathrm{nN}}(l)$ are the source vectors of NF noncoherent, FF noncoherent, NN coherent, and FF coherent signals, respectively. The matrix Γ_{c} contains information about the FCs, where $\boldsymbol{\alpha}_g = \left[1\ \alpha_{g,2}\ \alpha_{g,3}\ \ldots\ \alpha_{g,P_g}\right]^T \in \mathbb{C}^{P_g\times 1}$ and $\boldsymbol{\alpha}_{g'} = \left[1\ \alpha_{g',2}\ \alpha_{g',3}\ \ldots\ \alpha_{g',P_{g'}}\right]^T \in \mathbb{C}^{P_{g'}\times 1}$. According to Fresnel approximation [56], [155], one can write

$$\mathbf{a}(\theta_k, r_k) = \left[e^{j(-M\gamma_k+M^2\chi_k)}\ e^{j((-M+1)\gamma_k+(-M+1)^2\chi_k)} \ldots e^{j(M\gamma_k+M^2\chi_k)}\right]^T, \tag{80}$$

$$\mathbf{a}(\theta_k) = \left[e^{-jM\gamma_k}\ e^{j(-M+1)\gamma_k}\ \ldots\ e^{jM\gamma_k}\right]^T, \tag{81}$$

$$\mathbf{a}\left(\theta_{K_{\mathrm{n}}+g,\mu}, r_{K_{\mathrm{n}}+g,\mu}\right) = \left[e^{j(-M\gamma_{K_{\mathrm{n}}+g,\mu}+M^2\phi_{K_{\mathrm{n}}+g,\mu})}\ e^{j((-M+1)\gamma_{K_{\mathrm{n}}+g,\mu}+(-M+1)^2\phi_{K_{\mathrm{n}}+g,\mu})} \ldots e^{j(M\gamma_{K_{\mathrm{n}}+g,\mu}+M^2\phi_{K_{\mathrm{n}}+g,\mu})}\right]^T, \tag{82}$$

$$\mathbf{a}\left(\theta_{K_{\mathrm{n}}+g,\mu}\right) = \left[e^{-jM\gamma_{K_{\mathrm{n}}+g,\mu}}\ e^{j(-M+1)\gamma_{K_{\mathrm{n}}+g,\mu}}\ \ldots\ e^{jM\gamma_{K_{\mathrm{n}}+g,\mu}}\right]^T. \tag{83}$$

For the array in Fig. 3, the signal $x_m(l)$ in (65) takes the form below [69], [156]:

$$x_{m'}(l) = \sum_{k=1}^{K_{\mathrm{n}}} s_k(l)\, e^{j\frac{2\pi}{\lambda}\left(r_k - r_{m'}(\theta_k,\phi_k,r_k)\right)} + \sum_{g=1}^{G}\sum_{\mu=1}^{P_g} \alpha_{g,\mu} s_{K_{\mathrm{n}}+g}(l)\, e^{j\frac{2\pi}{\lambda}\left(r_{K_{\mathrm{n}}+g,\mu} - r_{m'}(\theta_{K_{\mathrm{n}}+g,\mu},\phi_{K_{\mathrm{n}}+g,\mu},r_{K_{\mathrm{n}}+g,\mu})\right)} + n_{m'}(l). \tag{84}$$

Since if the source is in the FF, for the range parameter, it is assumed that $r_k,\ r_{K_{\mathrm{n}}+g,\mu} \to \infty$, so according to (84) [69], [157],

$$x_{m'}(l) = \begin{cases} \sum_{k=1}^{K_{\mathrm{n}}} s_k(l) + \sum_{g=1}^{G}\sum_{\mu=1}^{P_g} \alpha_{g,\mu} s_{K_{\mathrm{n}}+g}(l) + n_{m'}(l), \\ m' = 0, \\ \sum_{k=1}^{K_{\mathrm{nN}}} s_k(l)\, e^{j\frac{2\pi R}{\lambda}\left(\eta_{m'}(\theta_k,\phi_k) - \frac{R}{2r_k}\left(1-\eta_{m'}^2(\theta_k,\phi_k)\right)\right)} \\ + \sum_{k=K_{\mathrm{nN}}+1}^{K_{\mathrm{n}}} s_k(l)\, e^{j\frac{2\pi R}{\lambda}\eta_{m'}(\theta_k,\phi_k)} \\ + \sum_{g=1}^{G_N}\sum_{\mu=1}^{P_g} \alpha_{g,\mu} s_{K_{\mathrm{n}}+g}(l) \times \\ e^{j\frac{2\pi R}{\lambda}\left(\eta_{m'}(\theta_{K_{\mathrm{n}}+g,\mu},\phi_{K_{\mathrm{n}}+g,\mu}) - \frac{R}{2r_i}\left(1-\eta_{m'}^2(\theta_{K_{\mathrm{n}}+g,\mu},\phi_{K_{\mathrm{n}}+g,\mu})\right)\right)} \\ + \sum_{g=G_{\mathrm{N}}+1}^{G}\sum_{\mu=1}^{P_g} \alpha_{g,\mu} s_{K_{\mathrm{n}}+g}(l) \\ e^{j\frac{2\pi R}{\lambda}\eta_{m'}(\phi_{K_{\mathrm{n}}+g,\mu},\theta_{K_{\mathrm{n}}+g,\mu})} + n_m(l), \\ m' = 1, 2, \ldots, M. \end{cases} \tag{85}$$

The array output in matrix form is similar to (66), where [69], [158]

$$\mathbf{A}_{\mathrm{nN}} = \left[\boldsymbol{\eta}_{\mathrm{N}}(\theta_1, \phi_1, r_1)\ \boldsymbol{\eta}_{\mathrm{N}}(\theta_2, \phi_2, r_2) \ldots \boldsymbol{\eta}_{\mathrm{N}}\left(\theta_{K_{\mathrm{nN}}}, \phi_{K_{\mathrm{nN}}}, r_{K_{\mathrm{nN}}}\right)\right], \tag{86}$$

$$\mathbf{A}_{\mathrm{nF}} = \left[\boldsymbol{\eta}_{\mathrm{F}}\left(\theta_{K_{\mathrm{nN}}+1}, \phi_{K_{\mathrm{nN}}+1}\right)\ \boldsymbol{\eta}_{\mathrm{F}}\left(\theta_{K_{\mathrm{nN}}+2}, \phi_{K_{\mathrm{nN}}+2}\right) \ldots \boldsymbol{\eta}_{\mathrm{F}}\left(\theta_{K_{\mathrm{n}}}, \phi_{K_{\mathrm{n}}}\right)\right], \tag{87}$$

$$\mathbf{A}_{K_{\mathrm{n}}+g} = \left[\boldsymbol{\eta}_{\mathrm{N}}\left(\theta_{K_{\mathrm{n}}+g,1}, \phi_{K_{\mathrm{n}}+g,1}, r_{K_{\mathrm{n}}+g,1}\right) \boldsymbol{\eta}_{\mathrm{N}}\left(\theta_{K_{\mathrm{n}}+g,2}, \phi_{K_{\mathrm{n}}+g,2}, r_{K_{\mathrm{n}}+g,2}\right) \ldots \boldsymbol{\eta}_{\mathrm{N}}\left(\theta_{K_{\mathrm{n}}+g,P_g}, \phi_{K_{\mathrm{n}}+g,P_g}, r_{K_{\mathrm{n}}+g,P_g}\right)\right], \tag{88}$$

$$\mathbf{A}_{K_{\mathrm{n}}+g'} = \left[\boldsymbol{\eta}_{\mathrm{F}}\left(\theta_{K_{\mathrm{n}}+g',1}, \phi_{K_{\mathrm{n}}+g',1}\right) \boldsymbol{\eta}_{\mathrm{F}}\left(\theta_{K_{\mathrm{n}}+g',2}, \phi_{K_{\mathrm{n}}+g',2}\right) \ldots \boldsymbol{\eta}_{\mathrm{F}}\left(\theta_{K_{\mathrm{n}}+g',P_{g'}}, \phi_{K_{\mathrm{n}}+g',P_{g'}}\right)\right], \tag{89}$$

$$\boldsymbol{\eta}_{\mathrm{N}}(\theta_k, \phi_k, r_k) = \left[1\ e^{j\frac{2\pi R}{\lambda}\left(\eta_1(\theta_k,\phi_k) - \frac{R}{2r_k}\left(1-\eta_1^2(\theta_k,\phi_k)\right)\right)} e^{j\frac{2\pi R}{\lambda}\left(\eta_2(\theta_k,\phi_k) - \frac{R}{2r_k}\left(1-\eta_2^2(\theta_k,\phi_k)\right)\right)} \ldots e^{j\frac{2\pi R}{\lambda}\left(\eta_M(\theta_k,\phi_k) - \frac{R}{2r_k}\left(1-\eta_M^2(\theta_k,\phi_k)\right)\right)}\right]^T, \tag{90}$$

$$\boldsymbol{\eta}_{\mathrm{F}}(\theta_k, \phi_k) = \left[1\ e^{j\frac{2\pi R}{\lambda}\eta_1(\theta_k,\phi_k)}\ e^{j\frac{2\pi R}{\lambda}\eta_2(\theta_k,\phi_k)} \ldots e^{j\frac{2\pi R}{\lambda}\eta_M(\theta_k,\phi_k)}\right]^T. \tag{91}$$

In [159] and [160], a two-step method for estimating the DOA of an FFS and localizing its NF multipath reflections is presented. In the first step, by using a calibration technique, the DOA of the FFS is estimated. In the second step, to remove the FF components and obtain the pure NF components, an NF to FF transformation is presented to estimate NF multipath signals. It exploits a UCA for 2-D DOA estimation and a virtual uniform linear array (ULA) structure for NF multipath localization. The approach presented in [159] and [160] is not able to resolve multiple sources and is applicable only in the presence of one FFS.

For the array in Fig. 7, a method called components separation algorithm (CSA) for localization of the mixed NF and FF multiple sources in multipath environments is presented in [56], which includes DOA estimation for FFSs and DOA and range estimations for NFSs. CSA is based on FOS, which, as mentioned earlier, increases the estimation accuracy, saves the number of sensors, and is insensitive to Gaussian noise types [112].

In summary, some key features of CSA are:

- It is the first algorithm that is presented for the problem of multiple mixed NFSs and FFFs that can resolve coherent signals.
- It does not require multidimensional searches.
- Designing a mechanism based on the integration of techniques of squaring, projection, array interpolation transform and spatial smoothing (SS) [161], [162] for the problem of mixed coherent signals is one of the innovations of problem solving.
- Due to the separation of noncoherent signals and coherent groups, and their separate resolve, it has low aperture loss.

In addition to the assumptions [A1] and [A3] in Section II-B, the following main assumptions are also considered for CSA:

[A5] Signals $\{s_k(l)\}_{k=1}^{K_n+G}$ are statistically independent, narrowband stationary processes.

[A6] The total number of sources (i.e. K_n+G) is known or properly estimated by conventional methods [72], [73], [74].

[A7] The multipath components due to FFSs are in the FF of the array and the multipath components due to NFSs are in the NF.

[A8] The DOAs of the signals are not the same.

The block diagram of CSA is given in Fig. 8, in which two cumulant matrices $\mathbf{C}_1$ and $\mathbf{C}_2$ are formed from the following cumulants, respectively, by using the array output stationary signals with different sensor lags [56]:

$$\text{cum}\left\{x_m^*(l), x_p(l), x_{-p}^*(l), x_{-m}(l)\right\}, \tag{92}$$

$$\text{cum}\left\{x_0^*(l), x_0(l), x_p^*(l), x_m(l)\right\}. \tag{93}$$

For decorrelation, the SS technique is applied to coherent estimation matrix, where the array is divided into N_u overlapping subarrays.

For the mixed sources scenario in multipath environments, the following are suggestions for future research in this area:

- As the results in [56] show, CSA has a poor performance in estimating coherent sources compared to noncoherent sources. One of the reasons for this is that the deviation of the estimate from the actual value in each step is transferred to the next step. Therefore, the percentage of error in the final estimates is higher than the estimates of the first stages. A solution could be to provide an algorithm that estimates the noncoherent and coherent signals independently as much as possible, instead of a hierarchical algorithm (such as CSA). For this purpose, the definition of special statistics matrices may help to achieve this. In addition, a more efficient technique, instead of using the array interpolation transform, can improve the parameter estimation of NF coherent signals.
- FCs provide multipath propagation characteristics. Therefore, by estimating them, the effect of multipath propagation can be removed, and the performance of DOA and range estimations can be improved [163], [164]. FCs can be extracted before DOA or range estimations and may be fruitful in purifying the information to estimate other parameters.
- The problem of estimating the parameters of mixed signals in multipath environments using 2-D arrays (to estimate the direction for both azimuth and elevation angles), can be presented and solved as a new scenario in future research.
- The use of radio-based simultaneous mapping and localization process [165], [166] and reconfigurable intelligent surface technology [167], [168] may provide efficient solutions for the complex assumptions of this subsection and more specific applications in this area.

B. CRAMÉR–RAO BOUND (CRB)

CRB is known as an important mathematical benchmark to achieve a reference for evaluating the efficiency of algorithms [169], [170]. CRB provides a lower bound on the variance (minimum variance) of unbiased estimators [171], [172]. CRB analyses in [155] and [173], for a linear array, assume that the set of radiation sources are all from FF and NF, respectively. Assuming the coexistence of FFS and NFS with linear array, stochastic CRBs have been presented in research [81]. Being uncorrelated of sources is the main assumption of all the above. The stochastic CRBs related to the problem mentioned in Section IV-A, for the linear array, are derived in [153].

Research [174] focuses on NF CRBs for planar arrays. As mentioned in Section II-B, among 2-D arrays, UCA is usually preferred. The CRB analyses in [175] and [176] assume that all signals impinging on the UCA are pure FF or pure NF, respectively. CRBs derived in the above references are not applicable to the localization problem of mixed NFSs and FFSs, including uncorrelated, partially correlated and coherent signals. The stochastic CRBs related to the above problem, corresponding to the data model presented

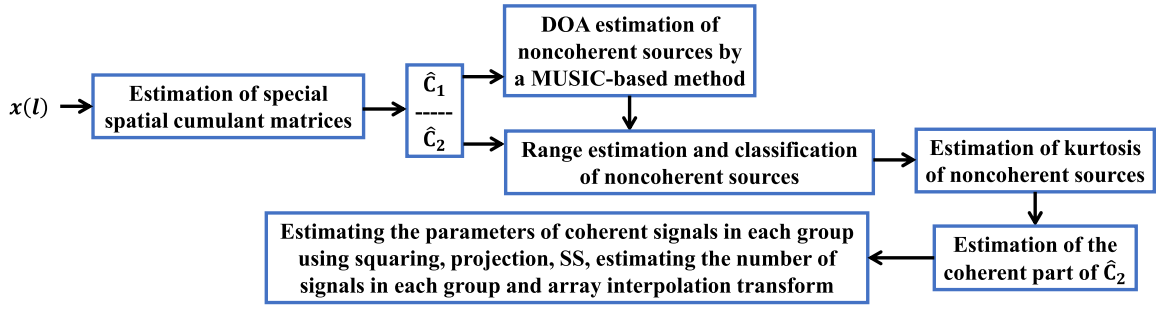

FIGURE 8. CSA block diagram.

in Section IV-A for the 2-D array, are derived as a compact closed-form expression in [69], which can be used as a benchmark to evaluate the accuracy of the estimation parameters of azimuth DOA, elevation DOA, and range, as well as complex FCs for the algorithms under the relevant scenario.

C. APPROXIMATE NEAR-FIELD MODEL

The approaches reviewed in the above sections use the NF approximation model [177], [178] to simplify the equations. The reviewed methods, by using the exact models in (8) and (26), definitely lose their effectiveness; because the basis of simplifying cumulants and the resulting equations from spatial statistics matrices is the use of (9) and (27).

More importantly, the studies [75], [179], [180] show that the standard array manifold models sometimes differ significantly from the model based on EM theory. In particular, it is shown that the standard models do not fit the equations governing the EM field near an antenna or an array. Also, linear prediction approaches do not take into account the characteristics of the NFS, such as the type and orientation of the transmitting antenna, which may have a profound effect on the signals received by the array. The mismatch between the highly idealized mathematical model and the actual array response raises concerns about the performance of conventional methods (both in resolving pure NFSs and in resolving mixed-field sources) with real arrays.

Unlike the majority of existing approaches that are based on the approximate model, in [181], [182], and [183], methods for NFSs localization are presented that consider the exact wavefront model. For the mixed sources scenario, there is a significant need for a comprehensive study of the errors caused by employing the approximate NF model, along with a solution to the problem when the exact model is considered [184].

D. WIDEBAND SIGNALS

A signal can be considered narrowband if [19], [185]

$$D/c \ll 1/B, \tag{94}$$

where D, c and B are the array length, speed of light and signal bandwidth, respectively. If the condition (94) is not satisfied, the signal is considered wideband and the measurement model in (15) cannot be applied. In this case, usually, first, the wide frequency band is decomposed into a set of narrow sub-bands [87], in each of which the condition of narrowband is fulfilled; so that the model (15) can be used. For example, if a wide frequency band is decomposed into I sub-bands, for each of them, (15) is applicable. Therefore, the wideband measurement model can be written in the following form [186], [187]:

$$\mathbf{x}_i(l) = \mathbf{A}(f_i)\,\mathbf{s}_i(l) + \mathbf{n}_i(l), \tag{95}$$

where $\mathbf{x}_i(l) \in \mathbb{C}^{N\times 1}$, $\mathbf{s}_i(l) \in \mathbb{C}^{K\times 1}$ and $\mathbf{n}_i(l) \in \mathbb{C}^{N\times 1}$ are respectively the measurement, signal and noise vectors in the l-th sample of the i-th sub-band. $\mathbf{A}(f_i)$ and f_i are the array steering matrix and frequency corresponding to the i-th sub-band, respectively. Therefore, the steering matrix of each sub-band is different, but the DOA of all sub-bands is the same.

In [188], the problem of localization of wideband sources in the NF of the sensor array has been addressed. Moreover, in [189], a two-step algorithm is developed to localize the mixed FF and NF acoustic sources using a N'-order spherical microphone array [190], [191] in a free-field environment. The algorithm proposed in [189] can localize multiple wideband mixed-field sources. Also, the proposed method presented in [192] works for FFSs in mixed wideband signals (FMW).

E. THE EFFECT OF ANTENNA MUTUAL COUPLING

MC between antennas reduces their efficiencies and thus the estimation accuracy [193], [194]. In fact, when such a phenomenon occurs, the voltage of each of the antennas is not only caused by the radiation wave, but the radiation signal also induces a current to the other elements of the array, which makes them act as secondary radiators and create an additional voltage on the adjacent elements [195], [196].

A simple way to solve this issue is to increase the distance between the elements, which leads to an increase in the physical area of the array. However, this solution not only conflicts with today's modern wireless communications [197], [198] but also adds the phase ambiguity problem to many algorithms presented in the mixed-field scenario. Obviously, the larger the aperture of the array, the higher the accuracy of

the results [199], [200]. On the other hand, the size of the aperture of the array is related to the number of array elements and the distance between adjacent array elements. Therefore, when the number of array elements and the distance between adjacent elements increases, the accuracy of the results also increases. However, according to the analysis of [29] and [98], for many algorithms in the mixed sources scenario, especially those that use FOS and even some algorithms that exploit SOS, when d (spacing between the array elements) is chosen larger than $\lambda/4$, although the accuracy increases, phase ambiguity occurs. Consider (56) and (57). The diagonal entries of Σ, i.e. $\sigma_k = e^{j4\pi d \sin\theta_k/\lambda}$, are the eigenvalues of $\mathbf{C}_{\mathrm{A}}$. Without placing any condition on d, a series of ambiguous DOA estimates are obtained as follows [29], [98]:

$$\theta_{k,z} = \arcsin\left(\nu_k + z\frac{\lambda}{2d}\right), \tag{96}$$

where $\nu_k = \lambda\angle\sigma_k/4\pi d$ and [29], [98]

$$\left\lceil \frac{2d}{\lambda}(-1-\nu_k)\right\rceil \le z \le \left\lfloor \frac{2d}{\lambda}(1-\nu_k)\right\rfloor. \tag{97}$$

For every θ_k and d, always $-\pi \le \angle\sigma_k \le \pi$. To avoid any cyclic ambiguity in $\angle\sigma_k$, it must be bounded to $0 \le \angle\sigma_k \le \pi$ and $-\pi \le \angle\sigma_k \le 0$ for $0 \le \angle\theta_k \le \pi/2$ and $-\pi/2 \le \angle\theta_k \le 0$, respectively. According to (97), to avoid ambiguity, $\lambda/4$ should be considered as the upper bound of d. This is the reason why in cumulant-based algorithms or some SOS-based algorithms (depending on how the statistics functions are defined) in the scenario of mixed sources, inter-element spacing $d \le \lambda/4$ is used.

The use of special antennas made or insulated with special materials, for example, using mantle cloaking [201], photonic bandgap structures between elements [202], [203] and neutralization line [204], [205] are other solutions in the physical layer for dealing with the problem of MC. It should be noted that the last two methods, in addition to making the design more complicated, do not work for dipole and monopole array antennas [206]. In addition to the above solutions, electrically small antennas [207], [208] with a size of $\lambda/10$ or less may be used. In this case, the distance between the antennas can be less than $\lambda/10$; and to reduce the MC effect in this case, metamaterials with cells less than $\lambda/100$ can be used.

Another strategy can be to use a compensator matrix in the RX processing part [209], [210]. This method is suitable for eliminating the effect of MC in dipole array antennas. The formation of the compensation matrix requires the calculation of the mutual impedance between the elements [211], [212]. Considering the effect of MC between array elements, (15) changes to the following form [213], [214]:

$$\mathbf{x}(l) = \mathbf{M}\mathbf{A}\,\mathbf{s}(l) + \mathbf{n}(l), \tag{98}$$

where $\mathbf{M}$ represents the MC matrix (MCM). It is often sufficient to consider the ULA coupling model with finite non-zero coefficients, and a symmetric Toeplitz matrix can be used to model the MC [215], [216]. Therefore, the MCM of the array in Fig. 2 can be written as [217] and [218]

$$\mathbf{M} = \begin{bmatrix} c_1 & c_2 & \dots & c_{\tilde{m}} & 0 & 0 & \dots & 0 \\ c_2 & c_1 & c_2 & \dots & c_{\tilde{m}} & 0 & \dots & 0 \\ \vdots & \ddots & \ddots & \ddots & \ddots & \ddots & \ddots & \vdots \\ c_{\tilde{m}} & \dots & c_2 & c_1 & c_2 & \dots & c_{\tilde{m}} & 0 \\ 0 & c_{\tilde{m}} & \dots & c_2 & c_1 & c_2 & \dots & c_{\tilde{m}} \\ 0 & 0 & c_{\tilde{m}} & \dots & c_2 & c_1 & c_2 & \vdots \\ \vdots & \ddots & \ddots & \ddots & \ddots & \ddots & \ddots & c_2 \\ 0 & \dots & 0 & 0 & c_{\tilde{m}} & \dots & c_2 & c_1 \end{bmatrix} \in \mathbb{C}^{N\times N}, \tag{99}$$

where $\tilde{m}$ indicates the number of non-zero MC coefficients (MCCs), and $1 = |c_1| > |c_2| > \ldots > |c_{\tilde{m}}| > 0$.

Based on the rank reduction (RARE) principle [219], [220], in [221], a localization algorithm called two-stage RARE (TSRARE) is presented for mixed FFSs and NFSs in the presence of unknown MC. The TSRARE algorithm only requires SOS and 1-D spectral search. Another localization algorithm for mixed-field sources under unknown MC is proposed in [222], which is based on rectilinearity [223]. In this algorithm, the multiple parameters of DOA, range, and MCC are decoupled, so that only three 1-D spectral searches are needed to estimate the parameters of the mixed rectilinear signals [224]. In addition, the closed-form deterministic CRB form of the corresponding problem is also derived. In [225], the authors have proposed a symmetric thinned coprime array (STCA) with the aim of reducing MC in a mixed sources scenario. The simulation results in this work show that STCA can achieve better performance than other symmetric nested arrays under the same array sensors and MC effects. In [226], an effective approach to resolve FFSs in mixed signals (FM) using SULA is presented, which in addition to considering MC effects, gain/phase imperfections are also addressed. The issue of array gain/phase uncertainties for mixed sources is also addressed in [227]. The authors in [227] have developed an algorithm using partly calibrated nonuniform linear arrays, which is compatible with exact spatial geometries. Also, in [76], a method called calibration for mixed FF and NF signals (CFN) has been proposed for the scenario of mixed sources, in which gain/phase error array is considered.

F. SPARSE ARRAYS

Achieving high resolution and estimation accuracy necessitates a large array aperture [227], [228]. To fulfill this requirement, it becomes imperative to augment the number of array elements, consequently escalating the number of circuit connections for the antennas. This increment, in turn, results in heightened hardware complexity within the system, accompanied by an associated increase in overall costs. One of the ways to overcome this problem is the sparse array structure [229]. By using sparse array structures, it is possible to estimate the direction of $\mathcal{O}(N^2)$ sources through only $\mathcal{O}(N)$ sensors [230].

In the study [231], an algorithm based on MUSIC has been developed for locating mixed FFSs and NFSs using

a structured sparse array and FOCs. A geometric proof is also provided to justify the utilisation of the proposed sparse linear array and to calculate the effective aperture of the array. The proposed algorithm enhances the resolution, estimation accuracy and the number of resolvable sources. In [52], a localization approach for mixed sources using a symmetric double-nested array (SDNA), by applying the oblique projection technique and constructing a special NF cumulant matrix is presented. Also, under a given number of sensors, the consecutive range of difference coarray and optimum array configurations for SDNA have been extracted. In the study [232], a generalized symmetric linear array framework is proposed that unifies all SULAs or symmetric SLAs, including symmetric nested arrays, cantor array and fractal arrays, for mixed sources localization. To increase the degrees of freedom of these arrays, the HOC matrix of the array output from the coarray perspective is used. The angle and range information are obtained by using the atomic norm technique from the gridless manner [233], [234] and applying the norm minimization technique to the covariance signal model, respectively. The authors claim that this method can be applied to any ULAs or symmetric SLAs to localize a mixture of FFSs and NFSs. In the study [235], in addition to designing an enhanced symmetric nested array, which can achieve more consecutive lags [236] and more unique lags [237] compared to a generalized nested array, a special cumulant matrix has been developed, which can automatically generate the largest consecutive lags. A symmetric flipped nested array (SFNA) for the localization of mixed-field non-circular (NC) sources is proposed in [238], where NC phase information can be removed by taking advantage of the special geometry of the array. In [239], two sparse symmetric linear arrays (SSLAs) named extended symmetric nested array (ESNA) and translation and transformation symmetric nested array (TTSNA) are designed for mixed sources localization. The ESNA configuration consists of three sparse SULAs with specified inter-element spacing and can achieve a higher number of unique lags than other SSLAs under the same number of array elements. Also, TTSNA is designed on the basis of nested arrays, which makes it possible to achieve a higher number of consecutive lags than other SSLAs. In addition, closed-form expressions of the two array configurations are provided in terms of the number of unique and consecutive lags.

G. TRACKING PARAMETERS

Tracking the parameters of multiple moving sources is important in wide areas such as surveillance in military applications and air traffic control in civilian applications [240], [241], [242]. A basic method for DOA tracking is to first find the DOAs for each time frame by a DOA estimation algorithm under the assumption that the directions do not change in each time frame. Each of the recently estimated DOAs is then linked to the previous estimates to track DOA changes and source movement. The above assumes that the measurement can be done quickly enough concerning the coherence time of the channel with a non-stationary target.

Parameter estimation and tracking represent pivotal research areas within the domain of direction finding and localization. While significant strides have been made in addressing the former, the latter, pertaining to sources with dynamic and non-static positions, remains an active and evolving research frontier, warranting further investigation and scholarly attention. Although approaches have been presented for parameters tracking [243], [244], [245], [246], [247], [248], none have been developed for the mixed-field sources scenario. Regarding tracking parameters in the scenario of mixed sources, two cases may be imagined. First, it is assumed that despite the movement of sources, NFSs will remain in NF and FFSs will remain in FF; and a more complicated case is that during the tracking process the mobile source transitions between FF and NF.

H. ESTIMATION OF PARAMETERS IN THE PRESENCE OF TYPES OF NOISE

For noise, there are many sources; for example, natural and man-made environmental noise in the transmission path [249], [250], [251]. The RX also produces noise such as thermal noise, shot noise and flicker noise [252], [253]. The RX noise is often the main source of noise, and additive white Gaussian noise is a good model for it. In many studies, noise is considered spatially and temporally white with Gaussian distribution, so that [254] and [255]

$$\mathbb{E}\left\{\mathbf{n}\left(l\right)\right\}=0,\quad \mathbb{E}\left\{\mathbf{n}\left(l\right)\mathbf{n}^{H}\left(l'\right)\right\}=\sigma^{2}\mathbf{I}_{N}\delta\left[l-l'\right],$$
$$\mathbb{E}\left\{\mathbf{n}\left(l\right)\mathbf{n}^{T}\left(l'\right)\right\}=0,\quad \forall l,\ l'. \tag{100}$$

The reason for this assumption is that if there are multiple sources of noise, according to the central limit theorem, their sum has a Gaussian distribution [256], [257]. Also, the assumption of white Gaussian noise greatly simplifies the performance analysis of DOA estimation.

Generally, the reason for the presence of colored (correlated) noise is interference between channels, random radiation from distributed sources, echoes, unwanted interference, etc [258]. Prominent examples of this noise occur in sonar (where there is ocean noise due to marine life, waves or ships) and in radar (where the background noise consists of ground clutter, sea clutter and scattering interference) [259]. If the noise is considered correlated, then the spatial covariance of the noise will be non-diagonal [260], [261].

Radar, sonar and communication systems are instances of application areas in non-Gaussian and non-stationary environments [262], [263], [264]. Non-stationary or non-Gaussian noise environments can be caused by various reasons such as changing conditions during operation and the presence of impulsive noise [265], [266]. For example, the variance of Gaussian observation noise may change over time. In this case, $\mathbf{n}\left(l\right) \sim \mathcal{N}\left(0,\ \sigma_{l}^{2}\mathbf{I}_{N}\right)$, where $\sigma_{l}^{2}\mathbf{I}_{N}$ is the noise covariance matrix at time l. Also, noise samples $\mathbf{n}\left(l\right)$ may result from a spherically symmetric distribution

described by a multivariate PDF that is only a function of the Euclidean norm of the random vector $\mathbf{n}$ [267], [268]. Another type of non-Gaussian noise environment may occur in such a way that the noise vectors at some time instants have much more variance than at other instants. A common model for such a case is an ε-contaminated Gaussian distribution with a cumulative distribution function (CDF) of the following form [267], [269]:

$$F_{\mathbf{n}}(\mathbf{n}) = (1-\varepsilon)\,\Theta\left(\mathbf{n};\ \tilde{\sigma}^2\mathbf{I}_N\right) + \varepsilon\Theta\left(\mathbf{n};\ \widehat{\sigma}^2\mathbf{I}_N\right), \quad (101)$$

where $\Theta(\mathbf{n};\ \mathbf{I}_N)$ is the CDF of the zero mean Gaussian vector $\mathbf{n}$ with covariance matrix $\mathbf{I}_N$. $\varepsilon \in [0,\ 1]$, and $\tilde{\sigma}^2$ and $\widehat{\sigma}^2$ are the variance of the samples originating to the nominal and contaminating distributions, respectively. Typically, ε is a number close to zero and $\tilde{\sigma}^2 \ll \widehat{\sigma}^2$.

The scenario of mixed NFSs and FFSs has been addressed so far only under additive (white and color) Gaussian noise [50], [54], [98], [111], [270]. As mentioned earlier, FOCs are insensitive to Gaussian noise types. Note that the algorithms developed by FOCs all have a limiting assumption that the source signals must be non-Gaussian; because the fourth-order moment and cumulant of Gaussian processes is zero [271], [272]. However, the non-Gaussianity of signals is not a strong limiting assumption; because non-Gaussian signals include a wide range of applications such as seismology, sonar, radio astronomy and digital communications [273], [274].

In wireless communications, signal degradation may occur due to the propagation of waves through random heterogeneous media such as urban areas or indoor environments. As a result, these waves, before impinging onto the antenna array, undergo random amplitude variation, which can be considered as a type of multiplicative noise from the point of view of the signal. Exploring the estimation of parameters for mixed-field sources in the presence of both additive noise and multiplicative noise constitutes a promising avenue for future research in this area; because this is a scenario that often happens in real wireless communications systems. In this case, the general form of the received signal in (13) can be expressed as follows [275], [276]:

$$x_m(l) = u_m(l)\sum_{k=1}^{K} s_k(l)\,a_m(\theta_k,\ r_k) + n_m(l), \quad (102)$$

where $u_m(l)$ is the multiplicative noise corresponding to the m-th sensor.

I. TIME DIFFERENCE OF ARRIVAL (TDOA)

Measuring the transmitted signal by two separate RXs allows the calculation of the TDOA between the RXs [277], [278]. By estimating the TDOA, other parameters that describe the source location, including DOA and range, can be calculated [279]. Calculating the range for TDOA point positioning involves determining whether the source is in the NF or FF, estimating the DOA, and potentially utilizing the modified polar representation (MPR) [280] to achieve accurate localization [279]. The closed-form solution methods, such as successive unconstrained minimization [281] and generalized trust region subproblem [282], provide efficient algorithms for TDOA positioning in MPR, ensuring stable and accurate estimation even under noise [279].

In [283], a unified approach based on TDOA is presented for locating a source that can be in the NF or FF. It is also shown that it is not possible to obtain the Cartesian coordinates of a distant source from Gaussian measurements when applying the NF model and derive the DOA bias of a not-so-distant source when using the FF model [283]. The approach [283] is limited to one source only. In [284], a method for the localization of multiple sources is proposed to eliminate association ambiguity for mixed NFSs and FFSs. A spatial source localization model is constructed in the modified polar representation without needing prior knowledge of whether the source is in the NF or FF. The localization model for multiple sources is derived using all possible permutations of TDOA sequences obtained from the original array. In addition, comparative analysis is performed through simulation and experiment on real speech datasets under different localization scenarios.

It is worth mentioning that the performance of TDOA is completely related to the signal bandwidth, so as the signal bandwidth increases, its performance improves [285]. It is sometimes impossible or difficult to estimate parameters of unmodulated signals and narrowband signals by TDOA techniques [286].

J. COMPRESSIVE SENSING (CS) TECHNIQUES

By considering the sparsity of the angle and range domains of the targets/sources, the localization problem can be turned into a sparse estimation problem [88]. In this way, it is assumed that there is a limited number of sources to estimate the angle/range, and this causes there to be a small number of peaks corresponding to the sources in the spatial spectrum. Such a problem can be considered a sparse signal reconstruction problem, and it uses CS reconstruction algorithms to recover the location of the peaks (angles/ranges) [287]. CS-based parameter estimation methods are robust in the condition of low number of snapshots [288], [289].

Based on FOS, a sparse reconstruction algorithm for the localization of mixed NFSs and FFSs is presented in the study [80]. By exploiting the structural characteristics of an SULA, an FOC matrix is constructed that separates angular and range information. Based on the sparse representation framework, a weighted norm minimization algorithm is developed to obtain DOAs of mixed sources. Next, another FOC matrix containing both the DOA and range information of the mixed sources is constructed. With DOA estimates, the 2-D spatial dictionary can be reduced to a 1-D dictionary that depends on the parameters. Then, by using a similar sparse reconstruction method, an estimate of the range of mixed sources can be obtained, and the type of sources can be distinguished from those ranges.

In [290], complex variational mode decomposition (CVMD) [291], [292], [293] is used to localize mixed NFSs and FFSs sources, which works with a single snapshot. Taking advantage of the fact that the signal model of the source localization problem is similar to the time-domain frequency-modulated signal model, in [290], CVMD is extended for array signal processing. Decomposition results of array measurements can correspond to potential sources at different locations. The DOA and range of the sources are estimated by model fitting with the decomposed sub-signals.

K. HIGHER-ORDER STATISTICS

Statistics of orders higher than four (such as sixth- and eighth-order statistics) have been especially used in the area of automatic modulation classification [294], [295], [296]. Also, they have been used in a few works [297], [298], [299] in the area of sources DOA estimation.

The feasibility of using statistics of orders higher than four, to improve the performance (especially to enhance the accuracy and resolution of the results) in the scenario of mixed-field sources, can be studied in the future. It is shown in [297] that by using 2υth-order cumulants, it is possible to have a virtual array with an aperture of $\mathcal{O}\left((2\upsilon+1)N^{2\upsilon}\right)$. With such an enhancement, although one can expect an increase in resolving capabilities, identifiability, and estimation accuracy, the sharp increase in computational complexity and the need for many snapshots will be among the inevitable drawbacks of using these higher-order statistics [300], [301].

L. POLARIZATION

The effectiveness of polarization diversity has been proven in wireless communications and various types of radar systems [302], [303], [304]. Polarization is also incorporated in array antennas for improved estimation of FF and NF signals parameters (including DOA and range) [184], [305], [306], [307], [308], [309], [310]. It has been shown that the use of polarimetric information can significantly improve the accuracy of source parameter estimation [311], [312]. For the SULA of Fig. 9 consisting of dual-polarization sensors placed on a flat plane in a 2-D surface, the received signal model at the m-th sensor is expressed separately for x and y polarizations [311], [313].

A multidimensional parameter estimation method for mixed NFSs and FFSs based on polarization sensitive array, FOC, joint diagonalization technology [314], [315] and propagator method [316], [317] is presented in [318], which can jointly estimate DOA, range, frequency, polarization auxiliary angle [319], and polarization phase difference [320]. In this method, the FOC matrix is constructed using the output on the label of the specific dipole pairs of the received array, which effectively avoids the matrix rank reduction caused by the FFSs coexistence situation. In addition, the proposed method employs the orthogonal propagation algorithm for subspace decomposition and uses the total LS solution to replace the orthogonal solution of SVD, which is effective in reducing computational complexity.

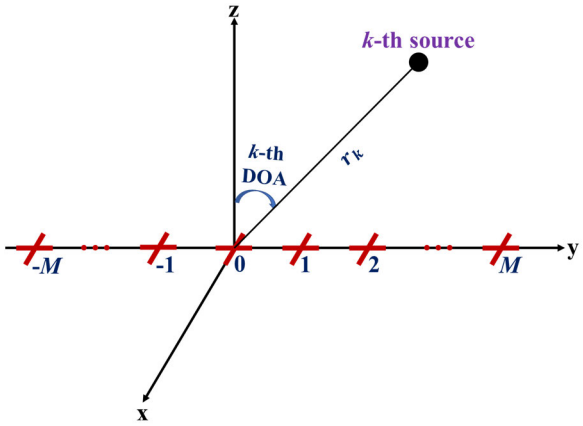

FIGURE 9. An example array geometry for polarized signals.

M. ONE-BIT MEASUREMENTS

One-bit DOA estimation represents a paradigm shift in wireless communication and radar systems, addressing the persistent challenge of high-resolution quantization [321]. Traditional methods require costly and complex hardware setups due to the exponential increase in power consumption with higher quantization bit numbers in analog-to-digital converters (ADCs) [322]. However, with the advent of one-bit ADCs, which utilize simple comparators and consume minimal circuit power, there is a promising avenue for improvement, particularly in massive multiple-input multiple-output systems [323].

Most of the researches in the area of one-bit DOA estimation have been carried out under the FF assumption [324], [325], [326], [327]. The NF localization approach in [328] is studied under one-bit measurement to show its robustness. However, the assumption of coexistence of FFSs and NFSs presents a significant challenge that has not yet been addressed in the literature. Future work in this area could focus on developing localization algorithms specifically tailored to handle the coexistence of NFSs and FFSs under one-bit measurement constraints.

N. METASURFACE ANTENNAS

Metasurface antennas represent a groundbreaking advancement in antenna technology, leveraging the principles of metamaterials and surface electromagnetics to achieve unprecedented control over electromagnetic waves [329]. By designing metasurfaces with tailored properties, such as phase modulation and beam steering, they have recently been widely employed in advanced imaging systems for enhancing resolution, reducing aberrations, and enabling novel imaging modalities [330], [331], [332], [333].

Metasurface antennas offer promising opportunities for enhancing the performance of DOA estimation and localization techniques [334]. By integrating metasurface structures into antenna arrays, researchers in the area of localization

of mixed-field sources can achieve precise control over the radiation patterns and beamforming capabilities, enabling accurate localization of signal sources in both azimuth and elevation domains [335]. Metasurface-based antennas can mitigate MC effects and improve array sensitivity, leading to enhanced DOA estimation accuracy, particularly in scenarios with complex propagation environments and interference [336]. Moreover, the reconfigurability and tunability of metasurface antennas allow for adaptive beamforming and dynamic localization, enabling robust operation in dynamic and cluttered environments [337].

O. DEEP LEARNING (DL)

DL is a subset of machine learning that involves the use of artificial neural networks to model and solve complex problems [338], [339], [340]. It has proven to be highly effective in handling complex and high-dimensional data, making it well-suited for ASP tasks [341], [342], [343].

In [344], convolutional neural networks (CNNs) are presented to achieve NFSs localization through SDNA. Due to the possibility of separating noncoherent NFSs in the frequency spectrum, first, the phase difference matrices are calculated, and the typical elements are considered as the input of the networks. To guarantee the accuracy of the angle estimation, autoencoders are implemented to divide the angle subregions, and the corresponding classification CNNs are constructed to obtain the angles of the NFSs. Then, a specific range vector without estimated angles is constructed, and regression CNN is used to obtain the sources range.

In the study [345], a DL-based DOA estimation approach considering N_c classes is presented to detect FFSs under correlated NF interferences. This approach consists of an NF interference rejection network and a DOA estimation network. The first network calculates the NF components of the covariance matrix by CNNs with a complex mapper. The NF components are rejected from the covariance matrix. The second network removes the interference residuals and estimates the DOAs of the interfered FFSs.

P. FULL-WAVE OR EXPERIMENTAL DATA

In most references related to DOA estimation and localization, the performance of the methods has been evaluated only with simulated data obtained from semi-analytical systems (e.g. MATLAB) [346]. Full-wave simulations (e.g. with Wireless InSite, CST Microwave Studio, FEKO, HFSS, etc.) or experimental data obtained directly from measurements in the real-world environment can provide a more realistic representation of the challenges faced in practical applications [347], [348].

In researches [157], [349], [350], [351], [352], full-wave simulations, and in researches [353], [354], [355], [356], [357], [358], experimental data (for radio or acoustic signals) have been used to evaluate the performance of DOA estimation or localization in pure fields. However, for the mixed-field sources scenario, only a limited real experiment has been performed in an anechoic chamber with microstrip patch antennas with a carrier frequency of 1.26 GHz in [51]. Also, in [159] and [160], EM simulations have been performed in Wireless InSite assuming only one FSS and its multipaths. A comprehensive study including a combination of numerically simulated data, full-wave data, and experimental data allows researchers to investigate both controlled conditions and the challenges posed by practical applications for the complex scenario of the coexistence of NFSs and FFSs.

Q. ARRAY GAIN

Array gain plays a pivotal role in the performance of DOA algorithms, especially when dealing with directional antenna arrays [359], [360], [361]. Unlike isotropic or omnidirectional arrays, which have uniform radiation patterns, directional arrays exhibit narrower radiation patterns that change as the main beam is directed towards different angular directions [359], [362].

Most of the DOA estimation and localization algorithms in the mixed-field sources scenario are designed to work with isotropic or omnidirectional antenna arrays. The shift from isotropic to directional elements alters the radiation pattern, subsequently impacting the maximum gain and directivity of the array [359], [363], [364]. As a result, any modifications to existing algorithms must consider these changes in array gain [359], [363], [364]. Consequently, there is a pressing need to adapt these algorithms to suit directional antenna arrays effectively. One promising avenue for addressing this challenge involves developing new approaches for calculating the statistics matrices, a crucial component in many existing algorithms. These approaches must inherently account for variations in array gain as the array is swept across different ''look directions'' in azimuth or elevation angles.

R. ROBUST STATISTICS

Traditional statistical signal processing relies heavily on the assumption of a normal (Gaussian) distribution, which often serves as a suitable model for the available data [365], [366]. This Gaussian model facilitates the derivation of optimal procedures in many cases [365], [367]. However, deviations from Gaussian behavior have been observed in various measurement studies [365], [368]. Robust statistical methods address the reality that assumed data models are only approximate rather than exact. Unlike classical parametric approaches, robust methods are less affected by minor variations in the data, such as outliers or slight deviations from the model [365], [369]. They also demonstrate nearly optimal performance even when the underlying assumptions are not precisely met. While achieving optimality is desirable, engineers often prioritize robustness in their decision-making processes.

The study [370] introduces a robust method for estimating the DOA based on sparse Bayesian learning (SBL). This method is designed to handle non-circular signals amidst

TABLE 2. Comparison of works available in the literature in the scenario of mixed-field sources in terms of design and implementation foundations.

Ref.	Array Type	Specific Assumptions/Scenario	Type of Statistics	The Basis of the Method
[77] TSMUSIC	SULA	Non-zero kurtosis signals; white or color Gaussian noise; $d \le \lambda/4$	FOS	Separation of a virtual steering vector into two parts
[81] OPMUSIC	SULA	Complex circular Gaussian and spatially uniformly white noise; $d \le \lambda/4$; along with deriving the relevant stochastic CRBs	SOS	Oblique projection
[100]	SULA	Non-zero kurtosis signals; $d \le \lambda/4$	FOS	Sparse signal reconstruction
[92]	SULA	Spatial white complex Gaussian noise	SOS	Power estimation of FSs
[83]	SULA	Cyclostationary sources with non-zero kurtosis; $d \le \lambda/4$	Third-order cyclic moment	ESPRIT-like
[91]	SULA	Complex circular Gaussian and spatially uniformly white noise; $d \le \lambda/4$	SOS	Polynomial rooting and ESPRIT-like
[87]	Symmetric SLA	Non-zero kurtosis signals; complex Gaussian white noise	FOS and SOS	Mixed-order MUSIC
[189]	Spherical microphone array	Acoustic wideband and narrowband sources; complex circular Gaussian and spatially uniformly white noise	SOS	Spherical ESPRIT-like
[101]	SULA	Non-zero kurtosis signals; complex circular Gaussian and spatially uniformly white noise; $d \le \lambda/4$	FOS	Sparse signal reconstruction
[102]	SULA	Circular Gaussian and spatially uniformly white noise; $d \le \lambda/4$	SOS	Jointly using MUSIC and sparse signal reconstruction
[93]	SULA	Circular Gaussian and spatially uniformly white noise	SOS	Spatial differencing
[94] TSMDA	SULA	Circular Gaussian and spatially uniformly white noise; $d \le \lambda/4$	SOS	Covariance matrix differencing
[159, 160]	UCA	FFS and its NF multipath reflections; 2-D angle estimation; temporally and spatially white Gaussian noise; along with numerical EM simulations in Wireless InSite; $K_F = 1$	SOS	Calibration technique and NF to FF transformation
[375]	ULA	FF acoustic signal in the presence of NF interferences; $K_F = 1$	SOS	Beamforming
[104]	SULA	Non-zero kurtosis signals; white or color Gaussian noise; $d \le \lambda/4$	FOS	Beamforming
[221] TSRARE	SULA	Under unknown MC; white Gaussian noise; $d \le \lambda/4$; along with deriving the corresponding deterministic CRBs	SOS	RARE principle
[51]	SULA	Non-zero kurtosis signals; white or color Gaussian noise; $d \le \lambda/4$; along with a real experiment	FOS	Polynomial decomposing
[76] CFN	SULA	Considering gain/phase error; white Gaussian noise; $d \le \lambda/2$	SOS	Simplifying the space spectrum function by matrix transformation
[106] MOS	SULA	Non-zero kurtosis signals; spatially white Gaussian noise; $d = \lambda/4$	FOS and SOS	Estimating the kurtosis of FSs
[192] FMW	SULA	DOA estimation for FMW with considering gain/phase error array; $d = \lambda/2$	SOS	Fast Fourier transformation
[226] FM	SULA	DOA estimation for FFSs in mixed signals with considering MC effects and gain/phase imperfections; white Gaussian noise; $d = \lambda/2$	SOS	Matrix transformation
[107]	SULA	Non-zero kurtosis signals; spatially white Gaussian noise; $d \le \lambda/4$	FOS and SOS	Cumulant matrix reconstruction
[82]	SULA	Non-zero kurtosis signals; white or color Gaussian noise; $d \le \lambda/4$	FOS	Differencing
[52]	SDNA	Non-zero kurtosis signals; spatially uniformly white noise	FOS and SOS	Oblique projection
[222]	SULA	Under unknown MC; circular Gaussian noise; $d \le \lambda/4$; along with deriving the corresponding deterministic CRBs	SOS	Rectilinearity
[111] HODA	SULA	Non-zero kurtosis signals; white or color Gaussian noise; $d \le \lambda/4$	FOS	High-order differencing
[376]	SULA	White Gaussian noise; $d \le \lambda/4$	None (single snapshot)	Discrete fractional Fourier transform
[56] CSA	SULA	Under multipath environments; non-zero kurtosis signals; white or color Gaussian noise; $d \le \lambda/4$; corresponding stochastic CRBs in [153]	FOS	Integration of squaring, projection, array interpolation transform and SS
[377]	SULA	Negative kurtosis signals; temporally and spatially white Gaussian noise; $d \le \lambda/4$	FOS	Gridless low-rank matrix reconstruction
[54] FOSA	UCA with a center sensor	2-D angle estimation; non-zero kurtosis signals; white or color Gaussian noise; $R \le \lambda/4$; corresponding stochastic CRBs in [69]	FOS	Fourth-order spatial-temporal cumulants

TABLE 2. *(Continued.)* **Comparison of works available in the literature in the scenario of mixed-field sources in terms of design and implementation foundations.**

[98] HOSTA	SULA	Non-zero kurtosis signals; white or color Gaussian noise; $d \leq \lambda/4$	FOS	Spatial-temporal full ESPRIT-like
[50]	SULA	Non-zero kurtosis signals; white or color Gaussian noise; $d \leq \lambda/4$	FOS	Rotational invariant
[124]	ULA	FFSs under NF interferences; sonar array	None	Beamforming
[290]	ULA	Robust with coherent sources; $d \leq \lambda/2$	None (single snapshot)	CVMD
[80]	SULA	Non-zero kurtosis signals; white or color Gaussian noise; $d \leq \lambda/4$	FOS	Sparse signal reconstruction
[79]	SULA	Non-zero kurtosis signals; complex Gaussian white noise; $d \leq \lambda/4$	FOS	High-order differencing
[227]	Nonuniform partly-calibrated linear array	Under array gain/phase uncertainties; along with deriving the corresponding CRBs; no simplification or approximation on the exact source-array geometry	FOS	Constructing two matrix pencils
[184]	Linear cocentered orthogonal loop and dipole array	Fully polarized sources; adaptability to non-uniform arrays; Exact spatial model; complex Gaussian noise	SOS	MUSIC-like and ESPRIT-like
[238]	SFNA	NC signals; Gaussian noise	FOS	Exchanging the positions of two subarrays in the traditional nested array
[225]	STCA	Non-zero kurtosis signals; white Gaussian noise; $d \leq \lambda/4$	FOS	Sparse signal reconstruction
[318]	Symmetric uniform polarization sensitive linear array	Joint estimation of DOA, range, frequency, polarization auxiliary angle and polarization phase difference; White Gaussian noise; $d \leq \lambda/4$	FOS and SOS	Joint diagonalization technology and propagator method
[345]	ULA	Detect FFSs under correlated NF interferences; $d \leq \lambda/2$	SOS	DL
[371]	SULA	Under impulsive noise with symmetric alpha-stable distribution; $d \leq \lambda/4$; along with deriving the corresponding CRBs	SOS	Weighted outlier filter
[270]	SULA	In the presence of alpha-stable noise	SOS	Noise reduction, sparse signal reconstruction and subspace decomposition

impulse noise and MC. Initially, the Toeplitz property of the MCM is leveraged to nullify the impact of array MC, while also extending the array aperture using non-circular signal properties. To mitigate the effects of impulse noise, the algorithm reconstructs the outlier segment of the impulse noise alongside the original signal in the signal matrix. Subsequently, a coarse estimation of DOA is achieved by balancing accuracy and efficiency through parameter estimation using the alternating SBL update algorithm. Finally, a 1-D search is employed around the identified spectral peaks to achieve precise DOA estimation.

To address the issue of declining performance in traditional localization methods caused by impulsive noise when dealing with a mix of NFSs and FFSs, a robust localization approach is proposed in [371]. This method begins by mitigating the effects of impulsive noise using a weighted outlier filter. Subsequently, the DOAs of FFSs are estimated through a MUSIC spectral peaks search. With the DOAs of FFSs identified, the mixed sources can then be separated. Additionally, the estimation of localization parameters for NFSs can avoid 2-D spectral peaks search through the decomposition of steering vectors. The CRB for unbiased estimations of DOA and range under impulsive noise are also derived.

V. SUMMARIZED COMPARATIVE EVALUATION

This section highlights and summarizes the main differences between the existing methods for DOA estimation and localization in the scenario of mixed NFSs and FFSs, which were discussed in detail in the previous sections, in tables, to make a general comparison between them. In Table 2, the comparison of the works available in the literature in the scenario of mixed-field sources is given in terms of design and implementation foundations. References are listed in order of publication year from the oldest to the newest in the first column. Abbreviated names of the methods are also mentioned, if any. In the second column of the table, the type of array used is mentioned. References that use the same array type are marked with the same color. At a glance, it can be seen that SULA is the dominant array that researchers have considered in their work due to its simplicity and the exploitation of its symmetry in developing algorithms. In the third column of the table, the main assumptions used in each work are mentioned. Wherever not stated, it is assumed that the source signal is narrowband, the array is calibrated, and the noise is additive. Although all works are under mixed-field sources scenario, some of them include more comprehensive/complex scenarios, such as mixed sources in multipath environments, mixed sources under MC, mixed sources with wideband signals, etc. These items are also highlighted in the third column. Special scenarios and issues are discussed in detail in eighteen subsections in Section IV. The inter-element spacing conditions are related to avoiding phase ambiguity, which was discussed in Section IV-E. In the fourth column of the table, the type of statistics used in each

TABLE 3. Comparison of works available in the literature in the scenario of mixed-field sources in terms of aperture loss and major computational complexities.

Ref.	Maximum Number of Resolvable Sources	Total Computational Complexity
[77] TSMUSIC	$N-1$ for $N \geq 7$	$\mathrm{O}\left(9\left(N^2+(2N-1)^2\right)L+4\left(N^3+(2N-1)^3+K(4N+1)^3\right)/3+(180/\Delta_\theta)N^2\right)$
[81] OPMUSIC	$(N-1)/2$	$\mathrm{O}\left(\left(N^2+(N+3)^2/4\right)L+4\left(N^3+(N+3)^3/8\right)/3+\left(2\times180/\Delta_\theta+K_\mathrm{N}\left(\left(2D^2/\lambda-0.62\sqrt{D^3/\lambda}\right)/\Delta_\mathrm{r}\right)\right)N^2\right)$
[100]	-	$\mathrm{O}\left(9N^3L+4N^5/3+4NL^2/3+K^3\bar{K}^3+K^6\left(\left(2D^2/\lambda-0.62\sqrt{D^3/\lambda}\right)/\Delta_\mathrm{r}+N_\mathrm{r}\right)^3\right)$
[83]	$(N-3)/2$	$\mathrm{O}\left((N-1)^2L/2+(N-1)^3/3+(180/\Delta_\theta)(N-1)^2/4\right)$
[91]	$N-2$	$\mathrm{O}\left(N^2L+4N^3/3+(N-1)K+(K-K')NK\right)$
[87]	-	$\mathrm{O}\left(9L\left((N+3)^2+1\right)/8+N^2L\right)$
[189]	$N'/2$	$\mathrm{O}\left((N'+1)^6+(N'+1)^4\left(2D^2/\lambda-0.62\sqrt{D^3/\lambda}\right)/\Delta_\mathrm{r}\right)$
[101]	$N-1$	$\mathrm{O}\left(9N^2L+9N(N-1)L+10\bar{K}^3+10K^3\left(\left(2D^2/\lambda-0.62\sqrt{D^3/\lambda}\right)/\Delta_\mathrm{r}+N_\mathrm{r}\right)^3\right)$
[102]	$(N-1)/2$	$\mathrm{O}\left(N^2L+(N+1-N_\mathrm{L})^2N_\mathrm{L}+4N^3/3+4(N+1-N_\mathrm{L})^3/3+\bar{K}^3+K^3\left((K-K_\mathrm{N})\left(2D^2/\lambda-0.62\sqrt{D^3/\lambda}\right)/\Delta_\mathrm{r}+K_\mathrm{N}\right)^3\right)$
[93]	$N-1$ for $K_\mathrm{N} \leq (N-1)/2$	$\mathrm{O}\left(N^2L+4N^3+(180/\Delta_\theta)(N-1)^2+\left(180/\Delta_\theta+K_\mathrm{N}\left(2D^2/\lambda-0.62\sqrt{D^3/\lambda}\right)/\Delta_\mathrm{r}\right)N^2\right)$
[94] TSMDA	$N-1$ for $K_\mathrm{N} \leq (N-1)/2$ and $K_\mathrm{F} \leq N-1$	$\mathrm{O}\left(N^2L+10N^3/3+(180/\Delta_\theta)(N-1)^2+\left(180/\Delta_\theta+K_\mathrm{N}\left(2D^2/\lambda-0.62\sqrt{D^3/\lambda}\right)/\Delta_\mathrm{r}\right)N^2\right)$
[375]	-	$\mathrm{O}\left(N^3\right)$, for $N<N_\mathrm{b}$; $\mathrm{O}\left(NN_\mathrm{b}^2\right)$, otherwise
[104]	N	$\mathrm{O}\left(\left(9\rho N^2+N^2\right)L+\rho\left(N^3+N^2\right)+4\left(N^3+\rho^3\right)/3+\left(180/\Delta_\theta+K\left(2D^2/\lambda-0.62\sqrt{D^3/\lambda}\right)/\Delta_\mathrm{r}\right)N^2\right)$
[221] TSRARE	$N-$ for $K_\mathrm{N} \leq (N-1)/2$	$\mathrm{O}\left(N^2L+8N^3/3+\left(2\times180/\Delta_\theta+K_\mathrm{N}\left(2D^2/\lambda-0.62\sqrt{D^3/\lambda}\right)/\Delta_\mathrm{r}\right)N^2\right)$
[51]	$N-2$	$\mathrm{O}\left(27(N-1)^2L+32(N-1)^3/3+8(N-2)^3/3+8K_\mathrm{N}\right)$
[76] CFN	-	$\mathrm{O}\left(N^2L+8N^3/3+2(180/\Delta_\theta)N^2\right)$
[106] MOS	$N-1$	$\mathrm{O}\left(10N^2L+KN^2+8N^3/3+\left(2\times180/\Delta_\theta+K_\mathrm{N}\left(2D^2/\lambda-0.62\sqrt{D^3/\lambda}\right)/\Delta_\mathrm{r}\right)N^2\right)$
[226] FM	$N-1$ for $K_\mathrm{F} < (N-1)/2$	$\mathrm{O}\left(N^2L+8N^3/3+(180/\Delta_\theta)N^2\right)$
[107]	$N-1$ for $K_\mathrm{N} \leq N-2$	$\mathrm{O}\left(10N^2L+4N^3+\left(180/\Delta_\theta+K_\mathrm{N}\left(2D^2/\lambda-0.62\sqrt{D^3/\lambda}\right)/\Delta_\mathrm{r}\right)N^2\right)$
[82]	$N-1$ for $K_\mathrm{N} \leq N-2$	$\mathrm{O}\left(9\left(4(N-2)^2+N^2\right)L+2\left(N^3+(N-2)^3\right)+(N-1)N^2+(N-2)^3\right)$
[222]	$\min\{2(N-),N-1\}$	$\mathrm{O}\left(4N^2L+32N^3/3+\left(8\times180/\Delta_\theta+4K_\mathrm{N}\left(2D^2/\lambda-0.62\sqrt{D^3/\lambda}\right)/\Delta_\mathrm{r}\right)N^2\right)$
[111] HODA	$N-1$ for $K_\mathrm{N} \leq N-2$	$\mathrm{O}\left(N^2L+9\left(4(N-2)^2+N^2\right)L_\mathrm{P}+4N^3/3+4(N-2)^3+N^2/\Delta_\mathrm{f}\right)$
[376]	-	$\mathrm{O}\left(\left(2(N-1)+2+(N/2)\log_2(N)\right)(180/\Delta_\theta)\right)$
[56] CSA	$N-1$ for $N \geq \max\{K_\mathrm{n}+G+1, \lceil(3\max\{P_1,P_2,\mathrm{K},P_G\}+1)/2\rceil\}$	$\mathrm{O}\left(18N^2L+4N^3+4(G+G_\mathrm{N})\left(N^3+N_\mathrm{u}^3\right)/3+(180/\Delta_\theta)N^2+(180/\Delta_\theta)\left((G+G_\mathrm{N})N_\mathrm{u}^2\right)+\left(\left(2D^2/\lambda-0.62\sqrt{D^3/\lambda}\right)/\Delta_\mathrm{r}\right)\left(N^2+G_\mathrm{N}N_\mathrm{u}^2\right)\right)$
[377]	$N-2$	$\mathrm{O}\left(9N^2L+9N(N-1)L^2+(N-1)^{4.5}\right)$
[54] FOSA	$M-1$	$\mathrm{O}\left(18(M+1)^2L+9M^2L+8(M+1)^3/3+8M^3/3+\left(\left(2\beta D^2/\lambda-0.62\zeta\sqrt{D^3/\lambda}\right)/\Delta_\mathrm{r}\right)KM^2\right)$
[98] HOSTA	$N-1$	$\mathrm{Min}:\mathrm{O}\left(9(\rho+2)N^2L+4(\rho+2)N^3/3\right)$; $\mathrm{Max}:\mathrm{O}\left(9(\rho+2)N^2L+4\left((\rho+(\rho-1)+\mathrm{K}+1)+2\right)N^3/3\right)$
[50]	$N-1$	$\mathrm{Min}:\mathrm{O}\left(9(\rho+1)N^2L+4\rho N^3\right)$; $\mathrm{Max}:\mathrm{O}\left(9(\rho+1)N^2L+4\left(\rho+(\rho-1)+\mathrm{K}+1\right)N^3\right)$

TABLE 3. *(Continued.)* **Comparison of works available in the literature in the scenario of mixed-field sources in terms of aperture loss and major computational complexities.**

[124]	-	$\mathrm{O}\left(N_{\mathrm{v}}N_{\mathrm{b}}^{2}\right)$
[80]	-	$\mathrm{O}\left(18N^{2}L+K^{3}\left(180/\Delta_{\theta}+\left(2D^{2}/\lambda-0.62\sqrt{D^{3}/\lambda}\right)/\Delta_{\mathrm{r}}+1\right)^{3}+9N^{4}L\right)$
[79]	N for $K_{\mathrm{N}}\leq(N-1)/2$	$\mathrm{O}\left(9N^{2}L+4N^{3}+\left(2\times180/\Delta_{\theta}+2K_{\mathrm{N}}\left(2D^{2}/\lambda-0.62\sqrt{D^{3}/\lambda}\right)/\Delta_{\mathrm{r}}\right)N^{2}\right)$
[227]	-	$\mathrm{O}\left(\left(6N^{2}+8N+3\right)L+54N^{3}+2K^{3}\right)$
[184]	$N-1$	-
[318]	$N-1$	$\mathrm{O}\left(36N^{2}L+N^{3}/3+3K\left(N+1\right)^{2}+3K^{2}\left(N+1\right)+3\left(N-1\right)^{3}/8+N^{2}L+KN^{2}\right)$
[345]	-	$\mathrm{O}\left(NN_{\mathrm{c}}\right)$
[371]	N	$\mathrm{O}\left(N^{2}L+8N^{3}/3+\left(2\times180/\Delta_{\theta}+K_{\mathrm{N}}\left(2D^{2}/\lambda-0.62\sqrt{D^{3}/\lambda}\right)/\Delta_{\mathrm{r}}\right)N^{2}\right)$

of the approaches is mentioned. References that have used the same type of statistics are marked with the same color. Most of the approaches have employed pure FOS or pure SOS; however, some works have used hybrid statistics. There are also a few methods that, being single-snapshot, do not rely on signal statistics. Finally, in the last column of Table 2, the basis of the method used in each of the approaches is given. More details of the algorithms and their implementation can be found in Sections III and IV.

In Table 3, the comparison of works available in the literature in the scenario of mixed-field sources in terms of aperture loss and computational complexity is given. Similar to Table 2, the references are listed in the order of publication year and with the abbreviated name in the first column. One of the quantitative criteria for comparing the performance of different DOA estimation and localization approaches is the amount of aperture loss. This criterion determines the degrees of freedom available for parameter estimation, in other words, the number of sources that can be resolved [50], [56]. The lower the aperture loss, the higher the number of resolvable sources. The maximum number of sources that can be resolved by each approach according to the given number of sensors is listed in the second column of Table 3. Note that the above upper bound, in some approaches, is a function of other parameters that the algorithm imposes, apart from the number of sensors. In addition, some approaches have a limit on the number of pure field sources. It is worth mentioning that in ESPRIT-based approaches, according to the theory of ESPRIT [372], the maximum number of resolvable uncorrelated sources is equal to the size of sub-arrays. A dash mark in Table 3 signifies that the value is not mentioned directly in the reference or is not easily verifiable. The last column of Table 3 shows the total computational complexity of each method. Computational complexity is another quantitative comparison measure that indicates the number of arithmetic operations of an algorithm and determines the amount of resources required to execute that algorithm [373]. The total computational complexities of the algorithms in Table 3 are calculated by considering the major multiplications involved in the construction of statistics matrices, eigendecomposition, spectral search, sparse signal recovery process, matrix inversion, selecting of tuning factor, constructing matrix, whitening reduction dimension, diagonalizing and orthogonal propagation [374]. All the parameters in the tables have already been introduced in the text. In general, various DOA estimation and localization approaches in the mixed-field sources scenario over the past fifteen years have gradually included more complex and practical assumptions, considered different types of arrays and statistics, employed more innovative techniques or tried to improve the performance in terms of estimation accuracy, resolution, aperture loss, computational complexity, etc.

Now let us examine the simulation results of some methods to evaluate their performance in the face of uncorrelated mixed sources. Consider two NFS and two FFS located at $\left(\theta_1=1^{\circ},\ r_1=7.3\lambda\right)$, $\left(\theta_2=-35^{\circ},\ r_2=5.2\lambda\right)$, $(\theta_3=-15^{\circ},\ r_3=\infty)$ and $(\theta_4=35^{\circ},\ r_4=\infty)$. For all experiments, a 17-element ULA with inter-element spacing $d=\lambda/4$ is assumed. The number of snapshots is equal to 500. The signals are equi-power and narrowband stationary. They are modeled in harmonic form $s_k(l)=e^{j(2\pi f_k l+\psi_k)}$ [50], [378], where the phases ψ_k are uniformly distributed in $[0,\ 2\pi)$. The additive noise is assumed to be a spatial-temporal white complex Gaussian random process. The Fresnel region is $R_{\mathrm{D}}\in\left[4.96\lambda,\ 32\lambda\right]$. Δ_θ, Δ_{r} and Δ_{f} are assumed 0.1°, 0.05λ and 0.0001 Hz, respectively. The number of time lags is 2. The performance of the methods of TSMUSIC, TSMDA, [51], HODA, HOSTA and CSA are compared with each other as well as with the corresponding theoretical CRB (see Sections IV-B). The results are evaluated in the estimated root mean square error (RMSE) based on the average results of 500 independent Monte Carlo runs. RMSE is calculated as follows [379]:

$$\mathrm{RMSE}=\sqrt{\frac{1}{N_{\mathrm{T}}}\sum_{n=1}^{N_{\mathrm{T}}}\left(\hat{\zeta}_n-\zeta\right)^{2}},\tag{103}$$

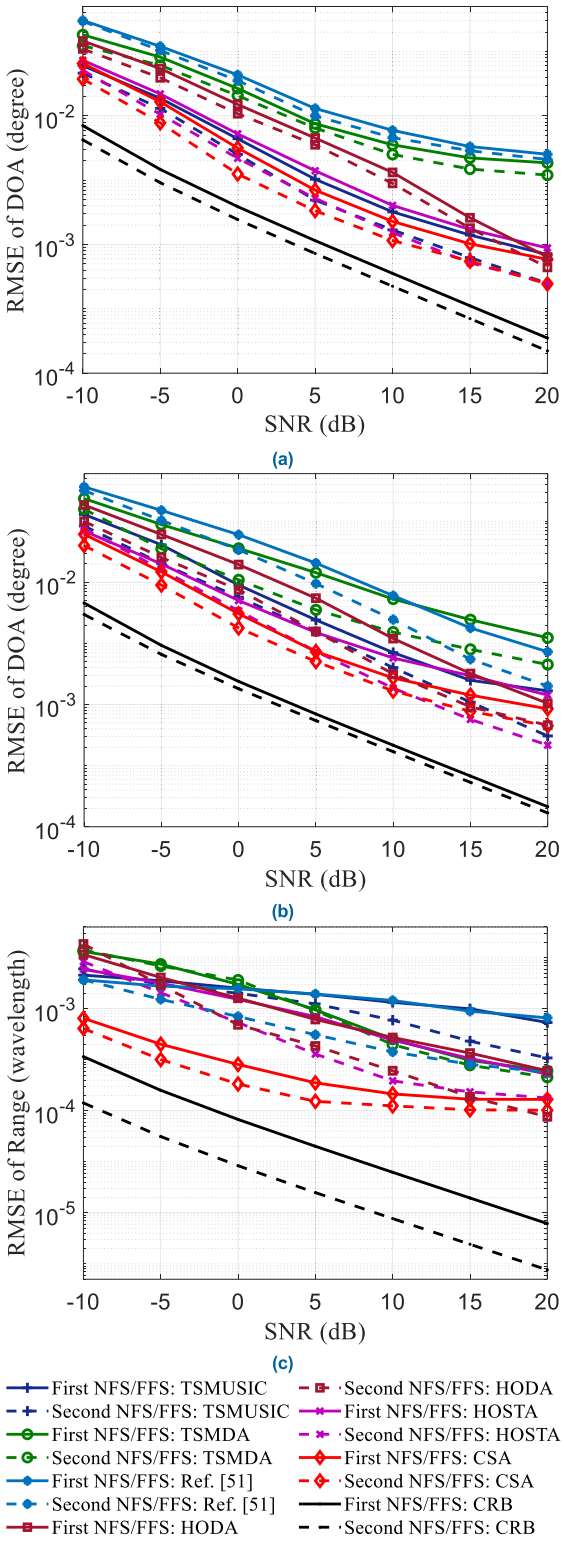

FIGURE 10. Comparison of RMSEs of DOA and range estimates of various algorithms versus SNR for mixed sources (two NFS and two FFS); (a) NFSs DOA, (b) FFSs DOA, (c) NFSs range.

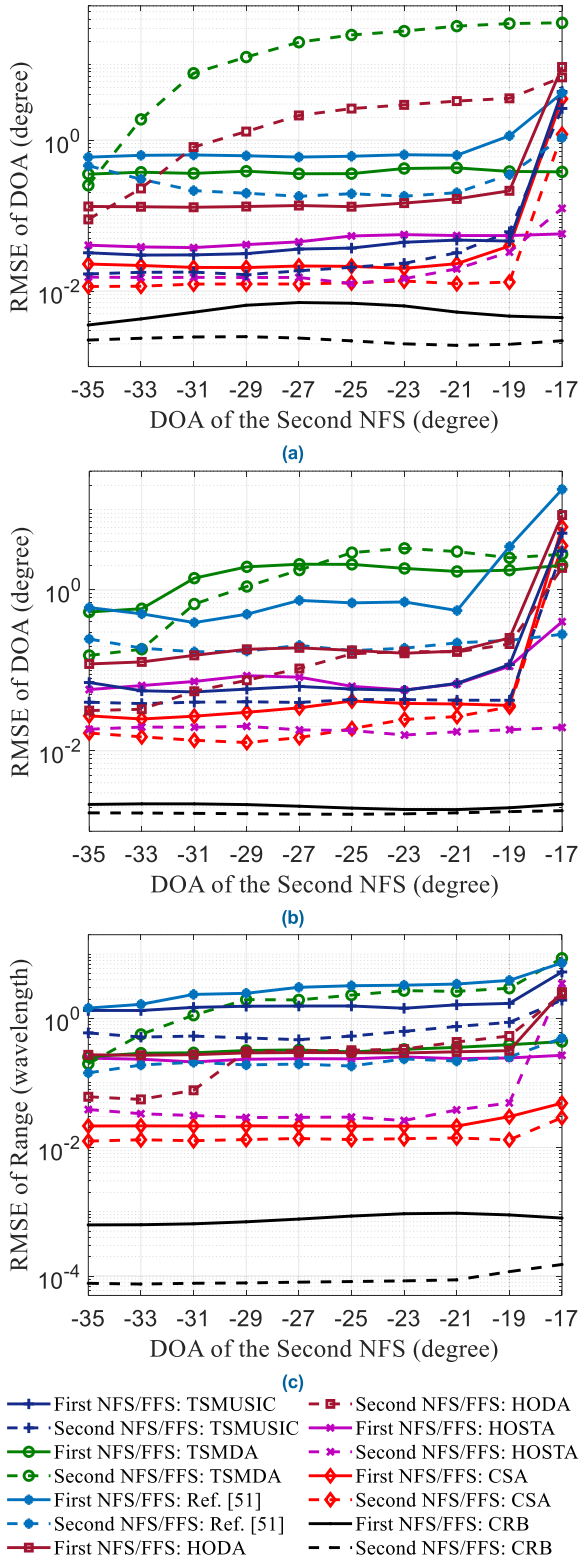

FIGURE 11. Comparison of RMSEs of DOA and range estimates of various algorithms versus DOA change of the second NFS for mixed sources (two NFS and two FFS); (a) NFSs DOA, (b) FFSs DOA, (c) NFSs range.

where $\hat{\zeta}_n$ is an estimate of the parameter ζ in the n-th test and N_T is the number of Monte Carlo runs.

When SNR varies from -10 to 20 dB, the RMSE of DOA and range estimations are shown in Fig. 10. As can be seen, in the DOA estimation, CSA, HOSTA, TSMUSIC have the best performance in terms of accuracy and are closer to the related CRBs. Especially in the case of the CSA and

TSMUSIC, this was expected; because in both methods, to estimate the DOA of uncorrelated sources, cumulant matrices of full size $N \times N$ are constructed and estimates are obtained based on MUSIC-like mechanisms. After these three methods, the best performance in DOA estimation belongs to HODA and TSMDA. The weakest performance in DOA estimation is provided by the method [51], one of the reasons for which is its greater aperture loss than other methods. As can be seen from Fig. 10(c), CSA has the best performance in terms of range estimation accuracy and is much closer to CRB than other methods. In the case of CSA, considering the high accuracy of DOA estimation of NFSs and the direct dependence of range estimation performance on the accuracy of DOA estimates of NFSs (refer to (17) from [56]), as well as the lack of spatial differencing, such performance was not far from expected (for more details, refer to [56]). After CSA, HOSTA and HODA have the best performance in terms of range estimation. According to the efficiency of CSA and HOSTA in the range estimation, and the analysis of Section IV-C of [56], these methods are expected to perform well in terms of signals classification. Notice that in the case of TSDMA and HODA, which are both based on spatial differencing, the results show that, in general, HODA performs better than TSMDA. This is due to the use of higher-order statistics and the reduction of differencing errors in HODA. Note that here the CRBs of the DOAs of the NFSs are almost equal, and the range CRB value of the second NFS, which is closer to the array, is smaller than that of the first NFS. This is fully consistent with the theoretical analysis of [109].

In the next experiment, to examine the angular resolution of the methods, the RMSE values are extracted versus the angular gaps. The SNR is assumed to be 10 dB. When the DOA of the second NFS varies from $-35°$ to $-17°$, the RMSE of the DOA and range estimates are shown in Fig. 11. As can be seen, DOA CRBs are almost insensitive to the angular gap. In most methods, this trend is almost maintained up to $-19°$. However, when the second NFS is placed at $-17°$, most results are faced with a relatively severe error. The reason for this is reducing the spatial gap and approaching the source located at $-15°$. HOSTA and TSMDA are the only methods that even when the second NFS is located at $-17°$, the DOA of the first NFS follows the CRB behavior. This holds true for the DOA of the second FFS for the methods of HOSTA and [51]. The justification for this superiority in the case of HOSTA is the use of spatial-temporal statistics matrices that improve the resolution and estimation accuracy [98], [122]. In general, the angular resolution of none of the methods reaches less than 4°, and their performance is reduced by decreasing the angular gap. In the case of range CRBs, it can also be observed that they are almost insensitive to the angular gap. The range RMSEs of various methods behave almost similarly to the general pattern of DOA RMSEs of NFSs. The reason for this is that in all these methods, the range estimation is either jointly obtained by estimating the DOAs of the NFSs, or at a later stage by inputting the estimated values of the DOAs of the NFSs.

VI. CONCLUDING REMARKS

The exploration of DOA estimation and localization in scenarios involving mixed NFSs and FFSs has been the focus of extensive research efforts, as evidenced by the comprehensive review presented in the preceding sections. In this section, we summarize the key findings and highlight future research directions in this domain.

Firstly, the reviewed literature showcases a diverse array of methodologies and techniques employed for DOA estimation and localization assuming the coexistence of NFSs and FFSs. Various array types, including ULA, UCA, SLA, spherical array, SDNA, SFNA and STCA have been utilized, each with its own advantages and suitability for specific applications. Additionally, a wide range of assumptions and scenarios have been considered, encompassing non-Gaussian noise models, multipath environments, and unknown MC effects, among others.

Secondly, the type of statistics used in the different approaches varies, with some methods relying on HOS to capture the complex characteristics of mixed-field sources, while others leverage SOS for simplicity or computational efficiency. These statistical approaches form the basis of many DOA estimation algorithms, ranging from beamforming, sparse signal reconstruction and differencing to the RARE principle, oblique projection and ESPRIT-like techniques.

Thirdly, the performance evaluation of DOA estimation and localization methods in mixed-field sources scenario involves considerations such as aperture loss and computational complexity. The ability to resolve multiple sources and the computational resources required for implementation are crucial factors that influence the practical applicability of these methods. Comparative evaluations have provided insights into the strengths and limitations of different approaches in terms of their ability to handle complex scenarios and achieve accurate localization results.

Looking ahead, several avenues for future research emerge from the existing literature. One promising direction is the exploration of advanced signal processing techniques, such as compressive sensing and DL, to further enhance the accuracy and robustness of DOA estimation algorithms in mixed-field sources environments. Moreover, the integration of polarization diversity, employing metasurface antennas, the development of efficient algorithms based on exact NF models and one-bit measurements, tracking parameters, and the utilization of full-wave or experimental data offer opportunities to improve the performance of localization systems in real-world applications.

In conclusion, the study of DOA estimation and localization in scenarios involving mixed NFSs and FFSs is a multifaceted and dynamic field that continues to evolve

with advancements in signal processing, array design, and experimental techniques. By addressing the challenges posed by complex noise environments, multipath propagation, and unknown system parameters, researchers can develop more robust and reliable localization systems with broad applicability across domains such as radar, wireless communications, and acoustic sensing.

REFERENCES

[1] P. Gupta and S. P. Kar, "MUSIC and improved MUSIC algorithm to estimate direction of arrival," in *Proc. Int. Conf. Commun. Signal Process. (ICCSP)*, Apr. 2015, pp. 757–761.

[2] J. Benesty, I. Cohen, and J. Chen, *Fundamentals of Signal Enhancement and Array Signal Processing*. Hoboken, NJ, USA: Wiley, 2017.

[3] L.-L. Wu and Z.-T. Huang, "Coherent SVR learning for wideband direction-of-arrival estimation," *IEEE Signal Process. Lett.*, vol. 26, no. 4, pp. 642–646, Apr. 2019.

[4] J. R. Wilson, "New frontiers in passive radar and sonar," Mil. Aerosp. Electron., Mil. Technol., Weapons, Equip. Syst. Mil. Ind. Complex, Feb. 2016. [Online]. Available: https://www.militaryaerospace.com/communications/article/16709052/new-frontiers-in-passive-radar-and-sonar

[5] S. Zekavat, R. M. Buehrer, G. D. Durgin, L. Lovisolo, Z. Wang, S. T. Goh, and A. Ghasemi, "An overview on position location: Past, present, future," *Int. J. Wireless Inf. Netw.*, vol. 28, no. 1, pp. 45–76, Mar. 2021.

[6] S. Mathew, C. MacBeth, J. Stevanovic, and M.-D. Mangriotis, "Detection of dynamic phenomena associated with underground nuclear explosion using multiple seismic surveys and machine learning," *Pure Appl. Geophys.*, vol. 180, no. 4, pp. 1287–1301, Apr. 2023.

[7] B. Stump, C. Hayward, P. Golden, J. Park, R. Kubacki, C. Cain, S. Arrowsmith, M. H. M. Taylor, S. Jeong, T. Ivey, M. MacPhail, C. C. Pace, J.-S. Jeon, I.-Y. Che, K. Kim, B.-I. Kim, T.-S. Kim, I.-C. Shin, and M.-S. Jun, "Seismic and infrasound data recorded at regional seismoacoustic research arrays in South Korea from the six DPRK underground nuclear explosions," *Seismological Res. Lett.*, vol. 93, no. 4, pp. 2389–2400, Jul. 2022.

[8] A. Bertrand, "Applications and trends in wireless acoustic sensor networks: A signal processing perspective," in *Proc. 18th IEEE Symp. Commun. Veh. Technol. Benelux (SCVT)*, Nov. 2011, pp. 1–6.

[9] N. Yousefian and P. C. Loizou, "A dual-microphone speech enhancement algorithm based on the coherence function," *IEEE Trans. Audio, Speech, Language Process.*, vol. 20, no. 2, pp. 599–609, Feb. 2012.

[10] C. Li and D. Shi, "A novel spatial three-dimensional spherical array antenna for OAM waves generation," in *Proc. Photon. Electromagn. Res. Symp. Fall (PIERS-Fall)*, Dec. 2019, pp. 373–377.

[11] S. Senthilkumar, U. Surendar, X. S. Christina, and J. William, "A compact phased array antenna for 5G MIMO applications," *Wireless Pers. Commun.*, vol. 128, no. 3, pp. 2155–2174, Feb. 2023.

[12] Z. Yang, J. Li, P. Stoica, and L. Xie, "Sparse methods for direction-of-arrival estimation," in *Academic Press Library in Signal Processing*, vol. 7. Amsterdam, The Netherlands: Elsevier, 2018, pp. 509–581.

[13] E. Björnson, L. Sanguinetti, H. Wymeersch, J. Hoydis, and T. L. Marzetta, "Massive MIMO is a reality-what is next?: Five promising research directions for antenna arrays," *Digit. Signal Process.*, vol. 94, pp. 3–20, Nov. 2019.

[14] M. Muhammad, M. Li, Q. Abbasi, C. Goh, and M. A. Imran, "A covariance matrix reconstruction approach for single snapshot direction of arrival estimation," *Sensors*, vol. 22, no. 8, p. 3096, Apr. 2022.

[15] J. Luo, Y. Zhang, J. Yang, D. Zhang, Y. Zhang, Y. Zhang, Y. Huang, and A. Jakobsson, "Online sparse DOA estimation based on sub–aperture recursive LASSO for TDM-MIMO radar," *Remote Sens.*, vol. 14, no. 9, p. 2133, Apr. 2022.

[16] Z. Li, W. Wang, R. Jiang, S. Ren, X. Wang, and C. Xue, "Hardware acceleration of MUSIC algorithm for sparse arrays and uniform linear arrays," *IEEE Trans. Circuits Syst. I, Reg. Papers*, vol. 69, no. 7, pp. 2941–2954, Jul. 2022.

[17] J. Chen, J. Benesty, and Y. Huang, "Time delay estimation in room acoustic environments: An overview," *EURASIP J. Adv. Signal Process.*, vol. 2006, no. 1, pp. 1–19, Dec. 2006.

[18] W. S. Leite and R. C. de Lamare, "List-based OMP and an enhanced model for DOA estimation with nonuniform arrays," *IEEE Trans. Aerosp. Electron. Syst.*, vol. 57, no. 6, pp. 4457–4464, Dec. 2021.

[19] J. Foutz, A. Spanias, and M. Banavar, *Narrowband Direction of Arrival Estimation for Antenna Arrays*. Switzerland: Springer, 2022.

[20] P. Wang, Y. Kong, X. He, M. Zhang, and X. Tan, "An improved squirrel search algorithm for maximum likelihood DOA estimation and application for MEMS vector hydrophone array," *IEEE Access*, vol. 7, pp. 118343–118358, 2019.

[21] S. K. Yadav and N. V. George, "Coarray MUSIC-group delay: High-resolution source localization using non-uniform arrays," *IEEE Trans. Veh. Technol.*, vol. 70, no. 9, pp. 9597–9601, Sep. 2021.

[22] R. Schmidt, "Multiple emitter location and signal parameter estimation," *IEEE Trans. Antennas Propag.*, vol. AP-34, no. 3, pp. 276–280, Mar. 1986.

[23] R. Roy, A. Paulraj, and T. Kailath, "Estimation of signal parameters via rotational invariance techniques—ESPRIT," in *Proc. IEEE Mil. Commun. Conf. Commun. Comput. (MILCOM)*, Oct. 1986, pp. 41.6.1–41.6.5.

[24] Z.-B. Shen, C.-X. Dong, Y.-Y. Dong, G.-Q. Zhao, and L. Huang, "Broadband DOA estimation based on nested arrays," *Int. J. Antennas Propag.*, vol. 2015, pp. 1–7, Jan. 2015.

[25] S. Chakrabarty and E. A. P. Habets, "Broadband DOA estimation using convolutional neural networks trained with noise signals," in *Proc. IEEE Workshop Appl. Signal Process. Audio Acoust. (WASPAA)*, Oct. 2017, pp. 136–140.

[26] O. Neitz, R. A. M. Mauermayer, Y. Weitsch, and T. F. Eibert, "A propagating plane-wave-based near-field transmission equation for antenna gain determination from irregular measurement samples," *IEEE Trans. Antennas Propag.*, vol. 65, no. 8, pp. 4230–4238, Aug. 2017.

[27] H.-T. Chou, "Conformal near-field focus radiation from phased array of antennas to enhance power transfer between transmitting and receiving antennas," *IEEE Trans. Antennas Propag.*, vol. 68, no. 5, pp. 3567–3577, May 2020.

[28] A. Guerra, F. Guidi, D. Dardari, and P. M. Djuric, "Near-field tracking with large antenna arrays: Fundamental limits and practical algorithms," *IEEE Trans. Signal Process.*, vol. 69, pp. 5723–5738, 2021.

[29] A. M. Molaei, P. del Hougne, V. Fusco, and O. Yurduseven, "Efficient joint estimation of DOA, range and reflectivity in near-field by using mixed-order statistics and a symmetric MIMO array," *IEEE Trans. Veh. Technol.*, vol. 71, no. 3, pp. 2824–2842, Mar. 2022.

[30] P. Ramezani, Ö. T. Demir, and E. Björnson, "Localization in massive MIMO networks: From near-field to far-field," 2024, *arXiv:2402.07644*.

[31] P. Paitz, N. Lindner, P. Edme, P. Huguenin, M. Hohl, B. Sovilla, F. Walter, and A. Fichtner, "Phenomenology of avalanche recordings from distributed acoustic sensing," *J. Geophys. Res., Earth Surf.*, vol. 128, no. 5, May 2023, Art. no. e2022JF007011.

[32] A. M. Molaei, S. Hu, V. Skouroliakou, V. Fusco, X. Chen, and O. Yurduseven, "Fourier compatible near-field multiple-input multiple-output terahertz imaging with sparse non-uniform apertures," *IEEE Access*, vol. 9, pp. 157278–157294, 2021.

[33] S. Park, J. Ryu, and H. Kim, "Method for selecting network node in wireless communication system and device therefor," U.S. Patent 3 736 614 B2, Feb. 26, 2020.

[34] D. Pei, D. Gong, K. Liu, X. Zeng, S. Zhang, M. Chen, and K. Zheng, "MmCTD: Concealed threat detection for cruise ships via mmWave radar," *IEEE Trans. Veh. Technol.*, early access, Jan. 10, 2024, doi: 10.1109/TVT.2024.3352039.

[35] G. Giovannetti, N. Fontana, A. Flori, M. F. Santarelli, M. Tucci, V. Positano, S. Barmada, and F. Frijia, "Machine learning for the design and the simulation of radiofrequency magnetic resonance coils: Literature review, challenges, and perspectives," *Sensors*, vol. 24, no. 6, p. 1954, Mar. 2024.

[36] D. A. Horne, P. D. Jones, M. S. Adams, J. C. Lotz, and C. J. Diederich, "LIPUS far-field exposimetry system for uniform stimulation of tissues in-vitro: Development and validation with bovine intervertebral disc cells," *Biomed. Phys. Eng. Exp.*, vol. 6, no. 3, May 2020, Art. no. 035033.

[37] Q. H. Nguyen, A. B. Nagorski, D. V. Setty, R. L. Loud, and L. T. Mortellaro, "Cloud-based acoustic monitoring, analysis, and diagnostic for power generation system," U.S. Patent 2022 0068 057 A1, Mar. 3, 2022.

[38] G. M. Djuknic, "Method of measuring a pattern of electromagnetic radiation," U.S. Patent 6 657 596 B2, Dec. 2, 2003.

[39] T. Saeidi, I. Ismail, A. R. Alhawari, and W. P. Wen, "Near-field and far-field investigation of miniaturized UWB antenna for imaging of wood," *AIP Adv.*, vol. 9, 2019, Art. no. 035232.

[40] Z. Yang, *Wireless Power Transfer Platform for Hydrocephalus Intracranial Pressure Sensing and Shunt Control*. Madison, WI, USA: The University of Wisconsin-Madison, 2022.
[41] K. H. Pho, T. D. C. Ho, T. K. Tran, and W. K. Wong, "Moment generating function, expectation and variance of ubiquitous distributions with applications in decision sciences: A review," *Adv. Decis. Sci.*, vol. 23, no. 2, pp. 1–85, 2019.
[42] T. Iori and T. Ohtsuka, "Nonlinear Bayesian filtering via holonomic gradient method with quasi moment generating function," *Asian J. Control*, vol. 25, no. 4, pp. 2655–2670, Jul. 2023.
[43] F. Wu and X. Zhuang, "CF distance: A new domain discrepancy metric and application to explicit domain adaptation for cross-modality cardiac image segmentation," *IEEE Trans. Med. Imag.*, vol. 39, no. 12, pp. 4274–4285, Dec. 2020.
[44] J. Xu, J. Song, Q. Yu, and F. Kong, "Generalized distribution reconstruction based on the inversion of characteristic function curve for structural reliability analysis," *Rel. Eng. Syst. Saf.*, vol. 229, Jan. 2023, Art. no. 108768.
[45] L. Accardi and A. Boukas, "On the characteristic function of random variables associated with boson lie algebras," *Commun. Stochastic Anal.*, vol. 4, no. 4, p. 3, Dec. 2010.
[46] D. Pollard, "The moment generating function method," Yale Univ., Mini-Empirical Rep., 2021. [Online]. Available: http://www.stat.yale.edu/ pollard/Books/Mini/MGF.pdf
[47] Z. Gao, Z. Sun, and S. Liang, "Probability density function for wave elevation based on Gaussian mixture models," *Ocean Eng.*, vol. 213, Oct. 2020, Art. no. 107815.
[48] A. Boyle, A. Barthelemy, S. Codis, C. Uhlemann, and O. Friedrich, "The cumulant generating function as a novel observable to cumulate weak lensing information," 2022, *arXiv:2212.10351*.
[49] S. Mitra, P. Hegde, and C. Schmidt, "New way to resum the lattice QCD Taylor series equation of state at finite chemical potential," *Phys. Rev. D*, vol. 106, no. 3, Aug. 2022, Art. no. 034504.
[50] A. M. Molaei, B. Zakeri, and S. M. H. Andargoli, "A one-step algorithm for mixed far-field and near-field sources localization," *Digit. Signal Process.*, vol. 108, Jan. 2021, Art. no. 102899.
[51] K. Wang, L. Wang, J.-R. Shang, and X.-X. Qu, "Mixed near-field and far-field source localization based on uniform linear array partition," *IEEE Sensors J.*, vol. 16, no. 22, pp. 8083–8090, Nov. 2016.
[52] Z. Zheng, M. Fu, W.-Q. Wang, S. Zhang, and Y. Liao, "Localization of mixed near-field and far-field sources using symmetric double-nested arrays," *IEEE Trans. Antennas Propag.*, vol. 67, no. 11, pp. 7059–7070, Nov. 2019.
[53] H. Ma, H. Tao, and J. Xie, "Mixed far-field and near-field source localization using a linear tripole array," *IEEE Wireless Commun. Lett.*, vol. 9, no. 6, pp. 889–892, Jun. 2020.
[54] A. M. Molaei and M. Hoseinzade, "High-performance 2D DOA estimation and 3D localization for mixed near/far-field sources using fourth-order spatiotemporal algorithm," *Digit. Signal Process.*, vol. 100, May 2020, Art. no. 102696.
[55] H. Ma, H. Tao, and H. Kang, "Mixed far-field and near-field source localization using a linear electromagnetic-vector-sensor array with gain/phase uncertainties," *IEEE Access*, vol. 9, pp. 132412–132428, 2021.
[56] A. M. Molaei, B. Zakeri, and S. M. H. Andargoli, "Components separation algorithm for localization and classification of mixed near-field and far-field sources in multipath propagation," *IEEE Trans. Signal Process.*, vol. 68, pp. 404–419, 2020.
[57] H. J. Landau, "Sampling, data transmission, and the Nyquist rate," *Proc. IEEE*, vol. 55, no. 10, pp. 1701–1706, Oct. 1967.
[58] G. S. Bhat, *Real-Time Speech Processing Algorithms for Smartphone Based Hearing Aid Applications*. Dallas, TX, USA: The University of Texas, 2021.
[59] J. Wang, B. Wang, S. Li, and W. Yi, "DOA estimation for mixed field of distributed arrays," in *Proc. Int. Conf. Control, Autom. Inf. Sci. (ICCAIS)*, Oct. 2021, pp. 849–854.
[60] A. M. Molaei, B. Zakeri, and S. M. H. Andargoli, "Two-dimensional DOA estimation for multi-path environments by accurate separation of signals using k-medoids clustering," *IET Commun.*, vol. 13, no. 9, pp. 1141–1147, Jun. 2019.
[61] H. Fu, S. Abeywickrama, C. Yuen, and M. Zhang, "A robust phase-ambiguity-immune DOA estimation scheme for antenna array," *IEEE Trans. Veh. Technol.*, vol. 68, no. 7, pp. 6686–6696, Jul. 2019.
[62] D. Chen and Y. Joo, "Novel approach to 2D DOA estimation for uniform circular arrays using convolutional neural networks," *Int. J. Antennas Propag.*, vol. 2021, pp. 1–15, Jul. 2021.
[63] A. R. Carballeira, F. A. P. de Figueiredo, and J. M. C. Brito, "Simultaneous estimation of azimuth and elevation angles using a decision tree-based method," *Sensors*, vol. 23, no. 16, p. 7114, Aug. 2023.
[64] X. Ding, W. Xu, and Y. Wang, "Efficient wideband DoA estimation with a robust iterative method for uniform circular arrays," 2022, *arXiv:2210.16768*.
[65] D. He, X. Chen, L. Pei, F. Zhu, L. Jiang, and W. Yu, "Multi-BS spatial spectrum fusion for 2-D DOA estimation and localization using UCA in massive MIMO system," *IEEE Trans. Instrum. Meas.*, vol. 70, pp. 1–13, 2021.
[66] R. Chen, W.-X. Long, X. Wang, and L. Jiandong, "Multi-mode OAM radio waves: Generation, angle of arrival estimation and reception with UCAs," *IEEE Trans. Wireless Commun.*, vol. 19, no. 10, pp. 6932–6947, Oct. 2020.
[67] A. E. Willner, Z. Zhao, C. Liu, R. Zhang, H. Song, K. Pang, K. Manukyan, H. Song, X. Su, G. Xie, Y. Ren, Y. Yan, M. Tur, A. F. Molisch, R. W. Boyd, H. Zhou, N. Hu, A. Minoofar, and H. Huang, "Perspectives on advances in high-capacity, free-space communications using multiplexing of orbital-angular-momentum beams," *APL Photon.*, vol. 6, 2021, Art. no. 030901.
[68] L. Zuo, J. Pan, and Z. Shen, "Analytical algorithm for 3-D localization of a single source with uniform circular array," *IEEE Antennas Wireless Propag. Lett.*, vol. 17, pp. 323–326, 2018.
[69] A. M. Molaei and M. Hoseinzade, "Derivation of multidimensional stochastic Cramer–Rao bound for mixture of noncoherent and coherent near/far field signals," *Trans. Emerg. Telecommun. Technol.*, vol. 31, no. 6, Jun. 2020.
[70] G.-T. Lee, S.-M. Choi, B.-Y. Ko, and Y.-H. Park, "HRTF measurement for accurate sound localization cues," 2022, *arXiv:2203.03166*.
[71] H. Huang, H. C. So, and A. M. Zoubir, "Off-grid direction-of-arrival estimation using second-order Taylor approximation," *Signal Process.*, vol. 196, Jul. 2022, Art. no. 108513.
[72] P.-J. Chung, M. Viberg, and J. Yu, "DOA estimation methods and algorithms," in *Academic Press Library in Signal Processing*, vol. 3. Amsterdam, The Netherlands: Elsevier, 2014, pp. 599–650.
[73] K. Xu, W. Pedrycz, Z. Li, and W. Nie, "High-accuracy signal subspace separation algorithm based on Gaussian kernel soft partition," *IEEE Trans. Ind. Electron.*, vol. 66, no. 1, pp. 491–499, Jan. 2019.
[74] R. Muhamed, "Direction of arrival estimation using antenna arrays," M.S. thesis, Dept. Elect. Eng., Virginia Tech, Blacksburg, VA, USA, 1996.
[75] B. Friedlander, "Localization of signals in the near-field of an antenna array," *IEEE Trans. Signal Process.*, vol. 67, no. 15, pp. 3885–3893, Aug. 2019.
[76] J. Zhen and Y. Liu, "DOA estimation for mixed signals with gain-phase error array," *J. Syst. Eng. Electron.*, vol. 28, no. 6, pp. 1046–1056, Dec. 2017.
[77] J. Liang and D. Liu, "Passive localization of mixed near-field and far-field sources using two-stage MUSIC algorithm," *IEEE Trans. Signal Process.*, vol. 58, no. 1, pp. 108–120, Jan. 2010.
[78] D. Wang, P. Qi, Q. Fu, N. Zhang, and Z. Li, "Multiple high-order cumulants-based spectrum sensing in full-duplex-enabled cognitive IoT networks," *IEEE Internet Things J.*, vol. 8, no. 11, pp. 9330–9343, Jun. 2021.
[79] Q. He, Z. Cheng, Z. Wang, and Z. He, "Mixed far-field and near-field source separation and localization based on FOC matrix differencing," *Digit. Signal Process.*, vol. 131, Nov. 2022, Art. no. 103753.
[80] M. Kuang, Y. Wang, L. Wang, J. Xie, and C. Han, "Localisation and classification of mixed far-field and near-field sources with sparse reconstruction," *IET Signal Process.*, vol. 16, no. 4, pp. 426–437, Jun. 2022.
[81] J. He, M. N. S. Swamy, and M. O. Ahmad, "Efficient application of MUSIC algorithm under the coexistence of far-field and near-field sources," *IEEE Trans. Signal Process.*, vol. 60, no. 4, pp. 2066–2070, Apr. 2012.
[82] A. M. Molaei, A. Ramezani-Varkani, and M. R. Soheilifar, "A pure cumulant-based method with low computational complexity for classification and localization of multiple near and far field sources using a symmetric array," *Prog. Electromagn. Res. C*, vol. 96, pp. 123–138, 2019.
[83] G. Liu, X. Sun, Y. Liu, and Y. Qin, "Low-complexity estimation of signal parameters via rotational invariance techniques algorithm for mixed far-field and near-field cyclostationary sources localisation," *IET Signal Process.*, vol. 7, no. 5, pp. 382–388, Jul. 2013.
[84] A. Napolitano, "Cyclostationarity: New trends and applications," *Signal Process.*, vol. 120, pp. 385–408, Mar. 2016.

[85] F. Sekak, F. Elbahhar, and M. Haddad, "Study and evaluation of the vital signs detection based on the third order cyclic temporal moment and cumulant," *IEEE Access*, vol. 10, pp. 59603–59611, 2022.

[86] H. Abdi, "Singular value decomposition (SVD) and generalized singular value decomposition," in *Encyclopedia of Measurement and Statistics*. Thousand Oaks, CA, USA: SAGE, 2007, pp. 907–912.

[87] B. Wang, Y. Zhao, and J. Liu, "Mixed-order MUSIC algorithm for localization of far-field and near-field sources," *IEEE Signal Process. Lett.*, vol. 20, no. 4, pp. 311–314, Apr. 2013.

[88] Y. Ma, Y. Zeng, and S. Sun, "A deep learning based super resolution DoA estimator with single snapshot MIMO radar data," *IEEE Trans. Veh. Technol.*, vol. 71, no. 4, pp. 4142–4155, Apr. 2022.

[89] F. Gao and A. B. Gershman, "A generalized ESPRIT approach to direction-of-arrival estimation," *IEEE Signal Process. Lett.*, vol. 12, no. 3, pp. 254–257, Mar. 2005.

[90] T. Shu, L. Li, and J. He, "Near-field localization for non-circular sources in the presence of sensor phase uncertainties," *IEEE Wireless Commun. Lett.*, vol. 10, no. 3, pp. 562–566, Mar. 2021.

[91] J.-J. Jiang, F.-J. Duan, J. Chen, Y.-C. Li, and X.-N. Hua, "Mixed near-field and far-field sources localization using the uniform linear sensor array," *IEEE Sensors J.*, vol. 13, no. 8, pp. 3136–3143, Aug. 2013.

[92] G. Liu and X. Sun, "Efficient method of passive localization for mixed far-field and near-field sources," *IEEE Antennas Wireless Propag. Lett.*, vol. 12, pp. 902–905, 2013.

[93] G. Liu and X. Sun, "Spatial differencing method for mixed far-field and near-field sources localization," *IEEE Signal Process. Lett.*, vol. 21, no. 11, pp. 1331–1335, Nov. 2014.

[94] G. Liu and X. Sun, "Two-stage matrix differencing algorithm for mixed far-field and near-field sources classification and localization," *IEEE Sensors J.*, vol. 14, no. 6, pp. 1957–1965, Jun. 2014.

[95] F. Xu, X. Yang, and T. Lan, "Search-free direction-of-arrival estimation for transmit beamspace multiple-input multiple-output radar via tensor modelling and polynomial rooting," *IET Radar, Sonar Navigat.*, vol. 15, no. 6, pp. 574–580, Jun. 2021.

[96] C. Cheng, S. Liu, H. Wu, and Y. Zhang, "Mixed-field source localization based on robust matrix propagator and reduced-degree polynomial rooting," *Signal Process.*, vol. 208, Jul. 2023, Art. no. 108988.

[97] S. A. Mojallal, J.-H. Jung, G.-S. Cheon, S.-R. Kim, and B. Kang, "Structural properties of Toeplitz graphs," *Discrete Math.*, vol. 345, no. 11, Nov. 2022, Art. no. 113016.

[98] A. M. Molaei, B. Zakeri, and S. M. H. Andargoli, "High-performance localization of mixed fourth-order stationary sources based on a spatial/temporal full ESPRIT-like method," *Signal Process.*, vol. 171, Jun. 2020, Art. no. 107468.

[99] J. Xie, H. Tao, X. Rao, and J. Su, "Comments on 'near-field source localization via symmetric subarrays,'" *IEEE Signal Process. Lett.*, vol. 22, no. 5, pp. 643–644, May 2015.

[100] B. Wang, J. Liu, and X. Sun, "Mixed sources localization based on sparse signal reconstruction," *IEEE Signal Process. Lett.*, vol. 19, no. 8, pp. 487–490, Aug. 2012.

[101] Y. Tian and X. Sun, "Mixed sources localisation using a sparse representation of cumulant vectors," *IET Signal Process.*, vol. 8, no. 6, pp. 606–611, Aug. 2014.

[102] Y. Tian and X. Sun, "Passive localization of mixed sources jointly using MUSIC and sparse signal reconstruction," *AEU Int. J. Electron. Commun.*, vol. 68, no. 6, pp. 534–539, Jun. 2014.

[103] E. Aboutanios and S. A. Vorobyov, "Advances in DOA estimation and source localization," *Int. J. Antennas Propag.*, vol. 2017, Aug. 2017, Art. no. 1352598.

[104] J. Xie, H. Tao, X. Rao, and J. Su, "Passive localization of mixed far-field and near-field sources without estimating the number of sources," *Sensors*, vol. 15, no. 2, pp. 3834–3853, Feb. 2015.

[105] J. Xie, L. Wang, and J. Su, "Parameters estimation of mixed far-field and near-field sources via second order statistics," in *Proc. Int. Appl. Comput. Electromagn. Soc. Symp. (ACES)*, Aug. 2017, pp. 1–2.

[106] Z. Zheng, J. Sun, W.-Q. Wang, and H. Yang, "Classification and localization of mixed near-field and far-field sources using mixed-order statistics," *Signal Process.*, vol. 143, pp. 134–139, Feb. 2018.

[107] Z. Zheng, M. Fu, D. Jiang, W.-Q. Wang, and S. Zhang, "Localization of mixed far-field and near-field sources via cumulant matrix reconstruction," *IEEE Sensors J.*, vol. 18, no. 18, pp. 7671–7680, Sep. 2018.

[108] A. M. Molaei, P. Del Hougne, V. Fusco, and O. Yurduseven, "Numerical-analytical study of performance of mixed-order statistics algorithm for joint estimation of DOA, range and backscatter coefficient in a MIMO structure," in *Proc. 23rd Int. Radar Symp. (IRS)*, Sep. 2022, pp. 396–401.

[109] N. Yuen and B. Friedlander, "Performance analysis of higher order ESPRIT for localization of near-field sources," *IEEE Trans. Signal Process.*, vol. 46, no. 3, pp. 709–719, Mar. 1998.

[110] R. N. Challa and S. Shamsunder, "High-order subspace-based algorithms for passive localization of near-field sources," in *Proc. Conf. Rec. 29th Asilomar Conf. Signals, Syst. Comput.*, vol. 2, Oct. 1995, pp. 777–781.

[111] A. M. Molaei, B. Zakeri, and S. M. H. Andargoli, "Passive localization and classification of mixed near-field and far-field sources based on high-order differencing algorithm," *Signal Process.*, vol. 157, pp. 119–130, Apr. 2019.

[112] E. M. Al-Ardi, R. M. Shubair, and M. E. Al-Mualla, "Investigation of high-resolution DOA estimation algorithms for optimal performance of smart antenna systems," in *Proc. 4th Int. Conf. 3G Mobile Commun. Technol.*, Jun. 2003, pp. 460–464.

[113] Y. Zhang, G. Zhang, and H. Leung, "Grid-less coherent DOA estimation based on fourth-order cumulants with Gaussian coloured noise," *IET Radar, Sonar Navigat.*, vol. 14, no. 5, pp. 677–685, May 2020.

[114] L. Saidi, J. B. Ali, E. Bechhoefer, and M. Benbouzid, "Wind turbine high-speed shaft bearings health prognosis through a spectral kurtosis-derived indices and SVR," *Appl. Acoust.*, vol. 120, pp. 1–8, May 2017.

[115] P. Stoica and R. L. Moses, *Spectral Analysis of Signals*. Upper Saddle River, NJ, USA: Prentice-Hall, 2005.

[116] O. Das, J. S. Abel, and J. O. Smith III, "FAST MUSIC-an efficient implementation of the MUSIC algorithm for frequency estimation of approximately periodic signals," in *Proc. 21st Int. Conf. Digital Audio Effects*, Sep. 2018, pp. 1–7.

[117] M. Kim, K. Ichige, and H. Arai, "Implementation of FPGA based fast DOA estimator using unitary MUSIC algorithm [cellular wireless base station applications]," in *Proc. IEEE 58th Veh. Technol. Conf. (VTC-Fall)*, vol. 1, Oct. 2003, pp. 213–217.

[118] U. M. Butt, S. A. Khan, A. Ullah, A. Khaliq, P. Reviriego, and A. Zahir, "Towards low latency and resource-efficient FPGA implementations of the MUSIC algorithm for direction of arrival estimation," *IEEE Trans. Circuits Syst. I, Reg. Papers*, vol. 68, no. 8, pp. 3351–3362, Aug. 2021.

[119] G. K. Gokeda, "Performance analysis of ESPRIT based algorithms for DOA estimation," M.S. thesis, Dept. Elect. Comput. Eng., Dalhousie Univ., Canada, May 2002.

[120] A. L. Swindlehurst, B. D. Jeffs, G. Seco-Granados, and J. Li, "Applications of array signal processing," in *Academic Press Library in Signal Processing*, vol. 3. Amsterdam, The Netherlands: Elsevier, 2014, pp. 859–953.

[121] H. Krim and M. Viberg, "Two decades of array signal processing research: The parametric approach," *IEEE Signal Process. Mag.*, vol. 13, no. 4, pp. 67–94, Jul. 1996.

[122] K. Kim, T. K. Sarkar, H. Wang, and M. Salazar-Palma, "Direction of arrival estimation based on temporal and spatial processing using a direct data domain (D^3) approach," *IEEE Trans. Antennas Propag.*, vol. 52, no. 2, pp. 533–541, Feb. 2004.

[123] S. Ouelha, A. Aïssa-El-Bey, and B. Boashash, "Improving DOA estimation algorithms using high-resolution quadratic time-frequency distributions," *IEEE Trans. Signal Process.*, vol. 65, no. 19, pp. 5179–5190, Oct. 2017.

[124] H. Lee, J. Ahn, Y. Kim, and J. Chung, "Direction-of-arrival estimation of far-field sources under near-field interferences in passive sonar array," *IEEE Access*, vol. 9, pp. 28413–28420, 2021.

[125] B. Xue, G. Fang, and Y. Ji, "Passive localisation of mixed far-field and near-field sources using uniform circular array," *Electron. Lett.*, vol. 52, no. 20, pp. 1690–1692, Sep. 2016.

[126] B. Xue, G. Fang, and Y.-C. Ji, "Efficient localization algorithm of mixed far-field and near-field sources using uniform circular array," *Prog. Electromagn. Res. M*, vol. 51, pp. 139–146, 2016.

[127] J. H. Lee, D. H. Park, G. T. Park, and K. K. Lee, "Algebraic path-following algorithm for localising 3-D near-field sources in uniform circular array," *Electron. Lett.*, vol. 39, no. 17, pp. 1283–1285, 2003.

[128] K. Wang, L. Wang, J. Xie, and M. Tao, "Classification and localization of mixed sources using uniform circular array under unknown mutual coupling," *Radioengineering*, vol. 27, no. 1, pp. 220–229, Apr. 2019.

[129] M. Fu, Z. Zheng, and W.-Q. Wang, "2-D DOA estimation for nested conformal arrays via sparse reconstruction," *IEEE Commun. Lett.*, vol. 25, no. 3, pp. 980–984, Mar. 2021.
[130] S. Qin, Y. D. Zhang, and M. G. Amin, "Improved two-dimensional DOA estimation using parallel coprime arrays," *Signal Process.*, vol. 172, Jul. 2020, Art. no. 107428.
[131] T. Erpek, T. J. O'Shea, Y. E. Sagduyu, Y. Shi, and T. C. Clancy, "Deep learning for wireless communications," in *Development and Analysis of Deep Learning Architectures*. Cham, Switzerland: Springer, 2020, pp. 223–266.
[132] N. Xie, Z. Li, and H. Tan, "A survey of physical-layer authentication in wireless communications," *IEEE Commun. Surveys Tuts.*, vol. 23, no. 1, pp. 282–310, 1st Quart., 2021.
[133] H. Shi, W. Leng, A. Wang, and T. Guo, "DOA estimation for mixed uncorrelated and coherent sources in multipath environment," *Int. J. Antennas Propag.*, vol. 2015, pp. 1–8, Jan. 2015.
[134] L. Wan, G. Han, J. J. P. C. Rodrigues, W. Si, and N. Feng, "An energy efficient DOA estimation algorithm for uncorrelated and coherent signals in virtual MIMO systems," *Telecommun. Syst.*, vol. 59, no. 1, pp. 93–110, May 2015.
[135] Y. Fang, S. Zhu, Y. Gao, and C. Zeng, "DOA estimation for coherent signals with improved sparse representation in the presence of unknown spatially correlated Gaussian noise," *IEEE Trans. Veh. Technol.*, vol. 69, no. 9, pp. 10059–10069, Sep. 2020.
[136] B.-S. Chen, C.-Y. Yang, and W.-J. Liao, "Robust fast time-varying multipath fading channel estimation and equalization for MIMO-OFDM systems via a fuzzy method," *IEEE Trans. Veh. Technol.*, vol. 61, no. 4, pp. 1599–1609, May 2012.
[137] F. A. P. de Figueiredo, F. S. Mathilde, F. P. Santos, F. A. C. M. Cardoso, and G. Fraidenraich, "On channel estimation for massive MIMO with pilot contamination and multipath fading channels," in *Proc. 8th IEEE Latin-American Conf. Commun. (LATINCOM)*, Nov. 2016, pp. 1–4.
[138] B. Jin and M. I. Vai, "An adaptive ultrasonic backscattered signal processing technique for instantaneous characteristic frequency detection," *Bio-Med. Mater. Eng.*, vol. 24, no. 6, pp. 2761–2770, 2014.
[139] B. M. Eckert, L. Rigazio, N. Khosla, and K. R. Joshi, "System and method for processing wireless backscattered signal using artificial intelligence processing for activities of daily life," U.S. Patent 2019 0057 777 A1, Jan. 7, 2021.
[140] C. Cheng, Y. Jiang, and Q. Sun, "Spatially distributed sampling and reconstruction," *Appl. Comput. Harmon. Anal.*, vol. 47, no. 1, pp. 109–148, Jul. 2019.
[141] J. Ye, A. Kammoun, and M.-S. Alouini, "Spatially-distributed RISs vs relay-assisted systems: A fair comparison," *IEEE Open J. Commun. Soc.*, vol. 2, pp. 799–817, 2021.
[142] A. M. Elbir, "Direction finding in the presence of array imperfections, model mismatches and multipath," Ph.D. thesis, Dept. Elect. Electron. Eng., Middle East Tech. Univ., Ankara, Turkey, 2016.
[143] O. J. Famoriji and T. Shongwe, "Source localization of EM waves in the near-field of spherical antenna array in the presence of unknown mutual coupling," *Wireless Commun. Mobile Comput.*, vol. 2021, pp. 1–14, Dec. 2021.
[144] A. Xhafa, F. Fabra, J. A. López-Salcedo, and G. Seco-Granados, "Preliminary results of 5G direction of arrival estimation using in-situ calibration with USRP," in *Proc. Int. Conf. Localization GNSS (ICL-GNSS)*, 2023, pp. 1–8.
[145] N. Peccarelli and C. Fulton, "A mutual coupling approach to digital predistortion and nonlinear equalization calibration for digital arrays," in *Proc. IEEE Int. Symp. Phased Array Syst. Technol. (PAST)*, Oct. 2019, pp. 1–8.
[146] W. Hu and Q. Wang, "DOA estimation for UCA in the presence of mutual coupling via error model equivalence," *IEEE Wireless Commun. Lett.*, vol. 9, no. 1, pp. 121–124, Jan. 2020.
[147] X. Han, M. Liu, S. Zhang, R. Zheng, and J. Lan, "A passive DOA estimation algorithm of underwater multipath signals via spatial time-frequency distributions," *IEEE Trans. Veh. Technol.*, vol. 70, no. 4, pp. 3439–3455, Apr. 2021.
[148] S. U. Pillai, *Array Signal Processing*. New York, NY, USA: Springer, 2012.
[149] H. Gantayat, T. Panigrahi, and P. Patra, "An efficient direction-of-arrival estimation of multipath signals with impulsive noise using satin bowerbird optimization-based deep learning neural network," *Expert Syst.*, vol. 41, no. 6, Jun. 2024, Art. no. e13108.
[150] P. Han, B. Ba, H. Xu, H. Li, and T. Qin, "Direction finding for both uncorrelated and coherent signals in improved uniform circular array," in *Proc. IEEE 8th Joint Int. Inf. Technol. Artif. Intell. Conf. (ITAIC)*, May 2019, pp. 553–558.
[151] J. Pan, M. Sun, Y. Wang, and X. Zhang, "An enhanced spatial smoothing technique with ESPRIT algorithm for direction of arrival estimation in coherent scenarios," *IEEE Trans. Signal Process.*, vol. 68, pp. 3635–3643, 2020.
[152] A. M. Molaei, B. Zakeri, and S. M. H. Andargoli, "Efficient clustering of non-coherent and coherent components regardless of Sources' powers for 2D DOA estimation," *Circuits, Syst., Signal Process.*, vol. 40, no. 2, pp. 756–771, Feb. 2021.
[153] A. M. Molaei, B. Zakeri, and S. M. H. Andargoli, "Closed-form expression of stochastic CRB for mixed near-field and far-field sources in multipath propagation environments," *IEEE Commun. Lett.*, vol. 23, no. 4, pp. 640–643, Apr. 2019.
[154] F. Liu, J. Wang, C. Sun, and R. Du, "Spatial differencing method for DOA estimation under the coexistence of both uncorrelated and coherent signals," *IEEE Trans. Antennas Propag.*, vol. 60, no. 4, pp. 2052–2062, Apr. 2012.
[155] E. Grosicki, K. Abed-Meraim, and Y. Hua, "A weighted linear prediction method for near-field source localization," *IEEE Trans. Signal Process.*, vol. 53, no. 10, pp. 3651–3660, Oct. 2005.
[156] J. Benesty, J. Chen, and Y. Huang, *Microphone Array Signal Processing*. Berlin, Germany: Springer, 2008.
[157] O. J. Famoriji and T. Shongwe, "Critical review of basic methods on DoA estimation of EM waves impinging a spherical antenna array," *Electronics*, vol. 11, no. 2, p. 208, Jan. 2022.
[158] Z. Zheng, Y. Huang, W.-Q. Wang, and H. C. So, "Augmented covariance matrix reconstruction for DOA estimation using difference coarray," *IEEE Trans. Signal Process.*, vol. 69, pp. 5345–5358, 2021.
[159] A. M. Elbir and T. E. Tuncer, "Far-field DOA estimation and near-field localization for multipath signals," *Radio Sci.*, vol. 49, no. 9, pp. 765–776, Sep. 2014.
[160] A. M. Elbir and T. E. Tuncer, "Direction finding and localization for far-field sources with near-field multipath reflections," in *Proc. IEEE Signal Process. Signal Process. Educ. Workshop (SP/SPE)*, Aug. 2015, pp. 130–135.
[161] J. Peng, G. Zheng, and Q. Zhu, "A novel weighted spatial smoothing DOA estimation algorithm for coherent signals," in *Proc. IEEE 3rd Int. Conf. Electron. Inf. Commun. Technol. (ICEICT)*, Nov. 2020, pp. 504–508.
[162] M. Yang, Y. Zhang, Y. Sun, and X. Zhang, "An enhanced spatial smoothing technique of coherent DOA estimation with moving coprime array," *Sensors*, vol. 23, no. 19, p. 8048, Sep. 2023.
[163] Y. Zhang, Z. Ye, and C. Liu, "Estimation of fading coefficients in the presence of multipath propagation," *IEEE Trans. Antennas Propag.*, vol. 57, no. 7, pp. 2220–2224, Jul. 2009.
[164] M. Hasib, S. Kandeepan, W. S. T. Rowe, and A. Al-Hourani, "Direction-of-arrival (DoA) estimation performance for satellite applications in a multipath environment with Rician fading and spatial correlation," *Sensors*, vol. 23, no. 12, p. 5458, Jun. 2023.
[165] B. Amjad, Q. Z. Ahmed, P. I. Lazaridis, M. Hafeez, F. A. Khan, and Z. D. Zaharis, "Radio SLAM: A review on radio-based simultaneous localization and mapping," *IEEE Access*, vol. 11, pp. 9260–9278, 2023.
[166] H. Kim, H. Chen, M. F. Keskin, Y. Ge, K. Keykhosravi, G. C. Alexandropoulos, S. Kim, and H. Wymeersch, "RIS-enabled and access-point-free simultaneous radio localization and mapping," *IEEE Trans. Wireless Commun.*, vol. 23, no. 4, pp. 3344–3360, Apr. 2024.
[167] R. Liu, Q. Wu, M. Di Renzo, and Y. Yuan, "A path to smart radio environments: An industrial viewpoint on reconfigurable intelligent surfaces," *IEEE Wireless Commun.*, vol. 29, no. 1, pp. 202–208, Feb. 2022.
[168] M. Khalily, O. Yurduseven, T. J. Cui, Y. Hao, and G. V. Eleftheriades, "Engineered electromagnetic metasurfaces in wireless communications: Applications, research frontiers and future directions," *IEEE Commun. Mag.*, vol. 60, no. 10, pp. 88–94, Oct. 2022.
[169] G. Chandrasekaran, M. A. Ergin, J. Yang, S. Liu, Y. Chen, M. Gruteser, and R. P. Martin, "Empirical evaluation of the limits on localization using signal strength," in *Proc. 6th Annu. IEEE Commun. Soc. Conf. Sensor, Mesh Ad Hoc Commun. Netw.*, Jun. 2009, pp. 1–9.
[170] A. N. D'Andrea, U. Mengali, and R. Reggiannini, "The modified Cramer–Rao bound and its application to synchronization problems," *IEEE Trans. Commun.*, vol. 42, no. 234, pp. 1391–1399, Apr. 1994.

[171] J. P. Delmas, "Performance bounds and statistical analysis of DOA estimation," in *Academic Press Library in Signal Processing*, vol. 3. Amsterdam, The Netherlands: Elsevier, 2014, pp. 719–764.

[172] E. Nitzan, T. Routtenberg, and J. Tabrikian, "Cramér–Rao bound for constrained parameter estimation using Lehmann-unbiasedness," *IEEE Trans. Signal Process.*, vol. 67, no. 3, pp. 753–768, Feb. 2019.

[173] P. Stoica, E. G. Larsson, and A. B. Gershman, "The stochastic CRB for array processing: A textbook derivation," *IEEE Signal Process. Lett.*, vol. 8, no. 5, pp. 148–150, May 2001.

[174] J. P. Delmas, M. N. El Korso, H. Gazzah, and M. Castella, "CRB analysis of planar antenna arrays for optimizing near-field source localization," *Signal Process.*, vol. 127, pp. 117–134, Oct. 2016.

[175] X. Lan, L. Wan, G. Han, and J. Rodrigues, "A novel DOA estimation algorithm using array rotation technique," *Future Internet*, vol. 6, no. 1, pp. 155–170, Mar. 2014.

[176] J.-P. Delmas and H. Gazzah, "CRB analysis of near-field source localization using uniform circular arrays," in *Proc. IEEE Int. Conf. Acoust., Speech Signal Process.*, May 2013, pp. 3996–4000.

[177] J. J. Handfield, R. M. Rao, and S. A. Dianat, "Near-field MVDR source localization," *Proc. SPIE*, vol. 6980, pp. 218–226, Apr. 2008.

[178] M. N. El Korso, A. Renaux, R. Boyer, and S. Marcos, "Deterministic performance bounds on the mean square error for near field source localization," *IEEE Trans. Signal Process.*, vol. 61, no. 4, pp. 871–877, Feb. 2013.

[179] B. Friedlander, "Comments on 'localization of near-field sources based on linear prediction and oblique projection operator,'" *IEEE Trans. Signal Process.*, vol. 69, pp. 6399–6400, 2021.

[180] Z. Ebadi, A. M. Molaei, M. A. B. Abbasi, S. Cotton, A. Tukmanov, and O. Yurduseven, "Electromagnetic informed data model considerations for near-field DOA and range estimates," *Sci. Rep.*, 2024.

[181] P. R. Singh, Y. Wang, and P. Charge, "Near field targets localization using bistatic MIMO system with spherical wavefront based model," in *Proc. 25th Eur. Signal Process. Conf. (EUSIPCO)*, Aug. 2017, pp. 2408–2412.

[182] P. Singh, Y. Wang, and P. Chargé, "An exact model-based method for near-field sources localization with bistatic MIMO system," *Sensors*, vol. 17, no. 4, p. 723, Mar. 2017.

[183] H. Chen, W. Wang, W. Liu, Y. Tian, and G. Wang, "An exact near-field model based localization for bistatic MIMO radar with COLD arrays," *IEEE Trans. Veh. Technol.*, vol. 72, no. 12, pp. 16021–16030, Dec. 2023.

[184] K. Yin, Y. Dai, and C. Gao, "Mixed near-field and far-field source localization using COLD arrays," *Circuits, Syst., Signal Process.*, vol. 41, no. 6, pp. 3642–3655, Jun. 2022.

[185] T. Li, *Underwater Direction-of-Arrival Finding: Maximum Likelihood Estimation and Performance Analysis*. St. Louis, MO, USA: Washington University, 2012.

[186] A. Asadzadeh, S. M. Alavi, M. Karimi, and H. Amiri, "A new wideband beamforming by fuzzy system for coherent signals," *Digit. Signal Process.*, vol. 96, Jan. 2020, Art. no. 102588.

[187] H. Sarieddeen, M.-S. Alouini, and T. Y. Al-Naffouri, "An overview of signal processing techniques for terahertz communications," *Proc. IEEE*, vol. 109, no. 10, pp. 1628–1665, Oct. 2021.

[188] W.-F. Lin, W.-D. Ma, M. Xie, L.-X. Xu, and P. Wei, "Direction-of-arrival and range estimation of wideband sources in the near field," *MATEC Web Conf.*, vol. 128, p. 01013, Oct. 2017.

[189] Q. Huang and T. Wang, "Acoustic source localization in mixed field using spherical microphone arrays," *EURASIP J. Adv. Signal Process.*, vol. 2014, no. 1, pp. 1–16, Dec. 2014.

[190] B. Rafaely, "Analysis and design of spherical microphone arrays," *IEEE Trans. Speech Audio Process.*, vol. 13, no. 1, pp. 135–143, Jan. 2005.

[191] T. Li, "A state-of-the-art review of measurement techniques on tire–pavement interaction noise," *Measurement*, vol. 128, pp. 325–351, Nov. 2018.

[192] J. Zhen and Y. Li, "DOA estimation for far-field sources in mixed signals with gain-phase error array," in *Proc. Int. Conf. Communicatins Netw.* Cham, Switzerland: Springer, 2017, pp. 41–50.

[193] S. Roshani, S. Koziel, S. I. Yahya, M. A. Chaudhary, Y. Y. Ghadi, S. Roshani, and L. Golunski, "Mutual coupling reduction in antenna arrays using artificial intelligence approach and inverse neural network surrogates," *Sensors*, vol. 23, no. 16, p. 7089, Aug. 2023.

[194] Z. Ebadi, A. M. Molaei, M. A. B. Abbasi, S. Cotton, A. Tukmanov, and O. Yurduseven, "Near-field localization with an exact propagation model in presence of mutual coupling," in *Proc. IEEE Veh. Technol. Conf.*, Jun. 2024.

[195] C. A. Balanis, *Antenna Theory: Analysis and Design*. Hoboken, NJ, USA: Wiley, 2016.

[196] D.-G. Fang, *Antenna Theory and Microstrip Antennas*. Boca Raton, FL, USA: CRC Press, 2017.

[197] T. S. Rappaport, Y. Xing, O. Kanhere, S. Ju, A. Madanayake, S. Mandal, A. Alkhateeb, and G. C. Trichopoulos, "Wireless communications and applications above 100 GHz: Opportunities and challenges for 6G and beyond," *IEEE Access*, vol. 7, pp. 78729–78757, 2019.

[198] I. F. Akyildiz, A. Kak, and S. Nie, "6G and beyond: The future of wireless communications systems," *IEEE Access*, vol. 8, pp. 133995–134030, 2020.

[199] P. E. Green, R. A. Frosch, and C. F. Romney, "Principles of an experimental large aperture seismic array (LASA)," *Proc. IEEE*, vol. 53, no. 12, pp. 1821–1833, Dec. 1965.

[200] A. M. Molaei, S. Hu, V. Skouroliakou, V. Fusco, X. Chen, and O. Yurduseven, "Fast processing approach for near-field terahertz imaging with linear sparse periodic array," *IEEE Sensors J.*, vol. 22, no. 5, pp. 4410–4424, Mar. 2022.

[201] S. Pawar, D. Lee, H. Skinner, S.-Y. Suh, and A. Yakovlev, "Decoupling and cloaking of rectangular and circular patch antennas and interleaved antenna arrays with planar coated metasurfaces at C-band frequencies—Design and simulation study," *Sensors*, vol. 24, no. 1, p. 291, Jan. 2024.

[202] M. Alibakhshikenari, M. Khalily, B. S. Virdee, C. H. See, R. A. Abd-Alhameed, and E. Limiti, "Mutual-coupling isolation using embedded metamaterial EM bandgap decoupling slab for densely packed array antennas," *IEEE Access*, vol. 7, pp. 51827–51840, 2019.

[203] M. Alibakhshikenari, M. Khalily, B. S. Virdee, C. H. See, R. A. Abd-Alhameed, and E. Limiti, "Mutual coupling suppression between two closely placed microstrip patches using EM-bandgap metamaterial fractal loading," *IEEE Access*, vol. 7, pp. 23606–23614, 2019.

[204] E. Fritz-Andrade, H. Jardon-Aguilar, and J. A. Tirado-Mendez, "Mutual coupling reduction of two 2×1 triangular-patch antenna array using a single neutralization line for MIMO applications," *Radioengineering*, vol. 27, no. 4, pp. 976–982, Sep. 2018.

[205] K. Vasu Babu and B. Anuradha, "Design of Wang shape neutralization line antenna to reduce the mutual coupling in MIMO antennas," *Anal. Integr. Circuits Signal Process.*, vol. 101, no. 1, pp. 67–76, Oct. 2019.

[206] N. Parhizgar, "A new mutual coupling compensation method for receiving antenna array-based DOA estimation," *Arch. Electr. Eng.*, vol. 67, no. 2, pp. 419–431, Jan. 2024.

[207] P. Kumar, T. Ali, and M. M. M. Pai, "Electromagnetic metamaterials: A new paradigm of antenna design," *IEEE Access*, vol. 9, pp. 18722–18751, 2021.

[208] C. Milias, R. B. Andersen, P. I. Lazaridis, Z. D. Zaharis, B. Muhammad, J. T. B. Kristensen, A. Mihovska, and D. D. S. Hermansen, "Metamaterial-inspired antennas: A review of the state of the art and future design challenges," *IEEE Access*, vol. 9, pp. 89846–89865, 2021.

[209] S. Henault, S. K. Podilchak, S. M. Mikki, and Y. M. M. Antar, "A methodology for mutual coupling estimation and compensation in antennas," *IEEE Trans. Antennas Propag.*, vol. 61, no. 3, pp. 1119–1131, Mar. 2013.

[210] H. Singh, H. L. Sneha, and R. M. Jha, "Mutual coupling in phased arrays: A review," *Int. J. Antennas Propag.*, vol. 2013, pp. 1–23, Jan. 2013.

[211] I. Nadeem and D.-Y. Choi, "Study on mutual coupling reduction technique for MIMO antennas," *IEEE Access*, vol. 7, pp. 563–586, 2019.

[212] O. J. Famoriji and T. Shongwe, "Electromagnetic machine learning for estimation and mitigation of mutual coupling in strongly coupled arrays," *ICT Exp.*, vol. 9, no. 1, pp. 8–15, Feb. 2023.

[213] Z. Zheng, W.-Q. Wang, Y. Kong, and Y. D. Zhang, "MISC array: A new sparse array design achieving increased degrees of freedom and reduced mutual coupling effect," *IEEE Trans. Signal Process.*, vol. 67, no. 7, pp. 1728–1741, Apr. 2019.

[214] Y. Wang, X. Yang, J. Xie, L. Wang, and B. W.-H. Ng, "Sparsity-inducing DOA estimation of coherent signals under the coexistence of mutual coupling and nonuniform noise," *IEEE Access*, vol. 7, pp. 40271–40278, 2019.

[215] Y. Wang, L. Wang, J. Xie, M. Trinkle, and B. W.-H. Ng, "DOA estimation under mutual coupling of uniform linear arrays using sparse reconstruction," *IEEE Wireless Commun. Lett.*, vol. 8, no. 4, pp. 1004–1007, Aug. 2019.

[216] B. Wang and J. Zheng, "Cumulant-based DOA estimation of noncircular signals against unknown mutual coupling," *Sensors*, vol. 20, no. 3, p. 878, Feb. 2020.

[217] D. Li, Y. Jiang, X. Wu, and W.-P. Zhu, "A gridless method for DOA estimation under the coexistence of mutual coupling and unknown nonuniform noise," in *Proc. IEEE 11th Sensor Array Multichannel Signal Process. Workshop (SAM)*, Jun. 2020, pp. 1–5.
[218] H. Wang, X. Wang, X. Lan, T. Su, and L. Wan, "BSBL-based auxiliary vehicle position analysis in smart city using distributed MEC and UAV-deployed IoT," *IEEE Internet Things J.*, vol. 10, no. 2, pp. 975–986, Jan. 2023.
[219] W. Lin, W. Cui, J. Wang, Y. Chen, and J. Zhang, "Localization of mixed-field sources based on fourth-order cumulant matrix rank reduction," *Electron. Lett.*, vol. 59, no. 18, Sep. 2023, Art. no. e12955.
[220] W. Lin, W. Cui, B. Ba, H. Xu, and J. Li, "A mixed-field circular and non-circular source localization algorithm based on exact spatial propagation geometry," *Sensors*, vol. 23, no. 14, p. 6516, Jul. 2023.
[221] J. Xie, H. Tao, X. Rao, and J. Su, "Localization of mixed far-field and near-field sources under unknown mutual coupling," *Digit. Signal Process.*, vol. 50, pp. 229–239, Mar. 2016.
[222] H. Chen, W. Liu, W.-P. Zhu, M. N. S. Swamy, and Q. Wang, "Mixed rectilinear sources localization under unknown mutual coupling," *J. Franklin Inst.*, vol. 356, no. 4, pp. 2372–2394, Mar. 2019.
[223] J. Xie, Q. Wang, Y. Wang, and X. Yang, "Efficient two-dimensional direction finding algorithm for rectilinear sources under unknown mutual coupling," *Sensors*, vol. 20, no. 7, p. 1914, Mar. 2020.
[224] Z. Meng, S. Dong, X. Shi, and X. Wang, "Robust beamforming for non-circular signals in uniform linear arrays with unknown mutual coupling," *Digit. Signal Process.*, vol. 122, Apr. 2022, Art. no. 103378.
[225] Y. Wang, W. Cui, B. Yang, B. Ba, and F. Mei, "Symmetric thinned coprime array with reduced mutual coupling for mixed near-field and far-field sources localization," *IET Radar, Sonar Navigat.*, vol. 16, no. 8, pp. 1292–1303, Aug. 2022.
[226] J. Zhen and B. Guo, "DOA estimation for far-field sources in mixed signals with mutual coupling and gain-phase error array," *EURASIP J. Wireless Commun. Netw.*, vol. 2018, no. 1, pp. 1–10, Dec. 2018.
[227] J. He, T. Shu, L. Li, and T.-K. Truong, "Mixed near-field and far-field localization and array calibration with partly calibrated arrays," *IEEE Trans. Signal Process.*, vol. 70, pp. 2105–2118, 2022.
[228] S. Wandale and K. Ichige, "Design of sparse arrays via deep learning for enhanced DOA estimation," *EURASIP J. Adv. Signal Process.*, vol. 2021, no. 1, p. 17, Dec. 2021.
[229] C. Larmour, N. Buchanan, V. Fusco, and M. A. B. Abbasi, "Sparse array mutual coupling reduction," *IEEE Open J. Antennas Propag.*, vol. 5, no. 1, pp. 201–216, Feb. 2024.
[230] M. Guo, Y. D. Zhang, and T. Chen, "DOA estimation using compressed sparse array," *IEEE Trans. Signal Process.*, vol. 66, no. 15, pp. 4133–4146, Aug. 2018.
[231] A. A. Ebrahimi, H. R. Abutalebi, and M. Karimi, "Localisation of mixed near-field and far-field sources using the largest aperture sparse linear array," *IET Signal Process.*, vol. 12, no. 2, pp. 155–162, Apr. 2018.
[232] X. Wu, "Localization of far-field and near-field signals with mixed sparse approach: A generalized symmetric arrays perspective," *Signal Process.*, vol. 175, Oct. 2020, Art. no. 107665.
[233] A. V. Delgado, "Atomic Norm decomposition for sparse model reconstruction applied to positioning and wireless communications," Ph.D. thesis, Universidad Carlos III de Madrid, 2022. [Online]. Available: https://e-archivo.uc3m.es/entities/publication/e39d1e7f-9132-4c01-9599-63b3a08e5d5a
[234] R. R. Pote and B. D. Rao, "Maximum likelihood-based gridless DoA estimation using structured covariance matrix recovery and SBL with grid refinement," *IEEE Trans. Signal Process.*, vol. 71, pp. 802–815, 2023.
[235] Y. Wang, W. Cui, Y. Du, B. Ba, and F. Mei, "A novel sparse array for localization of mixed near-field and far-field sources," *Int. J. Antennas Propag.*, vol. 2021, pp. 1–13, Dec. 2021.
[236] S. Zhang, A. Ahmed, Y. D. Zhang, and S. Sun, "Enhanced DOA estimation exploiting multi-frequency sparse array," *IEEE Trans. Signal Process.*, vol. 69, pp. 5935–5946, 2021.
[237] G. Qin, M. G. Amin, and Y. D. Zhang, "DOA estimation exploiting sparse array motions," *IEEE Trans. Signal Process.*, vol. 67, no. 11, pp. 3013–3027, Jun. 2019.
[238] Y. Wang, W. Cui, B. Ba, M. Quan, and Z. Yu, "Symmetric flipped nested array for mixed near-field and far-field non-circular source localisation," *IET Radar, Sonar Navigat.*, vol. 16, no. 11, pp. 1752–1760, Nov. 2022.
[239] H. Yan, Y. Wang, Y. Gong, Z. Zhang, and L. Wang, "Improved sparse symmetric arrays design for mixed near-field and far-field source localization," *IEEE Trans. Aerosp. Electron. Syst.*, vol. 59, no. 6, pp. 7486–7498, Dec. 2023, doi: 10.1109/TAES.2023.3291678.
[240] S. Hayat, E. Yanmaz, and R. Muzaffar, "Survey on unmanned aerial vehicle networks for civil applications: A communications viewpoint," *IEEE Commun. Surveys Tuts.*, vol. 18, no. 4, pp. 2624–2661, 4th Quart., 2016.
[241] T. Martelli, F. Colone, and R. Cardinali, "DVB-T based passive radar for simultaneous counter-drone operations and civil air traffic surveillance," *IET Radar, Sonar Navigat.*, vol. 14, no. 4, pp. 505–515, Apr. 2020.
[242] J.-P. Yaacoub, H. Noura, O. Salman, and A. Chehab, "Security analysis of drones systems: Attacks, limitations, and recommendations," *Internet Things*, vol. 11, Sep. 2020, Art. no. 100218.
[243] R. Pandey and S. Nannuru, "Parametric models for DOA trajectory localization," in *Proc. IEEE Int. Conf. Acoust., Speech Signal Process. (ICASSP)*, May 2022, pp. 5118–5122.
[244] X. Zhong, A. B. Premkumar, and W. Wang, "Direction of arrival tracking of an underwater acoustic source using particle filtering: Real data experiments," in *Proc. IEEE Tencon-Spring*, Apr. 2013, pp. 420–424.
[245] R. Pandey and S. Nannuru, "Localization of DOA trajectories—Beyond the grid," 2023, *arXiv:2308.07265*.
[246] J. Z. Stafsudd, R. E. Hudson, E. Taciroglu, and K. Yao, "Seismic-array signal processing for moving source localization," *Proc. SPIE*, vol. 6697, pp. 160–171, Sep. 2007.
[247] F. Gustafsson, G. Hendeby, D. Lindgren, G. Mathai, and H. Habberstad, "Direction of arrival estimation in sensor arrays using local series expansion of the received signal," in *Proc. 18th Int. Conf. Inf. Fusion (Fusion)*, Jul. 2015, pp. 761–766.
[248] M. Penhale and A. Barnard, "Direction of arrival estimation in practical scenarios using moving standard deviation processing for localization and tracking with acoustic vector sensors," *Appl. Acoust.*, vol. 168, Nov. 2020, Art. no. 107421.
[249] S. Ariyavisitakul, N. Sollenberger, and L. Greenstein, *Introduction to Radar System*. Delhi, India: Tata McGraw-Hill, 2001.
[250] I. van Kamp and F. van den Berg, "Health effects related to wind turbine sound, including low-frequency sound and infrasound," *Acoust. Aust.*, vol. 46, no. 1, pp. 31–57, Apr. 2018.
[251] I. Fiori, F. Paoletti, M. C. Tringali, K. Janssens, C. Karathanasis, A. Menéndez-Vázquez, A. Romero-Rodríguez, R. Sugimoto, T. Washimi, V. Boschi, A. Chiummo, M. Cieślar, R. De Rosa, C. De Rossi, F. Di Renzo, I. Nardecchia, A. Pasqualetti, B. Patricelli, P. Ruggi, and N. Singh, "The hunt for environmental noise in virgo during the third observing run," *Galaxies*, vol. 8, no. 4, p. 82, Dec. 2020.
[252] J. B. Johnson, "Thermal agitation of electricity in conductors," *Phys. Rev.*, vol. 32, no. 1, pp. 97–109, Jul. 1928.
[253] A. Van Der Ziel and E. Chenette, "Noise in solid state devices," in *Advances in Electronics and Electron Physics*, vol. 46. Amsterdam, The Netherlands: Elsevier, 1978, pp. 313–383.
[254] T. Svantesson, *Antennas and Propagation From a Signal Processing Perspective*. Goteborg, Sweden: Chalmers University of Technology, 2001.
[255] J. E. Chen, J. R. Polimeni, S. Bollmann, and G. H. Glover, "On the analysis of rapidly sampled fMRI data," *NeuroImage*, vol. 188, pp. 807–820, Mar. 2019.
[256] A. Papoulis and S. U. Pillai, *Probability, Random Variables and Stochastic Processes*. New York, NY, USA: McGraw-Hill, 2002.
[257] P. Hall and C. C. Heyde, *Martingale Limit Theory and Its Application*. New York, NY, USA: Academic, 2014.
[258] A. B. Kihero, A. Tusha, and H. Arslan, "Wireless channel and interference," in *Design and Analysis of Wireless Communication Signals: A Laboratory-Based Approach*. USA: Wiley, 2021.
[259] D. Neupane and J. Seok, "A review on deep learning-based approaches for automatic sonar target recognition," *Electronics*, vol. 9, no. 11, p. 1972, Nov. 2020.
[260] N. Tayem, H. M. Kwon, S. Min, and D. H. Kang, "Covariance matrix differencing for coherent source DOA estimation under unknown noise field," in *Proc. IEEE Veh. Technol. Conf.*, Sep. 2006, pp. 1–5.
[261] M. S. Veedu and M. V. Salapaka, "Topology identification under spatially correlated noise," *Automatica*, vol. 156, Oct. 2023, Art. no. 111182.
[262] A. Gholipour, B. Zakeri, and K. Mafinezhad, "Non-stationary additive noise modelling in direction-of-arrival estimation," *IET Commun.*, vol. 10, no. 15, pp. 2054–2059, Oct. 2016.
[263] H. You, X. Jianjuan, and G. Xin, *Radar Data Processing With Applications*. Hoboken, NJ, USA: Wiley, 2016.
[264] F. Wang, P. Wang, X. Zhang, H. Li, and B. Himed, "An overview of parametric modeling and methods for radar target detection with limited data," *IEEE Access*, vol. 9, pp. 60459–60469, 2021.

[265] J. Wodecki, A. Michalak, A. Wyłomańska, and R. Zimroz, "Influence of non-Gaussian noise on the effectiveness of cyclostationary analysis—Simulations and real data analysis," *Measurement*, vol. 171, Feb. 2021, Art. no. 108814.

[266] H. Shiri, P. Zimroz, J. Wodecki, A. Wyłomańska, R. Zimroz, and K. Szabat, "Using long-term condition monitoring data with non-Gaussian noise for online diagnostics," *Mech. Syst. Signal Process.*, vol. 200, Oct. 2023, Art. no. 110472.

[267] Y. Yardimci, A. E. Cetin, and J. A. Cadzow, "Robust direction-of-arrival estimation in non-Gaussian noise," *IEEE Trans. Signal Process.*, vol. 46, no. 5, pp. 1443–1451, May 1998.

[268] S. Zozor and C. Vignat, "Some results on the denoising problem in the elliptically distributed context," *IEEE Trans. Signal Process.*, vol. 58, no. 1, pp. 134–150, Jan. 2010.

[269] D. T. Hristopulos, *Random Fields for Spatial Data Modeling*. The Netherlands: Springer, 2020.

[270] T. Liu, M. Wang, H. Feng, S. Luan, and J. Zhang, "Joint estimation of DOA and range for near-field sources in the presence of far-field sources and alpha-stable noise," *IEEE Signal Process. Lett.*, vol. 31, pp. 406–410, 2024.

[271] C. J. Gaikwad, H. K. Samdani, and P. Sircar, "Signal parameter estimation using fourth order statistics: Multiplicative and additive noise environment," *SpringerPlus*, vol. 4, no. 1, pp. 1–26, Dec. 2015.

[272] T. Shu and J. He, "Passive direction finding with a pair of acoustic vector sensors using fourth-order cumulants," *Signal Process.*, vol. 201, Dec. 2022, Art. no. 108706.

[273] L. M. Garth and H. V. Poor, "Detection of non-Gaussian signals: A paradigm for modern statistical signal processing," *Proc. IEEE*, vol. 82, no. 7, pp. 1061–1095, Jul. 1994.

[274] J. L. Rojo-Álvarez, M. Martínez-Ramón, J. Munoz-Mari, and G. Camps-Valls, *Digital Signal Processing With Kernel Methods*. Hoboken, NJ, USA: Wiley, 2018.

[275] H. Jiang and S. Wang, "2-D direction finding of cyclostationary signals in the presence of both multiplicative noise and additive noise," in *Proc. 14th IEEE Pers., Indoor Mobile Radio Commun. (PIMRC)*, Sep. 2003, pp. 2393–2396.

[276] H. Jiang, S. Wang, and H. Lu, "Multipath direction finding in both multiplicative noise and additive noise environments via exploitation of cyclostationarity," in *Proc. IEEE 6th Circuits Syst. Symp. Emerg. Technol., Frontiers Mobile Wireless Commun.*, vol. 2, May 2004, pp. 765–768.

[277] S. Han, A. Khoryaev, Y. Tang, Z. Yu, and S. Bashar, "OTDOA (observed time difference of arrival) positioning enhancement by using heterogeneous reference signals," WO Patent 2016 122 812, Aug. 4, 2020.

[278] S. M. Sheikh, H. M. Asif, K. Raahemifar, and F. Al-Turjman, "Time difference of arrival based indoor positioning system using visible light communication," *IEEE Access*, vol. 9, pp. 52113–52124, 2021.

[279] Y. Sun, K. C. Ho, and Q. Wan, "Solution and analysis of TDOA localization of a near or distant source in closed form," *IEEE Trans. Signal Process.*, vol. 67, no. 2, pp. 320–335, Jan. 2019.

[280] B. Tang, Y. Sun, K. C. Ho, L. Zhang, and Y. Yang, "Multidimensional scaling-based TDOA localization in modified polar representation," in *Proc. IEEE Int. Conf. Acoust., Speech Signal Process. (ICASSP)*, Apr. 2024, pp. 8476–8480.

[281] S. Li, B. Hao, Y. Zhao, and Z. Li, "Unified near-field and far-field TDOA direction-finding with systematic uncertainties," in *Proc. IEEE Wireless Commun. Netw. Conf. (WCNC)*, Mar. 2023, pp. 1–6.

[282] R. Jiang and D. Li, "Exactness conditions for semidefinite programming relaxations of generalization of the extended trust region subproblem," *Math. Oper. Res.*, vol. 48, no. 3, pp. 1235–1253, Aug. 2023.

[283] Y. Wang and K. C. Ho, "Unified near-field and far-field localization for AOA and hybrid AOA-TDOA positionings," *IEEE Trans. Wireless Commun.*, vol. 17, no. 2, pp. 1242–1254, Feb. 2018.

[284] H. Liu, Y. Chen, Y. Lin, and Q. Xiao, "A multiple sources localization method based on TDOA without association ambiguity for near and far mixed field sources," *Circuits, Syst., Signal Process.*, vol. 40, no. 8, pp. 4018–4046, Aug. 2021.

[285] J. Pospisil, R. Fujdiak, and K. Mikhaylov, "Investigation of the performance of TDoA-based localization over LoRaWAN in theory and practice," *Sensors*, vol. 20, no. 19, p. 5464, Sep. 2020.

[286] H. Zeaiter, "Modeling and simulation of radio signals in confined environments using a software defined radio," Ph.D. thesis, School Eng. Sci. Microtechnology, Université Bourgogne Franche-Comté, Besançon, France, 2023.

[287] W. Lv, K. V. Mishra, and S. Chen, "Co-pulsing FDA radar," *IEEE Trans. Aerosp. Electron. Syst.*, vol. 59, no. 2, pp. 1107–1126, Apr. 2023.

[288] J.-X. Kou, M. Li, L. Wang, K. Yang, and C.-L. Jiang, "Generalized weight function selection criteria for the compressive sensing based robust DOA estimation methods," *Signal Process.*, vol. 175, Oct. 2020, Art. no. 107663.

[289] U. Hamid, S. Wyne, and N. R. Butt, "Joint model-order and robust DoA estimation for underwater sensor arrays," *Sensors*, vol. 23, no. 12, p. 5731, Jun. 2023.

[290] Q. Miao, X. Sun, B. Wu, L. Ye, and K. Song, "A source localization method using complex variational mode decomposition," *Sensors*, vol. 22, no. 11, p. 4029, May 2022.

[291] X. Hu, Q. Yu, Y. Han, Z. Chen, and Z. Geng, "Novel complex-valued long short-term memory network integrating variational mode decomposition for soft sensor," *J. Process Control*, vol. 129, Sep. 2023, Art. no. 103053.

[292] A. M. Molaei, O. Yurduseven, and V. Fusco, "An efficient waveform diversity based on variational mode decomposition of coded beat-frequency shifted signals algorithm for multiple-input multiple-output millimetre-wave imaging," *IET Radar, Sonar Navigat.*, vol. 15, no. 10, pp. 1266–1280, Oct. 2021.

[293] A. M. Molaei, S. Hu, V. Fusco, and O. Yurduseven, "A multi-resolution analysis-based approach to accelerate data acquisition for near-field MIMO millimeter-wave imaging," *Proc. SPIE*, vol. 12111, pp. 90–101, Jun. 2022.

[294] M. Sreekantamurthy, D. C. Popescu, and R. P. Joshi, "Classification of digital modulation schemes in multipath environments using higher order statistics," in *Proc. SoutheastCon*, Mar. 2016, pp. 1–6.

[295] M. Khosraviyani, H. Kalbkhani, and M. G. Shayesteh, "Higher order statistics for modulation and STBC recognition in MIMO systems," *IET Commun.*, vol. 13, no. 16, pp. 2436–2446, Oct. 2019.

[296] M. S. Pajic, M. Veinovic, M. Peric, and V. D. Orlic, "Modulation order reduction method for improving the performance of AMC algorithm based on sixth-order cumulants," *IEEE Access*, vol. 8, pp. 106386–106394, 2020.

[297] P. Gupta and M. Agrawal, "Higher-order statistics-based non-uniform linear array for underdetermined DoA estimation of non-circular signals," *Circuits, Syst., Signal Process.*, vol. 41, no. 5, pp. 2719–2749, May 2022.

[298] Y. Ma, C. Miao, Y. Li, and W. Wu, "Underdetermined DOA estimation exploiting the higher-order cumulants of harmonic steering vector with time-modulated arrays," *IET Signal Process.*, vol. 16, no. 3, pp. 239–247, May 2022.

[299] H. Wu, Q. Shen, W. Cui, and W. Liu, "DOA estimation with nonuniform moving sampling scheme based on a moving platform," *IEEE Signal Process. Lett.*, vol. 28, pp. 1714–1718, 2021.

[300] P. Chevalier, A. Ferréol, and L. Albera, "High-resolution DOA estimation with higher-order statistics," in *Classical and Modern Direction-of-Arrival Estimation*. Amsterdam, The Netherlands: Elsevier, 2009, pp. 289–341.

[301] Y. Wang, "Underdetermined DOA estimation of deterministic signals using high order statistics and noncircularity," Ph.D. thesis, School Elect. Electron. Eng., Univ. Adelaide, Adelaide, SA, Australia, 2017.

[302] Z. Feng, Z. Fang, Z. Wei, X. Chen, Z. Quan, and D. Ji, "Joint radar and communication: A survey," *China Commun.*, vol. 17, no. 1, pp. 1–27, Jan. 2020.

[303] T. V. Hoang, V. Fusco, T. Fromenteze, and O. Yurduseven, "Computational polarimetric imaging using two-dimensional dynamic metasurface apertures," *IEEE Open J. Antennas Propag.*, vol. 2, pp. 488–497, 2021.

[304] Y. Yi, L. Zhu, and X. Cao, "Signal fusion research in passive radar based on polarization diversity technology," *Int. J. Microw. Wireless Technol.*, vol. 15, no. 3, pp. 410–423, Apr. 2023.

[305] H. Chen, W. Wang, and W. Liu, "Joint DOA, range, and polarization estimation for rectilinear sources with a COLD array," *IEEE Wireless Commun. Lett.*, vol. 8, no. 5, pp. 1398–1401, Oct. 2019.

[306] T. Zhao, H. Chen, Y. Tian, and W. Liu, "An algorithm for 5-D parameters estimation of near-field sources using parallel factor analysis," *Multidimensional Syst. Signal Process.*, vol. 33, no. 4, pp. 1139–1150, Dec. 2022.

[307] H. Singh and R. M. Jha, "Trends in adaptive array processing," *Int. J. Antennas Propag.*, vol. 2012, Feb. 2012, Art. no. 361768.

[308] M. G. Amin, M. Amin, Y. Zhang, M. B. Obeidat, and M. P. Setlur, "Classification and discrimination of sources with time-varying frequency and spatial spectra," Center Adv. Commun., Office Naval Res., Villanova Univ., Annu. Rep. N00014-98-1-0176, Sep. 2005.

[309] S. Semper, M. Döbereiner, C. Steinmetz, M. Landmann, and R. S. Thomä, "High resolution parameter estimation for wideband radio channel sounding," *IEEE Trans. Antennas Propag.*, vol. 71, no. 8, pp. 6728–6743, Aug. 2023, doi: 10.1109/TAP.2023.3286024.

[310] T. V. Hoang, V. Fusco, M. A. B. Abbasi, and O. Yurduseven, "Single-pixel polarimetric direction of arrival estimation using programmable coding metasurface aperture," *Sci. Rep.*, vol. 11, no. 1, p. 23830, Dec. 2021.

[311] B. A. Obeidat, Y. Zhang, and M. G. Amin, "Range and DOA estimation of polarized near-field signals using fourth-order statistics," in *Proc. IEEE Int. Conf. Acoust., Speech, Signal Process.*, vol. 2, May 2004, pp. 92–97.

[312] M. Zhao, S. Zhu, R. Sharma, A. M. Molaei, X. Chen, and O. Yurduseven, "Metamaterial iris-based cavity antenna for mm-wave computational polarimetric imaging," *IEEE Antennas Wireless Propag. Lett.*, early access, Mar. 5, 2024, doi: 10.1109/LAWP.2024.3373041.

[313] Q. Ren, O. Eriksson, P. Thalya, R. Elezovic, C. Bencivenni, M. Hasselblad, J. Yang, Z. Zang, and A. U. Zaman, "An automotive polarimetric radar sensor with circular polarization based on gapwaveguide technology," *IEEE Trans. Microw. Theory Techn.*, early access, Nov. 9, 2023, doi: 10.1109/TMTT.2023.3329246.

[314] Q. Xie, X. Pan, J. Chen, and S. Xiao, "Joint DOD and DOA estimation for coherently distributed sources in bistatic MIMO radar based on joint diagonalization," *IEEE Access*, vol. 7, pp. 107805–107815, 2019.

[315] W. Hu and G. Xu, "DOA estimation with double L-shaped array based on Hadamard product and joint diagonalization in the presence of sensor gain-phase errors," *Multidimensional Syst. Signal Process.*, vol. 30, no. 1, pp. 465–491, Jan. 2019.

[316] X. Meng, J. Xue, F. Yan, and X. Yan, "Real-valued propagator method for fast DOA estimation via polynomial rooting," *J. Eng.*, vol. 2019, no. 21, pp. 7792–7795, Nov. 2019.

[317] N. Tayem, A. A. Hussain, V. R. Veramareddy, A.-H. Soliman, and J. M. Alghazo, "Propagator rooting method direction of arrival estimation based on real data," in *Proc. IEEE Mil. Commun. Conf. (MILCOM)*, Nov. 2021, pp. 975–980.

[318] L. Wang and B. Yu, "Estimation method for mixed near-field and far-field sources based on four-order cumulant and polarization sensitive array," *Secur. Commun. Netw.*, vol. 2022, pp. 1–11, May 2022.

[319] M. Dai, X. Ma, W. Sheng, and Y. Han, "Linear dipole array with element rotation for enhanced DOA and polarization estimation," *IEEE Trans. Aerosp. Electron. Syst.*, vol. 59, no. 6, pp. 9128–9141, Dec. 2023.

[320] L. Wan, K. Liu, Y.-C. Liang, and T. Zhu, "DOA and polarization estimation for non-circular signals in 3-D millimeter wave polarized massive MIMO systems," *IEEE Trans. Wireless Commun.*, vol. 20, no. 5, pp. 3152–3167, May 2021.

[321] S. Majumder, "One-bit spectrum sensing using Gustafson–Kessel fuzzy clustering for cognitive radio network," *Phys. Commun.*, vol. 62, Feb. 2024, Art. no. 102239.

[322] S. Zahrai and M. Onabajo, "Review of analog-to-digital conversion characteristics and design considerations for the creation of power-efficient hybrid data converters," *J. Low Power Electron. Appl.*, vol. 8, no. 2, p. 12, Apr. 2018.

[323] M. M. Kiasaraei, K. Nikitopoulos, and R. Tafazolli, "Towards ultra-power-efficient, tbps wireless systems via analogue processing: Existing approaches, challenges and way forward," *IEEE Commun. Surveys Tuts.*, early access, Dec. 13, 2023, doi: 10.1109/COMST.2023.3342775.

[324] C.-L. Liu and P. P. Vaidyanathan, "One-bit normalized scatter matrix estimation for complex elliptically symmetric distributions," in *Proc. IEEE Int. Conf. Acoust., Speech Signal Process. (ICASSP)*, May 2020, pp. 9130–9134.

[325] S. Sedighi, B. Shankar, M. Soltanalian, and B. Ottersten, "One-bit DoA estimation via sparse linear arrays," in *Proc. IEEE Int. Conf. Acoust., Speech Signal Process. (ICASSP)*, May 2020, pp. 9135–9139.

[326] S. Sedighi, B. S. Mysore R, M. Soltanalian, and B. Ottersten, "On the performance of one-bit DoA estimation via sparse linear arrays," *IEEE Trans. Signal Process.*, vol. 69, pp. 6165–6182, 2021.

[327] A. M. Molaei, V. Fusco, and O. Yurduseven, "Direct one-bit DOA estimation robust in presence of unequal power signals," *IEEE Access*, vol. 12, pp. 40011–40018, 2024.

[328] H. Liu, H. Meng, L. Gan, D. Li, Y. Zhou, and T.-K. Truong, "Subspace and sparse reconstruction based near-field sources localization in uniform linear array," *Digit. Signal Process.*, vol. 106, Nov. 2020, Art. no. 102824.

[329] A. K. Iyer, A. Alú, and A. Epstein, "Metamaterials and metasurfaces—Historical context, recent advances, and future directions," *IEEE Trans. Antennas Propag.*, vol. 68, no. 3, pp. 1223–1231, Mar. 2020.

[330] M. F. Imani, J. N. Gollub, O. Yurduseven, A. V. Diebold, M. Boyarsky, T. Fromenteze, L. Pulido-Mancera, T. Sleasman, and D. R. Smith, "Review of metasurface antennas for computational microwave imaging," *IEEE Trans. Antennas Propag.*, vol. 68, no. 3, pp. 1860–1875, Mar. 2020.

[331] A. M. Molaei, T. Fromenteze, S. Hu, V. Fusco, and O. Yurduseven, "Fourier-based near-field three-dimensional image reconstruction in a multistatic imaging structure using dynamic metasurface antennas," *IEEE Trans. Comput. Imag.*, vol. 8, pp. 1089–1100, 2022.

[332] A. M. Molaei, T. Fromenteze, V. Skouroliakou, T. V. Hoang, R. Kumar, V. Fusco, and O. Yurduseven, "Development of fast Fourier-compatible image reconstruction for 3D near-field bistatic microwave imaging with dynamic metasurface antennas," *IEEE Trans. Veh. Technol.*, vol. 71, no. 12, pp. 13077–13090, Dec. 2022.

[333] A. M. Molaei, V. Skouroliakou, V. Fusco, and O. Yurduseven, "Fourier-domain image reconstruction in near-field microwave imaging using a dynamic metasurface antenna: A sparse-sampling-based approach," *Proc. SPIE*, vol. 12535, pp. 239–249, Jun. 2023.

[334] Q. Yang, A. Guerra, F. Guidi, N. Shlezinger, H. Zhang, D. Dardari, B. Wang, and Y. C. Eldar, "Near-field localization with dynamic metasurface antennas," in *Proc. IEEE Int. Conf. Acoust., Speech Signal Process. (ICASSP)*, Jun. 2023, pp. 1–5.

[335] H. Lu, Y. Zeng, C. You, Y. Han, J. Zhang, Z. Wang, Z. Dong, S. Jin, C.-X. Wang, T. Jiang, X. You, and R. Zhang, "A tutorial on near-field XL-MIMO communications towards 6G," 2023, *arXiv:2310.11044*.

[336] F. Bilotti, M. Barbuto, Z. Hamzavi-Zarghani, M. Karamirad, M. Longhi, A. Monti, D. Ramaccia, L. Stefanini, A. Toscano, and S. Vellucci, "Reconfigurable intelligent surfaces as the key-enabling technology for smart electromagnetic environments," *Adv. Phys., X*, vol. 9, no. 1, Dec. 2024, Art. no. 2299543.

[337] A. Magbool, V. Kumar, Q. Wu, M. Di Renzo, and M. F. Flanagan, "A survey on integrated sensing and communication with intelligent metasurfaces: Trends, challenges, and opportunities," 2024, *arXiv:2401.15562*.

[338] I. H. Sarker, "Deep learning: A comprehensive overview on techniques, taxonomy, applications and research directions," *Social Netw. Comput. Sci.*, vol. 2, no. 6, p. 420, Nov. 2021.

[339] R. Gupta, D. Srivastava, M. Sahu, S. Tiwari, R. K. Ambasta, and P. Kumar, "Artificial intelligence to deep learning: Machine intelligence approach for drug discovery," *Mol. Diversity*, vol. 25, no. 3, pp. 1315–1360, Aug. 2021.

[340] J. Kufel, K. Bargieł-Łączek, S. Kocot, M. Koźlik, W. Bartnikowska, M. Janik, Ł. Czogalik, P. Dudek, M. Magiera, A. Lis, I. Paszkiewicz, Z. Nawrat, M. Cebula, and K. Gruszczyńska, "What is machine learning, artificial neural networks and deep learning? Examples of practical applications in medicine," *Diagnostics*, vol. 13, no. 15, p. 2582, Aug. 2023.

[341] H. Xiang, B. Chen, M. Yang, S. Xu, and Z. Li, "Improved direction-of-arrival estimation method based on LSTM neural networks with robustness to array imperfections," *Int. J. Speech Technol.*, vol. 51, no. 7, pp. 4420–4433, Jul. 2021.

[342] G. Jenkinson, M. A. B. Abbasi, A. M. Molaei, O. Yurduseven, and V. Fusco, "Deep learning-enabled improved direction-of-arrival estimation technique," *Electronics*, vol. 12, no. 16, p. 3505, Aug. 2023.

[343] K. Tekbıyık, O. Yurduseven, and G. K. Kurt, "Graph attention network-based single-pixel compressive direction of arrival estimation," *IEEE Commun. Lett.*, vol. 26, no. 3, pp. 562–566, Mar. 2022.

[344] X. Su, P. Hu, Z. Gong, Z. Liu, J. Shi, and X. Li, "Convolution neural networks for localization of near-field sources via symmetric double-nested array," *Wireless Commun. Mobile Comput.*, vol. 2021, pp. 1–8, Jun. 2021.

[345] H. Lee, Y. Kim, S. Seol, and J. Chung, "Deep learning-based direction-of-arrival estimation for far-field sources under correlated near-field interferences," *ICT Exp.*, vol. 9, no. 4, pp. 741–747, Aug. 2023.

[346] K. Magowe, A. Giorgetti, S. Kandeepan, and X. Yu, "Accurate analysis of weighted centroid localization," *IEEE Trans. Cognit. Commun. Netw.*, vol. 5, no. 1, pp. 153–164, Mar. 2019.

[347] D. De Witte, "Novel Bayesian optimization based uncertainty quantification frameworks for microwave design," Ph.D. thesis, Dept. Inf. Technol., Faculty Eng. Archit., Ghent Univ., Ghent, Belgium, 2023.

[348] A. M. Molaei, S. Hu, V. Skouroliakou, V. Fusco, X. Chen, and O. Yurduseven, "Fast image reconstruction for near-field terahertz imaging with multistatic non-uniform sparse arrays," *Proc. SPIE*, vol. 12535, pp. 264–272, Jun. 2023.

[349] O. Yurduseven, M. A. B. Abbasi, T. Fromenteze, and V. Fusco, "Frequency-diverse computational direction of arrival estimation technique," *Sci. Rep.*, vol. 9, no. 1, p. 16704, Nov. 2019.
[350] M. A. B. Abbasi, V. F. Fusco, O. Yurduseven, and T. Fromenteze, "Frequency-diverse multimode millimetre-wave constant-ϵ_r lens-loaded cavity," *Sci. Rep.*, vol. 10, no. 1, p. 22145, Dec. 2020.
[351] A. Cidronali, E. Ciervo, G. Collodi, S. Maddio, M. Passafiume, and G. Pelosi, "Analysis of dual-band direction of arrival estimation in multipath scenarios," *Electronics*, vol. 10, no. 11, p. 1236, May 2021.
[352] H. Paaso, N. Gulati, D. Patron, A. Hakkarainen, J. Werner, K. R. Dandekar, M. Valkama, and A. Mämmelä, "DoA estimation using compact CRLH leaky-wave antennas: Novel algorithms and measured performance," *IEEE Trans. Antennas Propag.*, vol. 65, no. 9, pp. 4836–4849, Sep. 2017.
[353] K. Yao, J. C. Chen, and R. E. Hudson, "Maximum-likelihood acoustic source localization: Experimental results," in *Proc. IEEE Int. Conf. Acoust., Speech, Signal Process.*, vol. 3, May 2002, pp. III-2949–III-2952.
[354] A. Bereketli, M. B. Guldogan, T. Kolcak, T. Gudu, and A. L. Avsar, "Experimental results for direction of arrival estimation with a single acoustic vector sensor in shallow water," *J. Sensors*, vol. 2015, pp. 1–10, Jan. 2015.
[355] H. Paaso, A. Hakkarainen, N. Gulati, D. Patron, K. R. Dandekar, M. Valkama, and A. Mämmelä, "Experimental results of novel DoA estimation algorithms for compact reconfigurable antennas," *Int. J. Antennas Propag.*, vol. 2017, pp. 1–13, Jul. 2017.
[356] H. Lim, K. Lim, I. Joo, J.-B. Kim, and S.-U. Lee, "Experimental performance of signal source localization based on distributed DoA measurements," in *Proc. 34th Int. Tech. Conf. Circuits/Syst., Comput. Commun. (ITC-CSCC)*, Jun. 2019, pp. 1–3.
[357] C.-B. Chen, T.-Y. Lo, J.-Y. Chang, S.-P. Huang, W.-T. Tsai, C.-Y. Liou, and S.-G. Mao, "Precision enhancement of wireless localization system using passive DOA multiple sensor network for moving target," *Sensors*, vol. 22, no. 19, p. 7563, Oct. 2022.
[358] W. A. P. van Kleunen, K. C. H. Blom, N. Meratnia, A. B. J. Kokkeler, P. J. M. Havinga, and G. J. M. Smit, "Underwater localization by combining time-of-flight and direction-of-arrival," in *Proc. OCEANS*, Apr. 2014, pp. 1–6.
[359] R. Sanudin, N. H. Noordin, and T. Arslan, "DOA estimation using modified covariance matrix," in *Proc. Loughborough Antennas Propag. Conf. (LAPC)*, Nov. 2012, pp. 1–4.
[360] X. Wang, M. Amin, and X. Wang, "Robust sparse array design for adaptive beamforming against DOA mismatch," *Signal Process.*, vol. 146, pp. 41–49, May 2018.
[361] Z. Xiao, Z. Han, A. Nallanathan, O. A. Dobre, B. Clerckx, J. Choi, C. He, and W. Tong, "Antenna array enabled space/air/ground communications and networking for 6G," *IEEE J. Sel. Areas Commun.*, vol. 40, no. 10, pp. 2773–2804, Oct. 2022.
[362] Z. Ahmad, M. Chen, and S.-D. Bao, "Beampattern analysis of frequency diverse array radar: A review," *EURASIP J. Wireless Commun. Netw.*, vol. 2021, no. 1, p. 189, Dec. 2021.
[363] P. Hyberg, "Antenna array mapping for DOA estimation in radio signal reconnaissance," Ph.D. thesis, Dept. Signals, Sensors Syst., Royal Inst. Technol. (KTH), Stockholm, Sweden, 2005.
[364] L. Guo, B. A. Gebre, and K. Pochiraju, "Parameter estimation of acoustic signals using linear microphone arrays," in *Proc. IEEE Sarnoff Symp.*, Mar. 2009, pp. 1–6.
[365] A. M. Zoubir, V. Koivunen, E. Ollila, and M. Muma, *Robust Statistics for Signal Processing*. Cambridge, U.K.: Cambridge Univ. Press, 2018.
[366] X.-D. Zhang, *Modern Signal Processing*. Berlin, Germany: Walter de Gruyter GmbH & Co KG, 2022.
[367] R. Cheng, Y. Jin, K. Narukawa, and B. Sendhoff, "A multiobjective evolutionary algorithm using Gaussian process-based inverse modeling," *IEEE Trans. Evol. Comput.*, vol. 19, no. 6, pp. 838–856, Dec. 2015.
[368] A. M. Zoubir, V. Koivunen, Y. Chakhchoukh, and M. Muma, "Robust estimation in signal processing: A tutorial-style treatment of fundamental concepts," *IEEE Signal Process. Mag.*, vol. 29, no. 4, pp. 61–80, Jul. 2012.
[369] M. Xu, J. Li, S. Wang, H. Hao, H. Tian, and J. Han, "Structural damage detection by integrating robust PCA and classical PCA for handling environmental variations and imperfect measurement data," *Adv. Structural Eng.*, vol. 25, no. 8, pp. 1815–1828, Jun. 2022.
[370] L. Jian, X. Wang, J. Shi, and X. Lan, "Robust sparse Bayesian learning scheme for DOA estimation with non-circular sources," *Mathematics*, vol. 10, no. 6, p. 923, Mar. 2022.
[371] G. Hongyuan, Z. Yuze, D. Ya'nan, C. Jianhua, and C. Menghan, "Localization for mixed near-field and far-field sources under impulsive noise," *J. Syst. Eng. Electron.*, early access, Jun. 30, 2023, doi: 10.23919/JSEE.2023.000065.
[372] A. Hu, T. Lv, H. Gao, Z. Zhang, and S. Yang, "An ESPRIT-based approach for 2-D localization of incoherently distributed sources in massive MIMO systems," *IEEE J. Sel. Topics Signal Process.*, vol. 8, no. 5, pp. 996–1011, Oct. 2014.
[373] S. Gulwani, K. K. Mehra, and T. Chilimbi, "SPEED: Precise and efficient static estimation of program computational complexity," *ACM SIGPLAN Notices*, vol. 44, no. 1, pp. 127–139, Jan. 2009.
[374] K.-L. Du, M. N. S. Swamy, Z.-Q. Wang, and W. H. Mow, "Matrix factorization techniques in machine learning, signal processing, and statistics," *Mathematics*, vol. 11, no. 12, p. 2674, Jun. 2023.
[375] L. Zhang, J. Mei, A. Zielinski, and P. Cai, "Direction-of-arrival estimation for far-field acoustic signal in presence of near-field interferences," *Electron. Lett.*, vol. 51, no. 1, pp. 101–103, Jan. 2015.
[376] Z. Huang, W. Wang, F. Dong, and D. Wang, "A one-snapshot localization algorithm for mixed far-field and near-field sources," *IEEE Commun. Lett.*, vol. 24, no. 5, pp. 1010–1014, May 2020.
[377] X. Wu and J. Yan, "Gridless mixed sources localization based on low-rank matrix reconstruction," *IEEE Wireless Commun. Lett.*, vol. 9, no. 10, pp. 1748–1752, Oct. 2020.
[378] D. Blanco, D. P. Ruiz, E. Alameda-Hernandez, and M. C. Carrion, "A fourth-order stationarity and ergodicity conditions for harmonic processes," *IEEE Trans. Signal Process.*, vol. 52, no. 6, pp. 1641–1649, Jun. 2004.
[379] M. Ć alasan, S. H. E. A. Aleem, and A. F. Zobaa, "On the root mean square error (RMSE) calculation for parameter estimation of photovoltaic models: A novel exact analytical solution based on Lambert *W* function," *Energy Convers. Manage.*, vol. 210, Apr. 2020, Art. no. 112716.

AMIR MASOUD MOLAEI (Senior Member, IEEE) received the M.Sc. degree in telecommunication systems engineering from the Sahand University of Technology, Tabriz, Iran, in 2013, and the Ph.D. degree (Hons.) in telecommunication systems engineering from the Babol Noshirvani University of Technology (BNUT), Babol, Iran, in 2019.

He was ranked first in the Ph.D. entrance exam/interview in telecommunication systems with BNUT and ranked first among the Ph.D. graduates from the Telecommunication Engineering Department. From 2015 to 2019, he was a Lecturer with the Faculty of Electrical and Computer Engineering, BNUT. From 2019 to 2020, he was a Mobile Networks GSM/UMTS/LTE Analyzer and Planner with Future Wave Ultratech Company, Tehran, Iran. Since 2020, he has been a Postdoctoral Research Fellow with the Centre for Wireless Innovation, School of Electronics, Electrical Engineering and Computer Science, Queen's University Belfast, Belfast, U.K. He has authored more than 55 refereed articles and has filed two patents. His current research interests include signal processing, radar imaging, and sensor arrays.

Dr. Molaei received the STAR Scheme Consolidated Performance Award for exceptional performance and contribution in the academic year 2022–2023. He was the General Chair of the 2022 IEEE International Conference on Manufacturing, Industrial Automation and Electronics (ICMIAE). He was the Session Chair of the Passive and MIMO Radar Session at the 2022 IEEE 23rd International Radar Symposium (IRS). He is the Senior Editor of *Cloud Computing and Data Science*. He has also served as a Technical Reviewer for numerous prestigious leading journals/magazines, including IEEE Wireless Communications, IEEE Transactions on Communications, and IEEE Journal of Selected Topics in Signal Processing.

BIJAN ZAKERI (Member, IEEE) was born in Babol, Iran, in 1974. He received the M.Sc. and Ph.D. degrees in electromagnetics engineering from the Amirkabir "Polytechnic" University of Technology, Tehran, Iran, in 1999 and 2007, respectively.

He is currently a Professor with the Electrical and Computer Engineering Faculty, Babol Noshirvani University of Technology, where he is also the Director of the Antenna and Microwave Laboratory and the Head of the Radar Research Team. His research interests include the application of electromagnetic computational techniques in solving radiation and scattering problems, radar microwave subsystems, ultra-wideband antenna, and Polin-SAR remote sensing. He is also a member of the Iranian Association of Information and Communication Technology.

SEYED MEHDI HOSSEINI ANDARGOLI received the B.Sc. degree in electronics engineering from Shahed University, Tehran, Iran, in 2004, and the M.Sc. and Ph.D. degrees in telecommunication systems engineering from the K. N. Toosi University of Technology, Tehran, in 2009 and 2011, respectively. He is currently an Associate Professor with the Electrical and Computer Engineering Faculty, Babol Noshirvani University of Technology, Babol, Iran. His current research interests include resource allocation of cellular networks, cognitive radio networks, sensor networks, optimization, and signal processing.

MUHAMMAD ALI BABAR ABBASI (Member, IEEE) received the B.S. degree in electrical engineering from COMSATS University Islamabad (CUI), Pakistan, the M.S. degree in electrical engineering from the National University of Sciences and Technology (NUST), Islamabad, Pakistan, in 2013, and the Ph.D. degree in electrical engineering from Frederick University, Nicosia, Cyprus, in 2017. From 2017 to 2019, he was a Research Fellow with the Centre of Wireless Innovation (CWI), Queen's University Belfast (QUB), Belfast, U.K., where he is currently a Lecturer (an Assistant Professor). He has authored or coauthored over 80 journals and conference papers and has contributed five book chapters. His research grant portfolio includes academic ownership of over B750k. His key projects include 6G-SANDBOX SNS HE, DSTL EME Hub, and REFLECT-MMWAVE. He was a recipient of the Erasmus Mundus INTACT Doctoral Scholarship by the European Union, in 2014. He has been an IEEE Antennas and Propagation Society (AP-S) Young-Professional Ambassador, since 2022; an IET-Young-Professional, since 2017; and a Grand Prize Winner of the Mobile World Scholar Challenge at the Mobile World Congress (MWC), in 2019. He has acted as the publication chair, the session chair, a technical program committee member, and a reviewer of several scientific conferences and workshops.

VINCENT FUSCO (Fellow, IEEE) is currently with the ECIT Research Institute, Queen's University Belfast, Belfast, U.K. His fundamental work on active antenna front-end techniques has provided generic advances in low-cost phased and self-tracking antenna array architectures. He has authored or coauthored more than 500 articles and two books. He holds several antenna-related patents. He is a fellow of the Institution of Engineering and Technology and the Royal Academy of Engineering. He was a recipient of the IET Senior Achievement Award and Mountbatten Medal for seminal contributions to the field of microwave electronics and its impact on the U.K. industry, in 2012, and the 2019 Royal Irish Academy Gold Medal for Engineering Science.

OKAN YURDUSEVEN (Senior Member, IEEE) received the Ph.D. degree in electrical engineering from Northumbria University, Newcastle upon Tyne, U.K., in 2014.

From 2014 to 2018, he was a Postdoctoral Research Associate with Duke University, USA. From 2018 to 2019, he was a NASA Research Fellow with the Jet Propulsion Laboratory, California Institute of Technology, USA. He is currently a Reader (Associate Professor) with the School of Electronics, Electrical Engineering and Computer Science, Queen's University Belfast, U.K. His research has been supported with extensive funding as a Principal Investigator and a Co-Investigator (over £15 million). He has authored more than 200 peer-reviewed technical journals and conference papers. His research interests include microwave and millimeter-wave imaging, multiple-input–multiple-output (MIMO) radars, wireless power transfer, antennas, and propagation and metamaterials.

Dr. Yurduseven is a fellow of the Institution of Engineering and Technology (IET) and a member of the European Association on Antennas and Propagation (EurAAP). He was a recipient of several awards, including the Outstanding Postdoctoral Award at Duke University, in 2017, the Duke University Professional Development Award, in 2017, the NASA Postdoctoral Program Award, in 2018, the British Council—Alliance Hubert Curien Award, in 2019, the Leverhulme Trust Research Leadership Award, in 2020 (£1M), the Young Scientist Award from the Electromagnetics Academy—Photonics and Electromagnetics Research Symposium, in 2021, the Queen's University Belfast Vice Chancellor's Early Career Researcher Prize, in 2022, and the Outstanding Associate Editor Award from IEEE ANTENNAS AND WIRELESS PROPAGATION LETTERS, in 2023. He serves as an Associate Editor for IEEE ANTENNAS AND WIRELESS PROPAGATION LETTERS and *Scientific Reports* (Nature).